Gonadotropin-releasing Hormone Receptor As
A Molecular Target for Contraception in Feral Cats

by

India Desiree Napier

A dissertation submitted to the Graduate Faculty of
Auburn University
in partial fulfillment of the
requirements for the Degree of
Doctor of Philosophy

Auburn, Alabama
December 12, 2015

Keywords: contraception, DNA vaccines, feline, gonadotropin-releasing hormone
receptor, superparamagnetic iron oxide nanoparticles, ubiquitin

Approved by

Tatiana I Samoylova, Chair, Research Professor of Scott-Ritchey Research Center
Frank F Bartol, Professor of Anatomy, Physiology, and Pharmacology
Timothy D Braden, Associate Professor of Anatomy, Physiology, and Pharmacology
Douglas R Martin, Professor of Anatomy, Physiology, and Pharmacology
Robyn R Wilborn, Associate Professor of Clinical Sciences

Abstract

The global overpopulation of feral cats generates concern regarding their welfare, negative impact on public health, and adverse effects on the environment. In the U.S. and other Westernized countries, the most common method for managing feral cat populations is impoundment in animal shelters, where they undergo surgical sterilization procedures as part of a shelter adoption or trap-neuter-release programs. However, such programs are labor-intensive, time-consuming, and costly. Further, several million, un-adopted cats are euthanized each year. Thus, there is a need for a permanent, nonsurgical, and low-cost method for controlling feral cat populations. Immunocontraception has the potential to provide the practical approach needed to manage stray cat populations. Gonadotropin-releasing hormone receptor (GnRHR) is an attractive target for immunocontraceptive vaccine development because it is highly expressed by anterior pituitary gonadotropic cells, important components of the hypothalamic-pituitary-gonadal axis that regulates normal mammalian reproduction. Therefore, induction of immune responses against pituitary gonadotropic cells by targeting GnRHR may impair normal reproductive function. The goal of this proof-of-concept work was to use a murine model to investigate the potentials of GnRHR as a target for immunocontraception. DNA plasmids were selected for immunocontraceptive vaccine construction because they are cost-effective, safe, and can elicit long-term

cytotoxic and humoral immune responses in animals. In order to overcome murine self-tolerance to the GnRHR, the nucleic acid sequence of feline (f)GnRHR was cloned into a plasmid with expectations of the murine immune system to elicit a stronger response to the heterologous antigen (fGnRHR) than to the homologous protein (mouse GnRHR). As an additional strategy for enhancing the potency of the vaccine against the self-antigen GnRHR, the DNA sequence for fGnRHR fused to ubiquitin (Ub) was incorporated into a plasmid in order to enhance presentation of GnRHR epitopes from Ub-fGnRHR to circulating CD4+ T cells. This strategy may efficiently activate these T cells, producing GnRHR-specific antibodies that ultimately target GnRHR-expressing pituitary gonadotropic cells. After DNA plasmid construction, adult male mice were vaccinated once with DNA encoding fGnRHR or Ub-fGnRHR. Vaccines were administered via intramuscular (IM) needle injection; IM injection with DNA-loaded, superparamagnetic iron oxide nanoparticles followed by magnetofection; or intradermal (ID) needle injection. Mice vaccinated with DNA encoding fGnRHR or Ub-fGnRHR via IM injection or magnetofection had normal serum testosterone levels at necropsy (or 12 weeks post-immunization) compared to pretreatment values. However, mice vaccinated with plasmid encoding Ub-fGnRHR via ID needle injection had significantly low testosterone concentrations 12 weeks post-immunization. Moreover, anti-GnRHR antibodies were detected in sera from mice intradermally vaccinated with DNA encoding Ub-fGnRHR. Also, PCR analysis indicated lower GnRHR mRNA expression in these animals. In summary, ID vaccination of mice with DNA encoding Ub-fGnRHR, a heterologous and ubiquitinated protein, abated serum testosterone concentrations and pituitary expression of GnRHR mRNA, as well as induced anti-GnRHR antibody

production in treated animals. The outcome of these parameters indicate induction of an immunological response to overcome self-tolerance to the endogenous GnRHR, resulting in impairment to anterior pituitary gonadotropes that affected testosterone production. Based on these findings, the Ub-fGnRHR DNA construct warrants further investigation, as such a vaccine profile would be beneficial as an immunocontraceptive for controlling the overpopulation of feral cats worldwide.

Acknowledgments

"It's not who I am underneath, but what I do that defines me."

Bruce Wayne, *Batman Begins*

First, I thank my advisor, Dr. Samoylova, for providing me the opportunity to conduct my dissertation research in her laboratory. I also thank the other members of my dissertation committee for their invaluable support during my tenure as a doctoral student. I would like to express my sincerest gratitude to my mentor, Dr. Frank Bartol, for inspiring me to be a leader in the Auburn University (AU) graduate student community and for having full confidence in my potential to be a biomedical researcher who can change the world. Dr. Timothy Braden has also been a great ally during my graduate studies at AU and taught me a valuable lesson: one must always make time for his/her family (even while enrolled in a graduate program). I also thank Drs. Douglas Martin and Robyn Wilborn for their positive attitudes, insightful comments, and encouragement throughout the dissertation process. Finally, I am thankful for the support of my family (especially my husband, Dr. James Morris-King) who encouraged me to pursue a doctoral degree and always reminded me that I am capable of achieving my educational, career, and personal goals.

Table of Contents

List of Tables

List of Figures

List of Abbreviations

AP   Adaptor protein

AQP-1   Aquaporin-1

AVMA   American Veterinary Medical Association

BamHI   *Bacillus amyloliquefaciens*

BBB   Blood brain barrier

BW   Body weight

CHO   Chinese hamster ovary

COS   African green monkey kidney

CSD   Cat-scratch disease

CTL   Cytotoxic T lymphocytes

DAG   Diacylglycerol

DMEM   Dulbecco's Modified Eagle Medium

DNA   Deoxyribonucleic acid

EPR   Enhanced permeation and retention

FSH   Follicle-stimulating hormone

GFP   Green fluorescent protein

GM-CSF   Granulocyte-macrophage colony-stimulating factor

GnRH   Gonadotropin-releasing hormone

GnRHR   Gonadotropin-releasing hormone receptor

GPCR	G-protein coupled receptor
HEK	Human embryonic kidney
HRP	Horseradish perioxidase
HTRF	Homogeneous Time Resolved Fluorescence
ID	Intradermal
IFNγ	Interferon γ
IGF-1R	Type 1 insulin-like growth factor receptor
IL	Interleukin
IM	Intradermal
IP	Intraperitoneal
IP$_3$	phophatidylinositol-triphosphate diacylglycerol
LH	Luteinizing hormone
LiCl	Lithium chloride
MGA	Megestrol acetate
MHC	Major histocompatibility complex
MOPS	3-(N-morpholino)propanesulfonic acid
MRI	Magnetic resonance imaging
mRNA	Messenger ribonucleic acid
MTT	(3-(4,5-Dimethylthiazol-2-yl)-2,5-Diphenyltetrazolium Bromide)
NK	Natural Killer cells
NMR	Nuclear magnetic resonance
NotI	*Nocardia otitidis-caviarum*
PCR	Polymerase chain reaction

PEG   Poly(ethylene) glycol

PEI   Polyethylenimine

POA   Preoptic area

SNARE   Soluble N-ethylmaleimide-sensitive factor attachment protein receptor

SPION   Superparamagnetic iron oxide nanoparticles

Th   T helper

TNR   Trap-neuter-release

TSH   Thyroid-stimulating hormone

Ub   Ubiquitin

UK   United Kingdom

US   United States

USD   United States dollars

USDA   United States Department of Agriculture

UPS   Ubiquitin proteasome system

XBaI   *Xanthomonas badrii*

ZP   Zona pellucida

CHAPTER 1

LITERATURE REVIEW

1.1 The Overpopulation of Feral Cats and its Implications

Stray cats may be classified into subcategories: feral; abandoned; or uncontrolled, owned cats. Feral cats are unowned, independent of human control, and poorly socialized to human handling [1]. Also, feral cats mainly survive through scavenging and hunting. Abandoned cats were once dependent on an owner who no longer provides care or resources [1]. Because of previous exposure to human handling, abandoned strays may be socialized enough to interact with people who provide intermittent resources. Similar to ferals, abandoned cats rely heavily on scavenging and hunting in order to survive. In contrast to abandoned and feral strays, owned, non-controlled cats are dependent on humans for resources [1]. These free-roaming cats are kept outdoors and well-socialized to people. Although the literature is rife with semantic disparity (as terms such as "feral", "stray" and "free-roaming" are used interchangeably), it is agreed that stray cats are overpopulating most areas worldwide [1,2].

In the United States (U.S.), the estimated population of stray cats ranges from 70 to 90 million [1,2]. The overpopulation of feral cats is not unique to North America, as it

exists on every continent except Antarctica. For example, the stray cat population in Australia is estimated at 12 million [3]. In the United Kingdom, there is a conservative estimate of 2 million stray cats [1]. The feline reproductive profile that includes early sexual maturity, polyestrous cyclicity, and multiparous pregnancies contribute to the prolific nature of cats. In addition, cats are exceptionally adaptable and thus thrive in various environments, ranging from isolated sub-Antarctic regions to densely-populated cities [2]. The unregulated reproduction of stray cats raises concern regarding their impact on public health and the environment.

Cats are a vector for numerous zoonotic diseases and parasites, thereby posing a threat to public health. Indisputably, rabies is the disease of greatest public concern due to low survival rate in humans manifesting clinical signs. For the past 25 years, rabies cases has been consistently documented in more cats than dogs in the U.S. [4]. In 2009, cats were one of the top five major contributors to over 6,000 rabies cases in the U.S. [5]. In 2010, the number of rabies cases decreased in all domestic animals except for cats, which constituted 62% of all rabies cases in domestic animals [5].

Felids serve as hosts for various zoonotic parasites. Toxoplasmosis is a common disease of cats that can be transmitted to humans via the protozoan *Toxoplasma gondii (T. gondii)*. Contact with infectious *T. gondii* parasitic eggs in cat feces is a primary risk factor for human toxoplasmosis [6]. Because human infections can occur months after the cat has excreted the oocysts, cat feces-contaminated playgrounds, garden soil, and other outdoor recreational venues are possible sources of infection for humans [7,8].

The ectoparasite *Ctenocephalides felis* (the cat flea) of domestic cats, plays an important role in the transmission of zoonotic diseases. It is the dominant vector for cat-scratch disease (CSD), one of the major flea-associated diseases of cats in the U.S. [9]. Cat fleas are the primary carriers of *Bartonella henselae* (*B. henselae*), the bacterium that causes CSD. Animal to animal or human infection commonly occurs by exposure to a cat scratch or bite, or *B. henselae*-contaminated flea feces. A small percentage (5-15%) of CSD-infected humans experience atypical yet serious complications such as encephalitis and endocarditis [10]. In humans, *Bartonella* spp. infection has correlated with chronic rheumatic symptoms that are clinically similar to chronic Lyme disease [11]. Feral cats have a significantly higher Bartonella seroprevalence than owned, controlled cats [12].

Stray cats exert a tremendous pressure on native wildlife populations. Provision of food resources from humans does not suppress a cat's instinct to hunt and kill [13]. As instinctive predators, cats are able to hunt as effectively as their wild ancestors. Because of this, stray cats kill up to a billion native North American birds, mammals, reptiles, amphibians, and fish each year [14,15]. This estimate does not account for the wounded animals reported to various rehabilitation and conservation institutions. Between January 1 and September 14, 2003, the Lindsay Museum of Walnut Creek, a wildlife rehabilitation facility in California, received 5,669 small mammals, birds, and reptiles [16]. Of these, 24% (1,050) of birds, 12% (143) of mammals, and 15% (11) of reptiles were presented because of cat-related injuries or conditions [16]. Specifically, birds that were admitted because of cat-related problems

represented 36 species, including songbirds [16]. Furthermore, many of the injured

birds are considered locally rare, sensitive, or migratory species, all of which are

mandated to be protected by law from illegal capture [16]. According to a survey

conducted in Michigan, free-roaming cats killed from 0.7 to 1.4 birds per week [16].

Twenty-three species were accounted for in this report, including two species of

conservation concern [16]. Further, it has been estimated that feral cats kill about 465

million birds per year in the U.S. [17]. Pimentel *et al.* estimated the value of those birds

at $17 million [17]. The predatory nature of free-roaming cats negatively impacts avian

populations such as piping plover, Florida scrub-jay, and tern, all federally-listed,

endangered bird species [18]. Thus, it is reasonable to speculate that cat predation

plays a critical role in the variation of bird populations.

In addition to negatively impacting bird populations, cats are predators to many

small, non-avian animals that become federally- or state-listed as "threatened" or

"endangered" species. For example, in Florida, domestic cats have been identified as

predators and a serious threat to the Key Largo cotton mouse, rice rat, Key Largo

woodrat, Choctawhatchee beach mouse, Perdido Key beach mouse, Anastasia Island

beach mouse, Southeastern beach mouse, green sea turtle, and Lower Keys marsh

rabbit, all federally-listed species [18]. Focusing in the latter, the Lower Keys marsh

rabbit has been dwindled down to a population of approximately 100 to 300 individuals

[19]. With predation as the greatest threat to the species, it is estimated that the Lower

Keys marsh rabbit could go extinct within two or three decades if current mortality rates

continue [19]. Also, it is estimated that 52% of marsh rabbit mortality was due to

predation by stray cats [20]. Population viability analyses indicated that control of free-roaming cats was an effective strategy for retarding marsh rabbit mortality [20]. Extensive research reveals that cat predation poses a major threat to the continued existence of beach mice, an important beacon of dune ecosystem health [18]. Beach mice are found only in the southeastern U.S. and are at least six subspecies of Florida beach mice federally-listed as "endangered" or "threatened". Indeed, beach mice appear to evade native predators such as birds, raccoons, fox and snakes, but experience difficulty in eluding non-native, feline predators [18]. Because of this, there is a push for public education aimed at informing people of the problems associated with supporting free-roaming cats with food supplemented by humans.

In addition to the detrimental impacts of the feral cat population on public health and the environment, there is concern regarding the welfare of stray cats. Many feral cats live short lives filled with hardships. The American Veterinary Medicine Association (AVMA) estimates that the average lifespan of unowned cats is two years, a figure significantly lower than ten-year mean lifespan of owned cats [21]. Mortality rates for feral cats can be up to 80% per year [16]. In one study evaluating survival rates of kittens born in a monitored cat colony, 48% of kittens died or disappeared before they were 100 days old, and 75% died or disappeared before they were six months old [12]. Investigators confirmed that trauma was the cause of death for most of the kittens in this study [12]. Feral cats suffer substantially higher rates of injury and disease than owned, controlled cats [21]. In addition, many feral cats succumb to vehicle trauma, predation,

or severe weather [16]. It is clear that these conditions and outcomes are impeding on the welfare of feral cats.

Overall, efforts to increase awareness of cat-related impacts on public heath, the environment, and cat welfare may prompt individuals to learn about companion animal responsibility and thus contribute to solving problems related to the global cat overpopulation.

1.2 Approaches to Controlling the Overpopulation of Feral Cats

1.2.1 Shelters

Various methods are used to control feral cats. In the U.S., temporary housing of cats into shelters is the primary method of controlling the population of free-roaming, unowned cats. An estimated 4 to 5 million animals are cared for or find permanent living arrangements through shelters each year [22]. As mediators of cat adoption into a household, shelter personnel educate soon-to-be owners about the importance of promoting public health by keeping the pet current on vaccinations or limiting the cat's access to the outdoors. Although the positive role that animal shelters play is unquestionable, there are limitations to the influence of shelters on reducing the stray cat population. Shelters are conditions of intensive housing where overcrowding is common and contributes to high rates of infectious disease exposure and transmission. It is estimated that eight to ten million animals were housed in animal shelters in 2014 [23]. Within the past decade, sheltered populations have been a source of emerging infectious diseases such as respiratory, neurologic, and virulent systemic feline

calicivirus infections, all of which have fatal tendencies [24,25]. In addition, restraints on housing space and financial resources to sustain daily operation limits the extent to which shelters can temporarily house and facilitate establishment of permanent homes for free-roaming cats.

1.2.2 Trap-neuter-release Programs

Some of the earliest scientific reports of trap-neuter-release/return (TNR) programs originated in the U.K. [26]. The ultimate goal of TNR programs is to decrease or, at least, stabilize a local colony population via sterilization. Generally, trap-neuter-release/return (TNR) involves the humane capture of cats, followed by surgical sterilization and permanent identification of sterilization status (e.g., ear tip removal). Identification of gonadectomized cats is an important step in TNR, as it is well-documented that cats, particularly toms, move between colonies [27]. Typically, the cats are minimally vaccinated for rabies, but in other cases, additional care is provided, including application of anti-flea and deworming medication, and vaccination against feline calici virus, panleukopenia, rhinotracheitis, and feline leukemia. Once captured and then neutered, these cats are released to their original site, thus resuming their occupancy in the colony. The expected outcome of this strategy is determent of new cats to move into an existing colony and, more importantly, natural reduction of the returned sterilized cats. TNR programs are well established in many countries, including, Canada, the Netherlands and the U.S.

While TNR offers a humane solution to controlling the population and improves the welfare of feral cats, these programs have limitations. For example, in Florida, a TNR program named "operation CatNip" is estimated to cost $17 USD per cat [28,29]. Therefore, consistent and greater financial support (by both private entities and government agencies) are critical for controlling the financial costs of trapping cats. However, there is opposition to TNR programs. Jessup claims that maintaining cat colonies facilitates the negative impact on public and environmental health destruction of wildlife and encourages people to abandon cats at the colony sites [16]. Others consider the TNR programs as morally unjustified [16]. Also, there is legal obstruction of TNR programs in some municipalities that considered them a form of 'abandonment' which is illegal under U.S. state laws [16].

Although there are some areas where TNR is illegal, those that can and do implement the program have positive outcomes. For example, in Florida TNR programs were found to be more efficient and cost effective than eradication methods [30]. Furthermore, they resulted in lower admissions rates to the local shelters [30]. Implementation of a TNR program on a Florida-based, university campus reduced a cat colony size by 85% over an 11-year period [27]. Within a five year period, over 99% of the individuals in that colony were sterilized through the program [27]. In addition, 47% of the colony cats were adopted into permanent homes and no new kittens were observed on the campus within the first five years of the TNR program [27]. Importantly, the study noted that a few of these colony cats went missing or were euthanized due to illnesses [27]. However, follow-up studies indicated that the remaining cats continued to

roam the area for over 6 years, suggesting that the welfare and lifespan of feral cats can be reasonable in some colonies [27].

Unfortunately, some TNR programs do not have such successful outcomes. Implementation of a 10-year TNR program in Rome, Italy, which has a 'no-kill' policy, initially decreased cat numbers [31]. However, the addition of new cats by both natural migration into the city and from the abandonment of pet cats offset the benefits of the TNR program [31]. These results emphasized that the TNR program would be optimized when combined with pet owner education about sterilization and containment of pets [31].

In conclusion, TNR is a practical, humane method of controlling the feral cat population. This is especially the case when the programs are supplemented with pet owner education about spay/neuter options and alternatives to abandonment. Financial costs and lack of collective efforts from the community (including local veterinarians) are major limitations to this method. In addition, sustainability of TNR requires endorsement by private and federal organizations.

1.2.3 Surgical Sterilization

Traditionally, the surgical removal of ovaries or testes (gonadectomy) is the most common method to achieve sterilization in companion animals. Potential benefits of gonadectomy include prevention of reproductive tract diseases, elimination of undesirable behaviors associated with hormonal cycling, and most importantly,

population control [32]. For female cats, sterilization can be accomplished by removing both the ovaries and uterus (ovariohysterectomy or "spaying") or by removing the ovaries alone (ovariectomy). Rather than ovariectomy, ovariohysterectomy is highly recommended for female cats because of the potential for uterine abnormalities such as cystic endometrial hyperplasia–pyometra complex and uterine neoplasia [33]. Sterilization of male cats is commonly attained through the removal of both the testes and spermatic cords (also known as orchiectomy, male castration, or neutering). Vasectomy, which is the occlusion or partial removal of the ductus deferens, has been reported since the 1980s [34]. However, this procedure has not been popularized because complete sterility is not guaranteed and there is a continuation of unwanted behaviors such as howling, aggressive behavior, and urine marking of territories [1].

From the position of population control, surgical sterilization of stray cats is typically performed prior to sexual maturity (i.e., at least six weeks of age and minimum weight of two pounds) [1]. Well-studied techniques for anesthesia protocols for feral cats are safe and result in very low mortality rates [35,36]. In addition, newer anesthetic protocols are being developed that focus on postoperative analgesia and short recovery times [37]. This form of pediatric neutering removes the prospect of accidental or intentional breeding of these animals.

Surgical sterilization as a method of controlling the feral cat population has limitations. Gonadectomies can be too time consuming and expensive to be performed on a large-scale. Sterile locations, surgical tools, medicines, and trained personnel have

an associated cost. Many shelters offer subsidized or low-cost surgical sterilization services. In the southern U.S., spays range from $35-$45 USD, while castration averages $25-$45 USD [1]. This greatly offsets the price of these procedures at private practices that have unsubsidized average costs of $75 for neuters and $150 for spays [1]. Also, surgical sterilization procedures are time-consuming. Although castration and ovariohysterectomy procedure lengths are five and twenty minutes, respectively, most veterinary facilities are not set up to solely perform these surgeries. Even agencies dedicated to surgical sterilization on a daily basis have been unable to significantly reduce the feral cat populations. Therefore, prospects of large-scale gonadectomies solving the problem of cat overpopulation are doubtful.

1.2.4 Non-Surgical Sterilization

The perfect fertility control agent for feral cats has several characteristics. First, the product must be safe and not cause negative side effects to feral cats. Developing an agent that is permanent and deliverable a single administration is important because there is likely only one opportunity to treat the feral cat population. Ideally a treatment that affects both male and female cats would have the greatest impact on controlling the feral cat population. In addition, the product needs to be set at a reasonable price-point which is important for both the manufacturer and consumer. Indeed, it is crucial to develop a product that is affordable to consumers who are (1) the shelters that rely on government assistance or private donations to run their daily operations, and (2) the individuals who will pay shelter cat adoption fees that include costs associated with the fertility control agent administered to the adopted cat. Additionally, the treatment should

11

be stable in field conditions. Lastly, the ability of a given product to be approved by relevant regulatory agencies is a key practical consideration. Various fertility control agents targeting different factors of the male and/or female reproductive systems have been formulated and tested in cats.

1.2.4.1   Chemical Sterilants

A nonsurgical approach to male contraception is injections of chemical sterilants designed to induce azoospermia in the testes. Pineda and Dooley were one of many groups in the 1980s to investigate the effects of chemical sterilant treatments in cats. In their studies, treatment with chlorhexidine digluconate caused azoospermia in seven of the eight treated cats [38]. Also, sperm production was reduced or eliminated for 4.5 months in five treated cats. Another chemical sterilant studied in cats is zinc gluconate. In one study, mature, mixed breed cats were administered a single injection of zinc gluconate into each testis [39]. Four months post-injection, histologic evaluation of the treated group revealed atrophic and dilated seminiferous tubules, a decrease in germ cell number, and abnormal spermatogenesis [39]. Azoospermia occurred in 73% (or eight out of eleven) of the treated cats [39]. In another study with the same design (N=11), penile spines were decreased in 55% and absent in 36% of the feline subjects, and there were substantial reductions in male sexual behavior [40]. However, plasma testosterone concentrations were not significantly different between treated and control cats at any time point in the study [40]. Calcium chloride solution is another chemical agent used in sterilization studies with feline subjects. Oliveira *et al.* injected cat testes with 5%, 10% or 20% calcium chloride dihydrate in saline solution with a local

anesthetic (N= six per group) [41]. On the 60th day post-injection, cat testes were observed to have complete testicular necrosis and very low sperm counts. Also, serum testosterone was significantly reduced by at least 70% in the 20% dose treatment group. In an unpublished study conducted by Jana and Samanta, three male cats were injected with 10-, 20-, 40-mg calcium chloride and then monitored for two months [41]. Two of the three cats treated with lowest concentrations were oligospermic and displayed necrotic seminiferious tubules [41]. Although intratesticular injection of chemical sterilants have negative impacts on many reproductive parameters, studies observing treated cats past five months were not conducted, making long-term effects of treatment unknown.

1.2.4.2   Hormonal Downregulation via Sex Steroids

Companion animal contraception through hormonal down-regulation has been practiced since the 1950s, with the first documented study by Murray and Eden. Megestrol acetate (MGA) is a synthetic progestin that is rapidly metabolized when administered orally, with a half-life of 8 days in the dog [42]. MGA was reported to be effective at suppressing estrus when given to queens at a dose of 5 mg/cat orally for 5 days and then once weekly [42,43]. Observed side effects of extensive MGA treatment in cats included: adrenal atrophy, profound adrenocortical suppression, polydipsia/polyuria, personality changes, possible hepatotoxicity, clinical and pathologic changes typical of diabetes mellitus [42,44,45]. Proligestone (14a,17a-propylidene-dioxy progesterone) is characterized with weaker activity than other synthetic progestins [46]. In Europe, proligestone is available (Delvosteron, Intervet) as an injectable canine

contraceptive, but can also be given to female cats (1 mL subcutaneously). Reports indicate that proligestone administration caused suppression of estrus for approximately 6.5 months [47]. In clinical trials, this regimen did not promote development of uterine disease or mammary tumors [46].

Mibolerone, a synthetic androgen, suppresses estrus in cats at a dose of 50 µg/day [48]. However, it is contraindicated for use in cats because the effective dose is very close to the toxic dose [42]. For example, queens dosed at 60 mg/day were observed with hepatic dysfunction [48]. Unfortunately, lower doses did not suppress estrus in queens. Furthermore, mortality ensues at doses of 120 mg/day [42,43]. Also, clitoral hypertrophy and cervical skin thickening was observed in cats and did not resolve after drug withdrawal [48].

1.2.4.3   Immunization against Zona Pellucida

In the ovary, where the eggs are produced, each egg is surrounded by a protective coating called the zona pellucida (ZP). The ZP is made up of several glycoproteins, including ZP1, ZP2, and ZP3. In each species, there are different, but similar, ZP proteins around the egg. For example, the ZP proteins from a pig (pZP1, -2, and 3) are similar to the ZP proteins of a cat. A great deal of work in animal contraception has been undertaken with ZP vaccines in cats.

For example, SpayVac, a commercially-manufactured pZP3 vaccine that has been a successful immunocontraceptive in many wild species, did not prevent estrous

14

cyclicity or pregnancy in queens [49]. Mature female cats produce high concentrations of anti-ZP3 antibodies that have a low affinity for feline ZP3 protein [49]. In other studies, vaccines constructed against native soluble-isolated ZP (siZP) from the ovaries of pigs, cows, cats, ferrets, dogs, and mink were also tested in female cats [50]. Despite all queens developing anti-siZP antibodies, all subjects became pregnant during a breeding trial [50]. Consistent with other studies, although the siZP from these species was immunogenic in the cat, *in situ* studies demonstrated that siZP antibodies did not bind to feline ZP, thus attributing to no observed contraception in treated animals [50].

In another study, pZP polypeptide and feline (f)ZP A, B and C subunits expressed by plasmid vectors were evaluated as anti-fertility vaccine candidates for domestic female cats [51]. Vaccination with pZP protein induced anti-pZP antibodies that did not, however, cross-react with fZP as assessed by immunohistochemistry [51]. Also no effect on fertility *in vivo* was observed after mating. Interestingly, vaccination with fZPA or fZPB+C DNA vectors elicited circulating fZP-specific antibodies [51]. *In situ* studies indicated that these antibodies were reactive to native fZP in ovarian follicles [51]. Further, conception rates in mated females were 25% and 20% in the ZPA and ZPB+C vaccinated groups respectively, compared with 83% in the control group [51]. However, sample sizes were small [51]. With such promising results, one is left to speculate the reason for no follow-up studies attempting to improve the efficacy of these DNA-based immunocontraceptive vaccines design for the domestic cat.

1.2.4.4   Gonadotropin-releasing Hormone-based Agents

1.2.4.4.1 Gonadotropin-releasing Hormone (GnRH) Agonists

Within the past decade, GnRH analogues have been developed to suppress fertility. GnRH agonists mimic endogenous GnRH but have a longer half-life in the blood. Sustained exposure to GnRH reduces GnRH-stimulated gonadotropin secretion through GnRH receptor down-regulation, internalization and signal uncoupling.

Deslorelin (brand name: Suprelorin) is an implant available in 6-month (4.7mg) or 12-month (9.4mg) forms. Developed in Australia and New Zealand for use in male dogs, deslorelin has been used off-label to suppress fertility in cats. Goericke-Pesch *et al.* launched a pilot study investigating the efficacy of a 4.7mg deslorelin implant on fertility suppression in male cats [52]. Within the first two days of treatment, serum testosterone concentrations increased. However, toms implanted with the 4.7mg dose had significantly decreased serum testosterone levels within 28 days of implantation. As early as twenty days post implantation, testosterone values were under the limit of detection of the radioimmunoassays in some of the male cats, an indication of suppressed fertility. Thirty-six weeks post implantation, absolute testicular size decreased by 73%. Approximately nine weeks after treatment, penile spines were absent, a characteristic of surgically castrated male cats. In addition, unwanted behaviors such as libido, mating, and urine marking were significantly abated in treated males eleven to sixteen weeks post implantation. Unfortunately, infertility of the treated toms is temporary and has an onset at approximately six weeks after implantation. Another flaw in the deslorelin product is its duration of efficacy ranging from 6 to 24

months in male cats. In queens, deslorelin has been established to suppress ovarian activity but is known to have variability in duration of suppression. In a blind study with mature cats (N = 20), Munson *et al.* subcutaneously administered a 6 mg deslorelin implant to ten cats and a placebo implant was administered to ten cats [53]. The typical "spike" in fecal estradiol levels were observed, followed by significant decrease for an extended period. Reestablishment of estrus varied from 7.5 to 14 months. Goericke-Pesch *et al.* reported that queens implanted during seasonal anestrus results in induction of estrus that was defined as increased estradiol levels [52]. Decreased estradiol levels start to occur two to four weeks after implantation of queens, followed by phases of sexual inactivity, an indication that the treatment is still effective. Also, injection of treated queens with a second 4.7mg implant during estrous suppression did not affect the duration of efficacy. In a study conducted by Toydemir and Kilicarslan, 21 queens were implanted with deslorelin. In addition to the deslorelin treatment, seven of these implanted females were administered MGA tablets 14.5 days before and 14 days after the deslorelin implants [54]. Over the course of the 18.5-month study, fecal estradiol concentrations were significantly decreased in all implanted females in comparison to the untreated group. In addition, there were more primordial and primary follicles and fewer corpora lutea in the implanted cats than the control subjects. However, there were no consistently significant differences in estradiol levels or follicle number between the MGA-administered and sham groups. Overall, studies on deslorelin continue to be conducted in hopes of improving the product's duration of efficacy.

Another GnRH agonist studied in cats is azagly-nafarelin. In the form of a commercialized implant (Gonazon), 20 mg azagly-nafarelin was administered subcutaneously in the necks of six queens [55]. After monitoring the ovarian activity of treated queens and six control queens for three years, all treated queens continuously displayed low progesterone concentrations until 2.5 years post implant insertion [55]. At this time point, two treated cats each experienced an isolated episode of follicular luteinization, but soon after all treated queens became anovulatory [55]. This research indicated that Gonazon efficiently prevented ovulation in queens for 3 years and was well tolerated. Interestingly, despite low azagly-nafarelin concentrations in some queens, return to estrus was not observed at the end of treatment [55].

1.2.4.4.2 GnRH Vaccines

Approximately 40 years ago, it was hypothesized that if an animal could be treated in such a way as to stimulate an immune response to GnRH, the GnRH antibodies would interfere with the action of GnRH and this could result in infertility. But since GnRH is a small decapeptide that is normally present in all mammals, it is not recognized as "foreign" by the immune system. Therefore, GnRH vaccines were developed to suppress production of the hypothalamic hormone.

Gonacon, manufactured by the U.S. Department of Agriculture (USDA), consists of GnRH coupled to carrier protein Keyhole limpet hemocyanin. Although initially developed for use in wild deer, Gonacon is frequently tested in research studies. In 2004, nine males cats (nine to twelve months old) were immunized only once with

Gonacon, and six out of nine male cats were considered immunocastrated 6 months after treatment (i.e, undetectable testosterone levels, high GnRH antibody titers, low to no sperm count) but the other 3 cats were considered nonresponders to the treatment (i.e, low GnRH antibody titres). In 2011, fifteen female cats (eight to fourteen months old) were injected with Gonacon and these vaccinated cats had a longer time to conception (median time: 39.7 months) compared to control cats (median time: 4.4 months). However, by the end of the five-year study, only four of the fifteen treated cats remained infertile. Although these and other studies using GnRH vaccines demonstrate difficulty in successful permanent sterilization of all subjects, this approach of targeting gamete production does show promise.

Baker and his research group reported on the effectiveness of a leukotoxin-GnRH antigen administered with the molecular immunostimulatory adjuvant CpG oligonucleotide [56]. One study involved immunizing cats via primary vaccination and a booster 4.5 months afterward [56]. In all treated adult female cats (N=6), contraception was maintained throughout the 38-week study period and no estrous behavior was recorded [56]. Ovariohysterectomy performed on treated and untreated cats showed that ovaries and uteri of treated cats were dramatically smaller than those of untreated animals [56]. In a separate study, five female, three-month-old kittens were given the vaccine with CpG, one received the vaccine with no CpG, and two kittens received control vaccines [56]. Abnormal reproductive cycling was observed in four kittens in the vaccine + CpG group and in the kitten receiving vaccine alone [56]. After administration of the booster, the fifth kitten in the vaccine plus CpG group achieved contraception

[56]. The GnRH antibody response remained high for six weeks and then plateaued until conclusion of the study [56]. Ovariohysterectomy of all cats showed that ovaries and uteri were dramatically smaller, similar to their adult counterparts [56]. In a final study, five male three-month old kittens were given the vaccine with CpG; four received the vaccine with no CpG; and four kittens were controls [56]. At the end of the study, serum testosterone was undetectable in all five vaccine/CpG-immunized [56]. Further, the vaccinated kittens did not develop secondary sex characteristics and displayed diminished aggressive male behavior typical of toms [56]. Surgical castration revealed atrophic testicles in all treated cats [56].

In 2004, Robbins *et al.* generated a vaccine designated IPS-21, a recombinant fusion protein consisting of tandem repeats of GnRH fused to leukotoxin [57]. Vaccines were further engineered by combining IPS-21 with the immunostimulant dimethyl dioctadecyl ammonium bromide and then tested in ten female cats and four male cats [57]. No estrous behavior or pregnancy was observed in any females [57]. Three of the four vaccinated males had decreased serum testosterone levels following the second immunization [57]. However, all subjects experienced injection site reactions that fortunately resolved within 28 days post-vaccination in the majority of animals [57].

The large number of tested contraceptive agents that have failed to induce permanent contraception in both male and female cats demonstrates the complexity in the feline reproductive system. Although many of the tested products have resulted in impairment to serum sex hormone levels, gonadal atrophy and dysfunction, all of them

20

are characterized by at least one of the following undesired effects for feral cat populations: inconsistent responses in individual animals; injection site reactions; reversibility of contraceptive effects; booster requirements; slow onset of activity; and ineffectiveness for both sexes. Thus, the re-evaluation of the entire hypothalamic-pituitary-gonadal axis coupled with novel adjuvants is needed to identify new targets for achieving permanent contraception in cats.

1.3 Gonadotropin-releasing Hormone (GnRH)

1.3.1 GnRH Structure

Gonadotropin-releasing hormone (GnRH) is a decapeptide produced by vertebrates. There are three types of GnRH that have distinct locations and functions in the brain. GnRH-1 is found in the preoptic area (POA) and anterior nuclei of the hypothalamus and is responsible for gonadotropin release from the anterior pituitary gland (i.e.,hypophysiotropic functions). GnRH-2 was first identified in chickens and is synthesized in a second population of GnRH neurons that are predominantly located in the midbrain and non-reproductive regions of the hypothalamus. GnRH-3, also known as salmon GnRH (after the species in which it was discovered) is found primarily in the terminal nerve and olfactory regions. GnRH-1 will be the main focus of this dissertation, where the generic term "GnRH" will refer to the hypophysiotropic GnRH-1 molecules.

GnRH is processed in hypothalamic neurons from a 92-amino acid, precursor polypeptide, prepro-GnRH, that undergoes several intracellular modifications before giving rise to the mature form of the GnRH peptide (Fig. 1.1). Prepro-GnRH has an N-

terminal signal sequence that is removed to generate pro-GnRH [58]. The decapeptide

GnRH sequence is near the N-terminus while the C-terminal region contains the GnRH-

associated peptide (GAP). These fragments are separated by a cleavage site that

allows for further processing to generate the mature forms of the GnRH and GAP

peptides [58]. The function of GAP is not clear but it has been shown to regulate

prolactin, LH, and FSH secretion [59]. Mature GnRH is packaged in storage granules

that are transported down axons to the external zone of the median eminence [60].

With the exception of the guinea pig, all mammals have the identical GnRH

decapeptide sequence (pGlu-His-Trp-Ser-Tyr-Gly-Leu-Arg-Pro-Gly-NH_2). Such

structural conservation of GnRH across mammalian species supports its fundamental

importance to reproductive function. Specifically, the amino terminus (Pro-Gly NH_2) and

carboxyl terminus (pGlu-His-Trp-Ser) are conserved, indicating that these amino acids

are critical for binding and activation of GnRH pituitary receptor. Although both termini

are involved in receptor binding, the NH_2 terminus is solely responsible for receptor

activation. GnRH forms a folded conformation when bound to its pituitary receptor. In

this configuration, GnRH bends around the flexible glycine in position six of the

decapeptide. Substitution of Gly^6 with d-amino acids stabilizes the folded conformation

and increases binding affinity of GnRH to the pituitary receptor. Arginine is required in

position eight of GnRH for the hormone to bind to its receptor, indicating an essential

role for the residue in ligand-selectivity for various GnRH receptors [61,62]. However,

substitution of Arg^8 with Gln^8 yields a predominant extended structure (rather than the

folded confirmation) and a low biological activity in mammalian GnRH [63]. Interestingly,

22

these extended GnRH conformers have high activity with many non-mammalian GnRH receptors [61,64-66]. The deleterious effects of Arg^8 substitution is overcome with a change of Gly^6 for a d-amino acid, resulting in a 1000-fold increase in the binding affinity for the mammalian receptor [65,67].

1.3.2 Hypothalamic-pituitary-gonadal Axis

The classical hypothalamic-pituitary-gonadal axis is a tiered and linearly organized set of endocrine tissues that mainly function to regulate and support reproductive activity (Fig. 1.2). This axis consists of a small population of GnRH-expressing hypothalamic neurons, anterior pituitary gonadotropic cells, and the gonads.

Surprisingly, only a small population of approximately 1000-2000 POA and anterior hypothalamic nuclei are responsible for GnRH synthesis in mammals. Generally, these perikarya project neuronal processes to the median eminence where GnRH is released into a portal capillary network known as the hypothalamo-hypophyseal portal system. The terminal boutons of the hypothalamic nuclei extend to the pituitary stalk (i.e., infundibulum) and terminate upon blood vessels of the primary portal plexus. The primary portal plexus is formed by the superior hypophyseal artery that supplies blood to this portal system. The hypophyseal portal vein transports blood containing releasing hormones (i.e., GnRH) from the primary portal plexus to the secondary plexus that delivers blood to the anterior pituitary (i.e., adenohypophysis). This is not the case for fish in which the GnRH neuroterminals are projected directly onto the anterior pituitary. In either case, GnRH is released in a pulsatile manner that is

highly conserved in vertebrates and required for maintenance of normal reproductive function. Each pulse of GnRH is released into the hypophyseal portal circulation. Once out of this circulation, GnRH binds to the GnRHR on the surface of anterior pituitary gonadotropes and stimulates secretion of luteinizing hormone (LH) and follicle-stimulating hormone (FSH). These gonadotropins are dimeric glycoprotein hormones comprised of distinct hormone-specific β subunits coupled with a common α subunit (αGSU) [68]. The β subunits of FSH and LH, along with the αGSU and GnRHR, are essential features of gonadotropes [68]. These gonadotropins are released into general circulation and promote steroidogenesis, gametogenesis, and reproductive tissue development. In the male, LH stimulates production of testosterone and androgen-binding protein by testicular Leydig cells and Sertoli cells, respectively. FSH binds to its receptor on the membranes of Sertoli cells that function concurrently with testosterone to promote the spermatogonia proliferation, along with the meiosis and post-meiotic development of germ cells. During the late stages of follicular growth in the female, LH drives the production of progesterone from the granulosa cells of the preovulatory follicle. Most importantly, a surge of LH causes ovulation and subsequent development and maintenance of the corpus luteum. FSH promotes follicular development and estradiol secretion from granulosa cells.

1.4 Gonadotropin-releasing Hormone Receptor (GnRHR)

The primary structure of mammalian GnRHR was first deduced by sequencing of cDNA isolated from the αT3-1 immortalized murine gonadotrophic cell line [69]. Analysis of the amino acid sequence of the cloned GnRHR revealed seven transmembrane

domains that are characteristic of the G protein-coupled receptor (GPCR) family (Fig,

1.3). Soon after elucidating the mouse receptor cDNA sequence, GnRHR cDNAs were

identified for additional mammalian species including the human [70,71], rat [72-74],

sheep [75,76], pig [77] and cow [70]. GnRHRs in the cow, pig, sheep, and human are

328 amino acids long, while the mouse and rat receptors contain only 327 amino acids,

due to an absent residue in the second extracellular domain. Typical of GPCRs, the

amino terminus of GnRHR is extracellular and is involved in ligand recognition and

binding. The intracellular carboxyl terminus contributes to effector binding and signal

transduction. Interestingly, mammalian GnRHR is the only GPCR that possesses a

clipped C-terminal cytoplasmic tail and has a short intracellular third loop [78]. The

carboxyl-terminal domain and the third loop of many other GPCRs are known to be

critical for receptor internalization and desensitization, and these processes require

phosphorylation of serine/threonine residues in these sites [79]. Like other GPCRs, the

functional protein structure of GnRHR is stabilized by a disulfide bridge. Important in

GnRHR function, these disulfide bonds are formed by conserved cysteines in the first

and second extracellular loops, specifically C114 and C196 of the mouse GnRH

receptor [80]. Studies show that disruption of these disulfide bonds significantly reduces

receptor binding affinity to GnRH [81]. Glycosylation sites are also critical features of

GnRHR. The murine, ovine, and human receptors include potential N-linked

glycosylation sites Asn^{18} and Asn^{102} but the rodent receptor contains an additional

glycosylation site on Asn^4 [82]. Mutations in the N-linked glycosylation sites significantly

decreased receptor numbers, indicating that these glycosylation sites play a critical role

in GnRHR stability [83].

1.4.1 Properties of GnRH Binding to GnRHR

Similar to other GPCRs that bind peptides (158) [84], amino acid residues in the extracellular and exofacial regions of the transmembrane domains of GnRHRs are suggested to participate in ligand-receptor interactions. Specifically, three residues have been identified and extensively studied: Asp at position 98 [Asp$^{(98)}$], Asn$^{(102)}$, and Asp$^{(302)}$. Studies show that mutation of Asp$^{(98)}$ to Asn significantly abated inositol phosphate production that was inconsistent with an interaction with Arg8 of GnRH [67], thus indicating the important role of Asp$^{(98)}$ in GnRHR signal transduction. Studies of GnRH receptor glycosylation showed that the Asn$^{(102)}$ residue is not glycosylated, but increased GnRH affinity to the Asn$^{(102)}$Gln mutant, suggesting involvement in ligand binding [83]. Mutation of human GnRH receptor Asp$^{(302)}$ to Asn showed that the Asp$^{(302)}$ residue contributes to hGnRHR selectivity for Arg8 of GnRH [85].

The existence of three GnRH forms in most vertebrates implied that additional receptors for GnRH may be expressed in tissues and organisms. Thus, two novel GnRH receptors have been identified [86]: GnRHR type I, the known mammalian pituitary receptor, and GnRHR type II that is expressed in many vertebrates including primates [87]. These forms of GnRHR primarily differ in the amino acid sequence of the third extracellular loop, which plays a role in distinguishing between the different structural variants of GnRH. Recently, three distinct types of GnRHR were characterized in bullfrog [88] where each receptor was shown to exhibit a differential ligand specificity and was proven to be a functional receptor as determined by its ability

to stimulate inositol phosphate production in transfected COS-7 cells. The chicken GnRHR exhibited differences in its primary structure and ligand selectivity as compared with mammalian GnRHR. It has been postulated that an ancestral GnRHR gave rise to putative GnRHR subtypes through gene duplication processes early in vertebrate evolution [89]. Thus, it is possible that cognate receptors have evolved together with the ligands to mediate differential effects in distinct species.

1.4.2   GnRHR Signaling

In pituitary gonadotropes, GnRH binding to GnRHR causes receptor conformational changes and subsequent GTP loading onto heterotrimeric G-protein subunit $G\alpha_q/11$. This leads to activation of phospholipase (PL)Cb that dissociates into second messengers, phophatidylinositol-triphosphate (IP_3) and diacylglycerol (DAG). IP_3 production generates intracellular calcium store release that causes a surge in intracellular calcium concentrations. DAG activates protein kinase C (PKC) isoforms that drives a sustained rise in intracellular calcium concentration derived from influx of extracellular calcium through L-type voltage gated channels [90]. These events lead to mitogen-activated protein kinase (MAPK) activity [91]. The pathways are highly conserved, signal transduction cascades that modulate cellular responses to a wide range of environmental stimuli. The fundamental organization of these pathways includes a multi-level phosphotransfer system. Activation of the MAPK pathway begins with phosphorylation of a primary MAP kinase-kinase kinase (MAPKKK), which phosphorylates and activates an intermediate level MAP kinase (MAPKK), which activates the final MAP kinase (MAPK). In addition to these essential kinases, various

scaffolding and adaptor proteins contribute to the functional organization of this pathway [92].

In mammals, there are four predominant MAPK pathways: the extracellular signal-regulated kinase (ERK), jun-N-terminal kinase (JNK), p38, and ERK5/BigMAPkinase (ERK/BMK). In the gonadotrope, GnRH stimulation leads to activation of the ERK, JNK, and p38 pathways [93-96]. Activation of these pathways has been linked to transcriptional regulation of the gonadotropin genes. The ERK pathway is most commonly implicated in the GnRH signal transduction cascade in the gonadotrope [97-99]. This is based on studies demonstrating that inhibition of ERK signaling in perifused LβT-2 primary pituitary cell cultures completely interferes with GnRH-induced FSHβ and LHβ transcription [97]. The dependence of LHβ transcription on the ERK pathway is consistent with other reports demonstrating the requirement of Egr1, an ERK-dependent transcription factor, for LHβ expression [100-103] .Contrastingly, the role of ERK signaling in modulating upregulation of FSHβ transcription by GnRH is less clear and conflicts with studies indicating intact FSHβ expression in mice with ERK-deficient gonadotropes [104].

PKC activity is required for activation of ERK pathway by GnRH in αT3-1 cells [94,105]. However the mechanism outlining this prerequisite is unclear. The leading theory involves Raf-1 kinase as the key activator of the ERK signaling module in gonadotropes. Many suggest that direct activation of Raf-1 by membrane-bound PKC is the mechanism by which GnRH-induced signaling at the plasma membrane is linked to

the ERK pathway that culminates in the nucleus [103,106]. Because membrane recruitment is an important step in the complicated events that lead to Raf-1 activation, activation of Raf-1 by PKC is an appealing concept. However, experiments with αT3-1 cells or LβT-2 cell lines do not conclusively demonstrate a role of Raf-1 in GnRH-induced ERK activation, let alone its direct influence on PKC. Thus, the mechanism of this portion of the GnRH signaling module, especially the networking between signaling events at the plasma membrane and the ERK pathway remains unknown.

1.4.3 GnRHR Trafficking

Similar to other plasma membrane-bound, GPCR proteins, GnRHR is synthesized by ribosomes attached at the cytosolic face of the endoplasmic reticulum (ER). Signal sequences encoded in the hydrophobic domains target GnRHR to the translocon that co-translationally transports the receptor protein into the ER lumen. Post-translational modifications such as N-linked glycosylation by glycosyl transferases, association with chaperone proteins, and folding transpire in this compartment and are required for export [107,108]. Studies indicate that the exit of GPCRs from the ER may be directed via specific motifs embedded within the receptors [109-111]. Membrane insertion of transmembrane domains of GnRHR is driven by the translocon and orientation signals contained in the polypeptide itself [108]. With the assistance of coat protein (COP)I-coated vesicles, GPCRs are trafficked through the ER and Golgi intermediate compartment, and Golgi apparatus [107,108]. COPII-coated vesicles assist the processes associated with conformation maturation and correct targeting to the cell membrane [107,108]. Vesicle fusion to the plasma membrane requires the soluble N-

ethylmaleimide-sensitive factor attachment protein receptor (SNARE) complex.

Specifically, SNAREs on the vesicle are recognized by SNAREs on the plasma

membrane [112]. After vesicle fusion with the membrane, cargo is finally inserted into

the plasma membrane. Further, these vesicles act as a tightly-regulated quality control

system for protein misfolding and accumulation [113,114]. In addition, the quality control

system guides correct association with chaperone proteins that regulate folding or

transport through the ER/Golgi [115]. This quality control system includes ER-located

chaperones, such as calnexin, calreticulin and protein disulfide-isomerase that detect

membrane insertion and disulfide bond formation [113]. If GnRHR is misfolded, the

defective protein is then targeted for degradation via the proteasome pathway.

Activation of most seven trans-membrane receptors by their respective ligands

results in change of the receptor's conformation that activates protein kinases.

Phosphorylation by these kinases commonly takes place at the receptor's carboxy-

terminal tail (C-tail). This facilitates binding to β-arrestins, mediators of receptor

desensitization and internalization, as well as signaling to arrestin-scaffolded effectors

[116]. Agonist-induced phosphorylation, arrestin-receptor binding, and arrestin-mediated

desensitization and internalization have all been verified with non-mammalian GnRHR

that have C-tails with many potential phosphorylation sites. However, mammalian

GnRHR lacks a carboxyl-terminal intracellular domain, implying that GnRHR may be

resistant to rapid desensitization and internalization, features that have been confirmed

by studies investigating the receptor. Indeed, several studies have indicated rapid

desensitization and internalization of chimeric receptors in which the C-tail of other

GPCRs was integrated onto the C-terminus of GnRHR. Moreover, the lack of a functionally relevant C-tail translates to the absence of a direct receptor desensitization mechanism [117]. This is an interesting phenomenon because experiments show that sustained stimulation of GnRHR by GnRH results in desensitization of GnRH-stimulated gonadotropin secretion [118]. However, this process occurs at a slower rate than other GPCRs [118]. Thus, researchers have explored mechanisms regulating desensitization of GnRH-stimulated gonadotropin secretion in the absence of a direct receptor desensitization pathway. For example, experiments revealed that continuous GnRH treatment caused marked down-regulation of inositol 1,4,5 trisphosphate (IP_3) receptors, thus preventing GnRH effects on the cytoplasmic calcium concentrations [118]. Additional mechanisms that are responsible for desensitization of GnRH influence on calcium gradients and ultimately gonadotropin secretion include GnRH-mediated inactivation of calcium channels and agonist-induced GnRHR internalization [119]. GnRHR mutations are commonly associated with impairment of intracellular IP_3 accumulation that can be rescued by molecular chaperones. Thus, misfolding and abnormal intracellular trafficking of newly synthesized receptor proteins play a role in the ultimate failure of mutated GnRH receptor expression [120]. Naturally occurring mutations inactivate LHβ and FSHβ genes and their receptors. Reports indicate that such mutations are commonly associated with hypogonadal phenotypes that are exceptionally rare given their adverse effects on reproductive function [121-123].

Once internalized, GnRHR goes through specific trafficking routes that further defines the signaling response. GnRHR can be rapidly targeted to the lysosome for

degradation, causing complete termination of receptor signaling activity [124]. The receptor can also be quickly recycled back to the plasma membrane, re-sensitizing and recovering hormone signaling [124]. Finally, GnRHR can be retained in endosomes, traversing the degrading or recycling pathways at a slow rate. Receptor endocytosis-recycling pathway is mediated by clathrin-coated pits [125]. This process proceeds through stages including initiation, cargo selection, pit formation, excision, and uncoating. Once GnRHR has been identified as the "cargo", adaptor protein (AP)-2 and AP-180 complexes bind to it, followed by clathrin recruitment to the AP-coated cargo [112]. After extensive clathrin polymerization, the clathrin-coated pit is formed and cytoplasmic accessory proteins are also recruited to the vesicle budding sites. Dynamin, a GTPase, is recruited and excises the nascent vesicle from the plasma membrane [112]. Finally, GnRHR is endocytosed and taken to an endosome to be either sent back to the cell surface or targeted for lysosomal degradation. Interestingly, GnRHR internalization is species-specific. For example, the rat GnRHR, which has no C-tail, internalizes in an arrestin-independent, clathrin- and dynamin-dependent manner [126]. Human GnRHR, which also lacks a C-tail, was also reported to internalize in a dynamin-independent manner [126]. However, the Xenopus GnRHR, having a C-tail, internalizes via both clathrin-dependent and dynamin-dependent pathways [126].

In essence, GnRHR trafficking is a complex event requiring numerous "checks and balances" to ensure a properly folded (and functional) receptor is inserted into the plasma membrane. In addition, the endocytosis-recycling pathway involves mechanisms unique to GnRHR and no other G-protein coupled receptor. Internalization

and recycling of GnRHR is fundamental to the regulation of plasma membrane and intracellular activities of the receptor. Such properties of GnRHR is essential to maintaining a homeostatic environment within eukaryotic cells.

1.5 DNA-based Vaccines

Genetic immunization is an emerging vaccine approach that integrates many advantageous characteristics of standard vaccine strategy. While conventional vaccines (e.g., live-attenuated or killed) have demonstrated their efficacy in the eradication of some diseases, current safety requirements and remaining resilient infectious agents require vaccine techniques of great complexity that will overcome the inadequacies of modern vaccine technology. Indeed, strong humoral immune responses induced by some traditional vaccines do not solely provide defense against many current agents and diseases such as malaria and human immunodeficiency virus (HIV), for which the elicitation of a strong cellular immune response is likely to be necessary. Satisfying this demand is currently under extensive research by many desiring DNA vaccine technology.

The strategy of most DNA vaccine-related investigations is straightforward. First, one starts with a DNA vector that is commonly bacterial-derived and encoded with sequences for eukaryotic or viral promoter/enhancer transcription elements that guides highly efficient transcription of the plasmid-encoded antigen within the host cell nucleus. A DNA plasmid encoding a protein of interest is injected (intramuscularly or intradermally) into an animal, where it enters host cells and instructs the synthesis of its

antigen target. Once the plasmid-antigen is processed and presented on the cell surface of transfected host cells, the expected outcome is cellular and humoral immune responses against the antigen (Fig. 1.4).

DNA immunization exhibits many advantageous features that trump traditional protein-based vaccines. While protein vaccines elicit humoral responses, DNA vaccines induce both humoral and cellular-mediated immune responses at very low plasmid concentrations in animal models [127]. Also, in contrast to protein immunizations, the intracellular synthesis of the target protein from the plasmid DNA sequences is routinely characterized as properly folded polypeptides in their native conformation with normal post-translational modifications (e.g., glycosylation) that occur in natural infection, thus favoring the generation of biologically-relevant, neutralizing antibodies. In addition, because of the incapability to revert into virulence, DNA vaccines are conceptually safer than live vaccines [127]. Furthermore, toxic chemical inactivation methods are not necessary for the use of DNA-based immunizations. Plasmid constructs are able to accommodate nearly any gene or its derivatives, an easy manipulation enabled by techniques of modern molecular biology [127]. Importantly, these recombinant plasmids can be produced at both low-cost and at large scale in bacteria, and simply collected using plasmid DNA isolation kits and reagents [127]. DNA vaccines are also regarded to have longer shelf-life than conventional vaccines due to temperature stability that is characteristic of nucleic acids [127]. This feature is of great value, as it would positively impact the transport and shipping requirements from the financial and packaging efficiency perspectives.

Since their inception in the early 1950s, thousands of manuscripts have been published on the ability of DNA vaccines to induce strong immune responses against various proteins. However, few of the vaccines constructed and used in these experiments have been commercialized for veterinary use. In 2005, researchers at the Centers for Disease Control and Prevention, the USDA, and Fort Dodge Animal Health developed the world's first licensed, veterinary DNA vaccine called West Nile Innovator [22]. This vaccine protects horses from West Nile virus. There is also a DNA vaccine (*Apex-IHN*) against novirhabdovirus infectious necrosis virus that is responsible for losses to the salmon-related fish industry in the U.S. and Canada [22]. LifeTide-SW5 is a growth hormone releasing hormone DNA vaccine that increases piglets weaned and decreases perinatal morbidity [22]. Oncept, a therapeutic cancer vaccine for melanoma in dogs, is another commercially available DNA vaccine that was manufactured by Merial [22].

The plasmid's immunogenicity may be enhanced in part by the presence of repeated immuno-stimulatory motifs (e.g., CpGs) that are recognized as foreign by the immune system of the host. Granulocyte/macrophage colony-stimulating factor may also be used as an adjuvant for DNA vaccines because of its capability to enhance CD4+ T cell proliferation and antibody responses. Encapsulation of plasmids by polymeric nanoparticles is a novel approach to enhancing immunogenicity of a DNA vaccine delivery because of its efficient uptake by antigen-presenting cells, subsequently inducing both antigen-specific humoral and cellular immune responses.

The ubiquitin-proteasome system (UPS) can be exploited for enhancing the potency of DNA vaccines against self-antigens. The UPS is responsible for the generation of most antigenic peptides presented to circulating lymphocytes. Antigens synthesized within somatic cells are first poly-ubiquitinated and then degraded into their peptide components by the proteasome. These peptides are subsequently transported into the endoplasmic reticulum through the transporter associated with antigen processing protein and then loaded onto major histocompatibility complex (MHC) class I molecules. Once the antigen peptides are bound to an MHC I molecule, the peptide-MHC class I complexes are transported to the surface of the cell via the Golgi. Based on this, vaccination with DNA encoding the target protein fused to ubiquitin will theoretically direct proteins to be degraded by the UPS. This strategy may enhance the expression of epitopes from the synthesized protein via MHC I molecules and thus break host tolerance to the self-antigen and will efficiently activate target protein-specific cytotoxic T lymphocytes that will ultimately destroy the endogenous polypeptides or cells expressing them on the cell surface.

DNA vaccines are a novel technology that may significantly decrease future human and animal morbidities. Conceptually, they exhibit many of the desirable attributes of traditional protein vaccines as well as elicit strong humoral and cellular immune responses in animal models. A variety of adjuvants can enhance the immunogenicity of DNA vaccination. Clearly DNA immunization is an important contributor to the next generation of prophylactic and therapeutic vaccines that are efficient and economically feasible to individuals worldwide.

1.6 Superparamagnetic Iron Oxide Nanoparticles

Biotherapeutics such as therapeutic cells, protein/peptides, and nucleic acids can be made highly target-specific through modifications such as antibody-antigen interactions and antisense oligonucleotide-target mRNA hybridization [128]. Compared to conventional chemical drugs, this new class of drugs functions in a relatively well-defined manner and possess advantageous properties that may greatly improve therapeutic effects while reducing adverse effects. Accordingly, over the last few decades, these modified biotherapeutics have been widely studied for treating autoimmune diseases and cancers [129,130]. However, application of such technology is hindered by the lack of effective mechanisms to protect these biotherapeutics during transport to disease sites. This is mainly due to the inherent physical and chemical characteristics such as protein/peptide and nucleic acid degradability that make their delivery problematic [131,132]. For example, proteins are easily degradable by proteinases in serum, and noncovalent interactions results in protein aggregation. In serum, DNAs and RNAs are susceptible to nucleases and acidic microenvironment, thus abating their biological half-life [133]. Because biotherapeutics are hydrophilic and of relatively high molecular weights, their delivery to and accumulation at target sites, such as tumors, can be challenging. Furthermore, the inability of negatively-charged nucleotide-based drugs to permeate cellular membranes resulting in poor intracellular delivery is a major concern. One strategy to overcome the biological barriers is to encapsulate biotherapeutics in nano-material formulations. In the design of these formulations, it is important to minimize damage to biotherapeutics and prevent loss of

their biological activities by physical stress [134,135]. Another approach is to construct vectors specially designed for the types of biotherapeutics with varying delivery requirements. A wide variety of nano-carriers mobilized with ligands or moieties that are responsive to external stimuli such as ultrasounds, lights, and magnetic fields have been developed for targeted delivery [136,137]. Among these delivery systems, superparamagnetic iron oxide nanoparticles (SPIONs) have drawn considerable attention because of their unique features such as biocompatibility, superparamagnetism that is useful for magnetic resonance imaging (MRI)-based monitoring for treatment response, and magnetofection that enables magnet-driven drug delivery and release [138-143].

SPIONs containing iron oxide cores (usually magnetite, Fe_3O_4, or maghemite, γ-Fe_2O_3) possess superparamagnetism that allow the particles to target a specific area only through external magnets [144]. With such properties, biotherapeutics coated on or mixed with SPIONs can be physically guided to localize and accumulate in specific tissues, thus enhancing target specificity and therapeutic efficacy [145]. However, once the external magnetic field is removed, the particles will cease to show magnetic interaction [144]. *In vitro* studies demonstrated that a majority of magnetic nanoparticles can be taken up by cancer cells within fifteen minutes in the presence of a magnetic field [146]. Thus, accompanying biotherapeutics with a delivery system that can significantly abate lengths of transport time for genes and proteins into cells is desirable. Magnetic fields are safe and are extensively used in clinics. In one study, application of a static, ten tesla magnetic field had no effect on cell growth and cell cycles for four

days in mammalian Chinese hamster ovary (CHO)K1 cells [147]. However, no studies

have been conducted with magnets greater than ten tesla. Due to loose vasculature in

tumors, a phenomenon known as an enhanced permeation and retention (EPR), less

than 5% of administered nanoparticles can reach tumor sites [148]. In the presence of a

magnetic field, one group significantly augmented accumulation of SPIONs for targeted

delivery of interferon γ in a mouse tumor model [149]. In fact, magnetic particles under

the influence of the external magnetic field were retained in tumors six- to ten-fold more

than those without magnetic field assistance [149]. In addition to having bio-applicable,

magnetic capabilities, it is critical for SPIONs to be stable and maintain their size,

homogeneity, and magnetic property during the course of treatment for successful

delivery of biotherapeutics [150]. To accomplish this, various SPION-based carriers

have been generated and investigated, including SPION micelles, SPION clusters,

SPION-encapsulated hydrogels, SPION liposomes, and surface-modified SPIONs.

Within the past decade, surface modifications to SPIONs have been widely

employed to accommodate numerous biomedical applications and a variety of

technologies including magnetic resonance imaging, magnetic hyperthermia, drug

delivery, and bio-separation [151,152]. Surface modifications help to maintain

physicochemical properties of SPIONs such as surface charge and hydrodynamic size.

This is important because SPION size and surface charge affect their affinity to target

cells *in vitro* and *in vivo* [140,153-155]. In particular, the particle size determines its fate

when confronted with biological barriers such as kidney filtration, phagocytosis, and

extravasation from tumor vasculature [156]. Chemical destabilization of SPIONs can

occur via oxidation in air and consequently lose their magnetic properties [157]. This can be prevented by the application of a surface coating. For example, SPIONs may be coated with a biocompatible polymer (e.g., starch) that can protect the particles from the surrounding environment. In addition, because of their large surface area-to-volume ratio, SPIONs can easily aggregate when suspended in salt- and serum protein-based solutions [158,159]. To overcome such a biological disadvantage as a drug delivery system, SPION surfaces may be modified with lipids, moieties, or polymers. For example, application of a hydrophilic layer coating the nanoparticle may conceal the nanoparticles' hydrophobic surfaces, thus producing stable SPIONs. Hydrophilic polymers such as poly(ethylene glycol) (PEG), dextran, chitosan, and poly(vinyl alcohol) can be immobilized onto SPIONs to achieve steric stabilization of SPIONs [150,160-164]. However, excessive steric hindrance of surface-modified SPIONs can also block interaction with target cells or tissues, resulting in poor intracellular uptake. Immobilizing cationic polymers such as PEG can prevent this undesirable property. Internalization of PEG-coated magnetic nanoparticles by cells occurs through amphiphilic affinity to plasma membrane lipid bilayers via fluid-phase endocytosis [165]. In one study, PEG modification facilitated nanoparticle internalization into BT20 breast cancer cells [166]. The possible mechanism for this uptake is that PEG dissolves in both polar and non-polar solvents and thus can take on a higher solubility in cell membranes [167]. Complexation of nanoparticles to DNA is even more beneficial from the perspective of potential applications in DNA isolation and directed assembly of nanostructures [168-170]. Thus, the choice of coating material for SPIONs is critical for successful *in vivo* delivery of biotherapeutics.

Surface coatings also serve to provide functional groups for further conjugation of ligands and therapeutics such as plasmid DNA. Because plasmid DNA should be delivered to the nucleus for gene expression, SPIONs must be constructed to mediate nuclear localization of plasmid DNA. When the surface is modified with positively-charged ligands, magnetic nanoparticles can adsorb negatively-charged nucleic acids through electrostatic interactions. Thus, modification of magnetic nanoparticles with cationic materials is necessary for DNA adsorption. Dendrimers, chitosan, lipids, poly(L-lysine), polyethylenimine (PEI), and PEG have all proven to be effective candidates for this purpose [171-173]. For example, PEI-coated SPIONs that were prepared using commercially available Chemicell nanoparticles showed successful DNA delivery into the cytoplasm via endocytosis by ten-minute magnetic exposure [174]. As a different formulation, PEI-PEG-chitosan copolymer was coated onto the surface of SPIONs for plasmid DNA delivery [175,176]. Also, using PEI-coated SPIONs, plasmid DNA expressing small hairpin RNA targeting type 1 insulin-like growth factor receptor (IGF-1R) was successfully delivered along with lipofectamines to suppress endogenous IGF-1R in tumor-bearing mice [177]. Furthermore, mice treated via magnetofection were observed to have two-fold higher gene suppression compared to those with lipofection [177]. In another study, PEI-coated SPIONs adsorbed with plasmid DNA was administered as microdroplets via a nebulizer for magnet-guided delivery to lungs in a mouse model [178]. Exposure of the right lung only to a magnetic field resulted in two-fold increase in DNA accumulation compared to the left lung that was not exposed to the magnetic field [178].

In essence, SPIONs based carrier systems are advantageous for biomedical application. They are biocompatible, biodegradable, easily manipulated, and superparamagnetic and thus can be targeted to specific areas by an external magnetic field. Surface modification to SPIONs aid in nanoparticle stability and conjugation to specific ligands or drugs. These attributes are attractive for efficient *in vivo* delivery of biotherapeutics such as plasmid DNA.
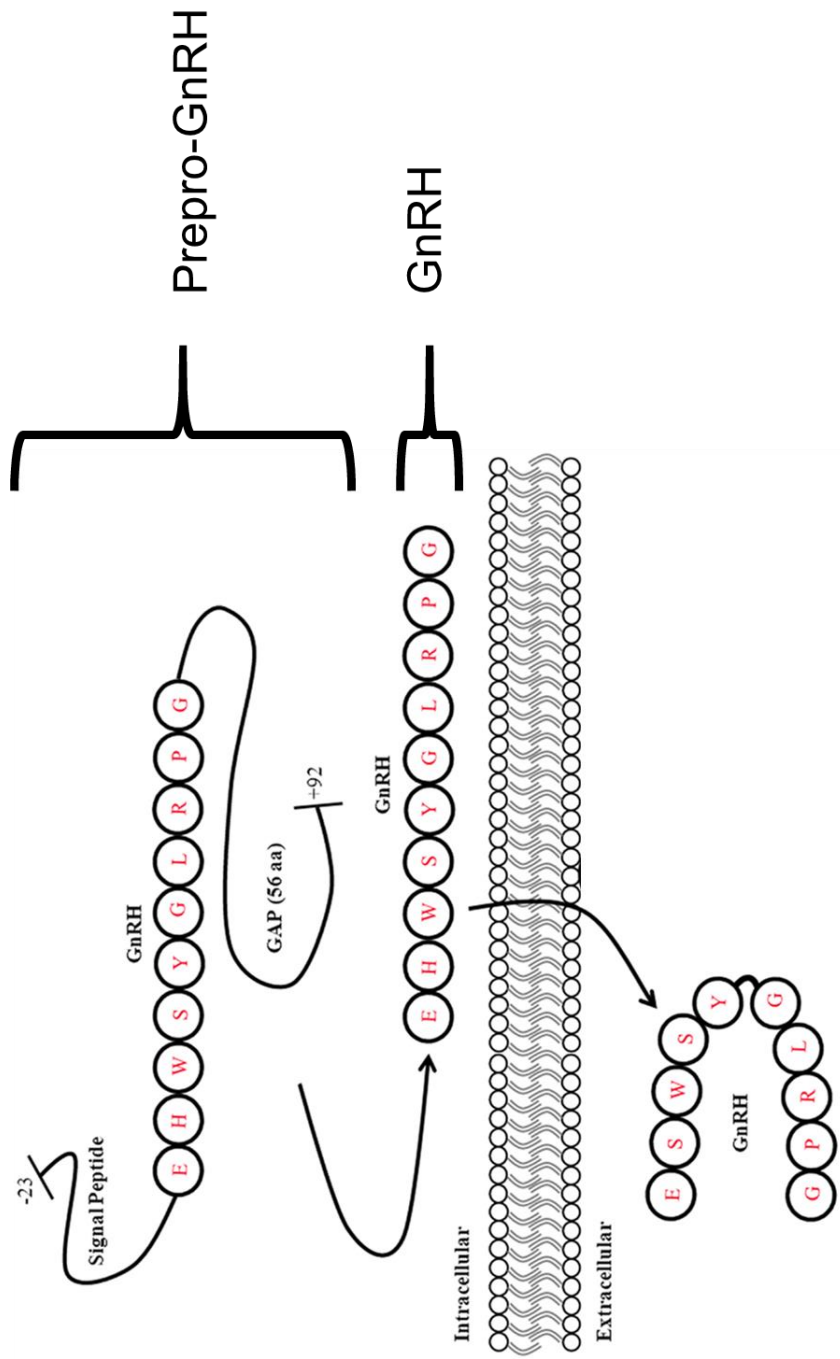
Figure 1.1: Gonadotropin-releasing Hormone Peptide Processing. The prepro-GnRH is processed intracellularly to generate the mature GnRH peptide. Mature GnRH is secreted and released into the hypothalamo-hypophyseal portal system. Modified from Roberts *et al.* 2007. Trends Endocrinol Metab. 18:386-92.
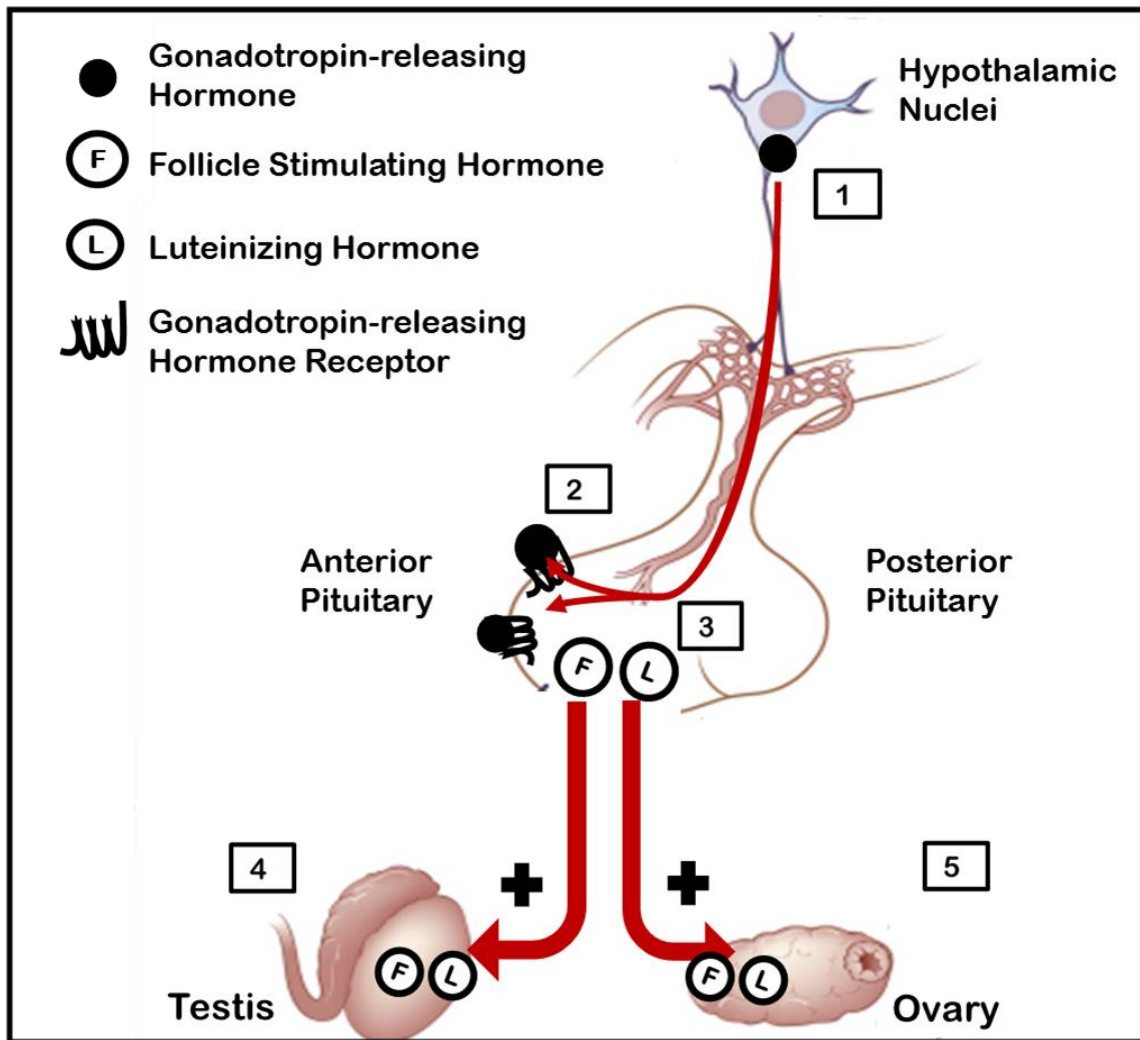
Figure 1.2: The hypothalamic-pituitary-gonadal axis. (1) The hypothalamus produces gonadotropin-releasing hormone receptor (GnRH) that travels through the hypophyseal portal system and is delivered to the anterior pituitary. (2) GnRH binds to the GnRH receptors (GnRHR) that are expressed on the surfaces of anterior pituitary gonadotropic cells. (3) Activation of GnRHR by GnRH stimulates gonadotropic production of luteinizing hormone (L) and follicle-stimulating hormone (F). L and F are released into general circulation and promote steroidogenesis, gametogenesis, and reproductive tissue development. (4) In the male, L mainly stimulates production of testosterone by testicular Leydig cells. F acts on Sertoli cells that mainly promote spermatogonia proliferation. (5) In the female, L is mainly responsible for progesterone production by preovulatory follicles and ovulation. F promotes follicular development and estradiol secretion from preovulatory follicles.
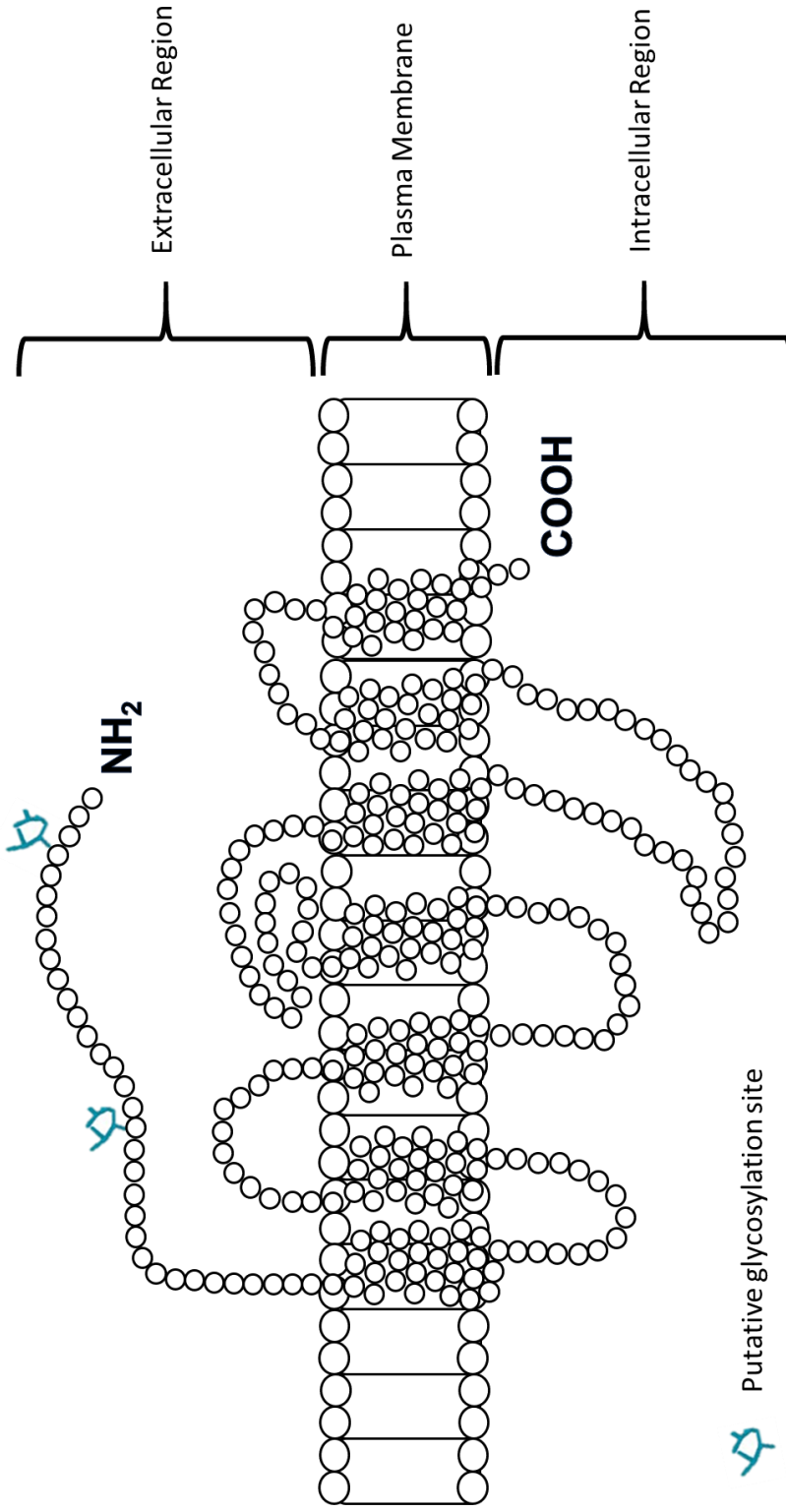
Figure 1.3: Structure of Gonadotropin-releasing Hormone Receptor. Modified from Ulloa-Aguirre *et al.* 2004. Hum. Reprod. Update. 10:177-192.
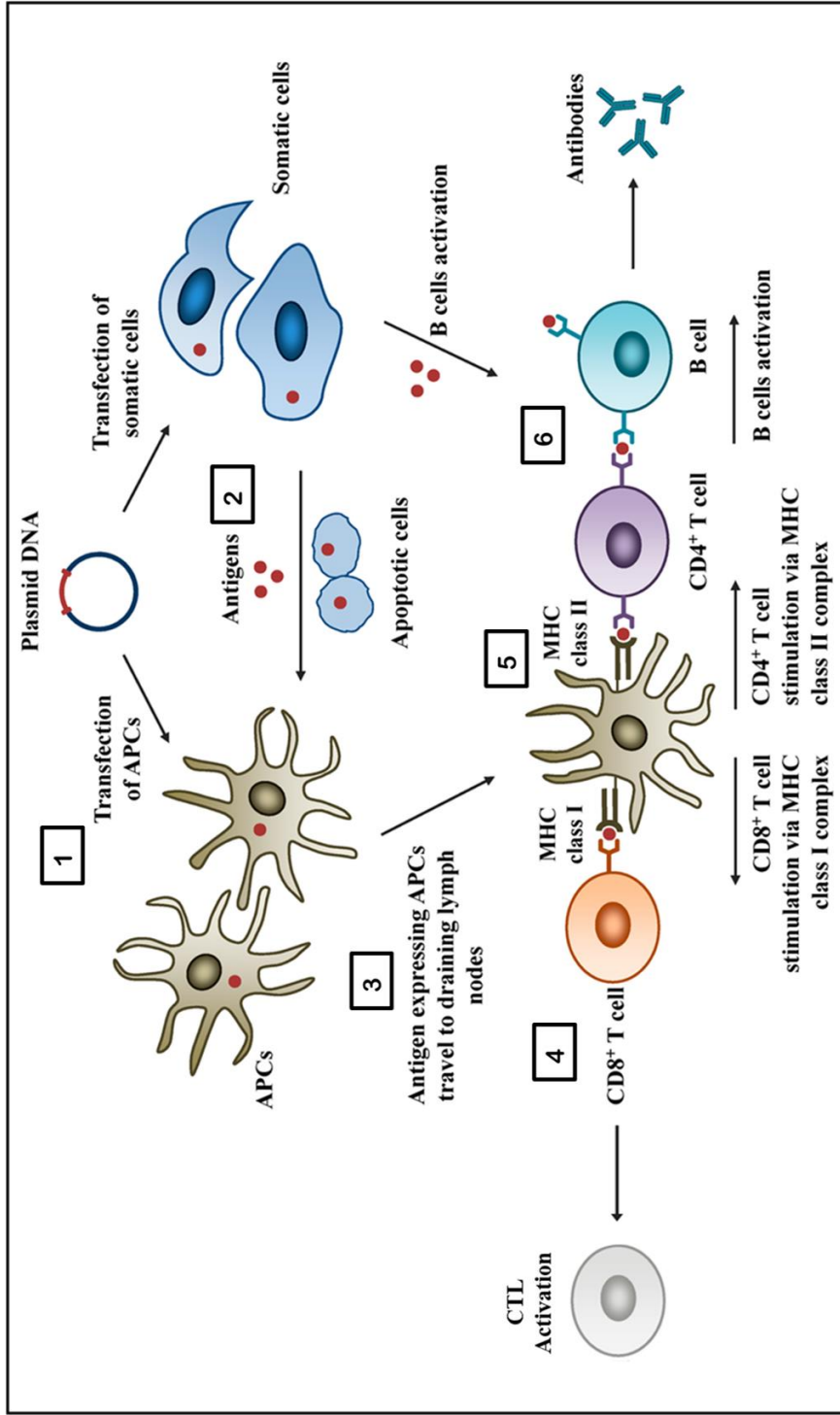
Figure 1.4: DNA vaccine mode of action. (1) Plasmid DNA encoding antigen of interest activate professional antigen presenting cells (APCs) via direct transfection or (2) cross-presentation (indirect transfer of antigens). (3) Professional APCs then migrate to the draining lymph nodes where they present antigenic peptides to naïve T cells via major histocompatibility complex (MHC) molecules. (4) Antigenic peptide presentation to CD8+ T cells via MHC-I results in activation of cytotoxic T lymphocyte (CTL) that kill cells expressing the antigen. (5) Antigenic peptide presentation to results in mature CD4+ T cells that activate B cells MHC-II Antigen presentation via MHC-II stimulates CD4+ T cells to become T helper cells that are involved in B cell activation and maturation. (6) Secreted antigens or T helper cells activate B cells, leading to production of antigen-specific antibodies. Modified from Xu *et al.* 2014. Pharmaceutics. 6:378-415.

CHAPTER 2

CONSTRUCTION AND *IN VITRO* CHARACTERIZATION OF
DNA-BASED CONTRACEPTIVE VACCINES DIRECTED AGAINST
GONADOTROPIN-RELEASING HORMONE RECEPTOR

2.1 Introduction

A contraceptive vaccine is needed to manage the global overpopulation of feral

cats that have negative impacts on human health and the environment. However, the

ideal target for development of a contraceptive product must meet several

requirements. First, the target must be a crucial component to normal reproduction.

Also, it must not play an important role in physiology other than reproduction. In

addition, the ideal target for inducing contraception should be essential for both female

and male reproduction so that the fertility control agent may be used for both sexes.

Moreover, it is preferable that the contraceptive product also eliminate unwanted sex-

related behaviors. Lastly, the target should be extracellular, because antibodies are

ineffective at targeting intracellular antigens are not readily available for the immune

system. There are several regulators of reproduction that meet these criteria. For

example, sex steroids, such as progesterone, estradiol, and testosterone, are logical

targets to be considered for contraceptive vaccine development. However, because sex

steroids share common precursors, antibodies would not be specific to the target

hormone, thus possibly resulting in deleterious side effects. Follicle-stimulating hormone

(FSH) and luteinizing hormone (LH), gonadotropins that regulate gonadal functions, could be targets for a contraceptive vaccine. While these gonadotropins possess unique beta subunits, they share an alpha subunit with each other and thyroid-stimulating hormone (TSH). Thus, targeting FSH and LH may be problematic for TSH that has many important physiological functions, including control of metabolism. Ovarian zona pellucida (ZP) glycoproteins are a popular target for contraception in animals, but only applicable to female animals. Further, decades' worth of studies evaluating ZP-based fertility control agents have only achieved temporary contraceptive effects in animals [49-51]. Hypothalamic gonadotropin-releasing hormone (GnRH) is also an extensively-studied target for contraceptive vaccine development because it is conserved across mammalian species and produced by both males and females [53,54,179-182]. However, GnRH is poorly immunogenic as a stand-alone decapeptide. Although fusion of GnRH with a larger, foreign protein greatly improves its immunogenicity, the contraceptive effects of GnRH-based vaccines in cats are commonly inconsistent between individuals [180-182]. Further, no study has demonstrated permanent contraception in feline subjects. Also, the blood-brain barrier (BBB) is a major obstacle for T cells and antibodies to access hypothalamic neurons, thus rendering immune mechanisms less effective at ablating these GnRH-secreting cells. Unlike GnRH neurons, the anterior pituitary gland, where LH- and FSH-secreting gonadotropic cells reside, is outside of the BBB and thus is accessible to both T cells and antibodies. Thus, targeting pituitary gonadotropes for ablation is a viable approach for inducing contraception in target species. Gonadotrophs of the anterior pituitary highly express GnRH receptor (GnRHR), a mediator of the hypothalamic GnRH signaling pathway.

48

Interestingly, GnRHR is rarely but should be considered a major target for contraception.

GnRHR is a seven transmembrane protein that is a member of the G-protein-coupled receptor (GPCR) superfamily. GnRH is the only endogenous molecule that activates the GnRHR signaling pathway. GnRH receptor activation by GnRH leads to dissociation of phospholipase C into second messengers phophatidylinositol-triphosphate (IP3) and diacylglycerol (DAG). IP3 production generates intracellular calcium store release that causes a surge in intracellular calcium concentrations. Soon after receptor activation, IP3 rapidly degrades into IP2 and finally IP1 [183,184]. Calcium influx leads to the extracellular signal-regulated kinase (ERK) pathway that has been linked to transcriptional regulation of the genes for the beta subunits of LH and FSH [97-99]. Because GnRHR is pivotal to hypothalamic-pituitary-gonadal axis, targeting the receptor will disrupt GnRH and gonadotropin signaling, thus impairing gonadotrope and overall reproductive functions. Thus, an immunocontraceptive directed against GnRHR is an appropriate strategy for controlling the feral cat population.

GnRHR-based immunocontraceptives for ablation of pituitary gonadotropes in feral cats must be safe, have inexpensive manufacturing costs, be stable in field conditions, and induce long-term immune responses that do not require boosters. DNA vaccines have such desirable characteristics. DNA immunization involves a plasmid encoding a desired protein to be injected into the muscle or the skin of an animal, where it thereupon enters host cells and begins its mechanism of action. The DNA plasmid

directs synthesis of its polypeptide antigen that is then presented on the surface of the transfected host cell. Subsequently, a cell-mediated immune response is elicited or the secreted antigen stimulates an antigen-specific antibody (or humoral) immune response. Thus, DNA vaccination induces both cellular and humoral immune responses against the antigen, unlike traditional protein vaccines that can only induce humoral immune responses [127]. DNA vaccines have been commercialized for veterinary use. Examples include Oncept, a therapeutic cancer DNA vaccine for treatment of melanoma in dogs, and LifeTide-SW5, a growth hormone releasing hormone DNA vaccine that increases piglets weaned and decreases perinatal morbidity [185].

DNA vaccines directed against GnRHR must also be designed to overcome host tolerance because it is a self-protein. One approach to overcoming self-tolerance to an autologous antigen is to vaccinate the host (e.g., cat) with DNA encoding a heterologous antigen (e.g., mouse GnRHR). Success with this strategy was demonstrated in cats and dogs who were observed to have suppressed fertility post-immunization with bovine LH receptor protein [186,187]. Another strategy for enhancing the potency of DNA vaccines against self-antigens is to exploit the ubiquitin-proteasome system (UPS). The UPS is responsible for the degradation of proteins and presentation of the resulting antigenic peptides to circulating lymphocytes. Antigens synthesized within cells are first poly-ubiquitinated and then degraded into their peptide components by the proteasome and subsequently presented on the cell surface. Based on this, vaccination with DNA encoding the target protein fused to ubiquitin (Ub) will theoretically direct proteins to be degraded by the UPS. This strategy may enhance the expression

of epitopes from the synthesized protein via MHC Class I molecules and thus break host tolerance to the self-antigen and will efficiently activate target protein-specific cytotoxic T lymphocytes (CTLs) that will ultimately destroy the endogenous polypeptides or cells expressing them on the cell surface [188]. The ability of DNA vaccines encoding for ubiquitinated proteins to break host tolerance to self-proteins was shown to be effective in a number of studies. For example, Chou's group demonstrated successful use of a DNA vaccine composed of Ub fused to endogenous aquaporin-1 (AQP-1) to induce AQP-1-specific CTL killing of AQP-1-supported melanoma tumor cells in mice [189]. Also, Eslami and colleagues' vaccine against Wilms tumor 1 epitope fused to Ub induced T helper cells activation that contributed to tumor rejection in mice [190].

No published work has described a DNA-based vaccine designed to target ablation of pituitary gonadotropes via GnRHR. Because of this, it is important to conduct a proof-of-concept study with the DNA-based agent before experimenting with the target population; that is, cats. The objectives for this chapter were to (1) construct novel DNA plasmids encoding feline (f) GnRHR alone (fGnRHR) or fGnRHR fused to Ub (Ub-fGnRHR), and (2) characterize DNA constructs for *in vitro* expression of cloned genes. There constructs were further characterized in mice, as described in Chapter 4.

2.2 Materials and Methods

2.2.1 Animal Samples

All tissue samples were collected at post mortem examinations from animals on several different research projects (not including this work) under protocols approved by

Auburn University Institutional Animal Care and Use Committee. This was done in

agreement with Auburn University animal care and use policies that permit *post mortem*

tissue collection for unrelated research projects. For molecular cloning of fGnRHR,

pituitary glands were obtained from three normal cats (a six-month-old male, an eleven-

month-old female, and a three-year-old female). For molecular cloning of Ub, whole

brain tissues were collected from eighteen-week-old, male CD-1 mice. Tissues were

flash frozen in liquid nitrogen and stored at -80°C before further processing.

2.2.2 RNA Isolation

RNA isolation was performed using an RNeasy Lipid Tissue Mini Kit (Qiagen,

Germantown, MD, USA) according to the manufacturer's protocol. Briefly, 5×10^6

mammalian cells or 5 mg tissues were added to 2 mL tubes with 1.4 mm zirconium

oxide beads (Bertin Technologies, Montigny-le-Bretonneux, France) and 600 µL QIAzol

Lysis reagent. Samples were homogenized using a Precellys 24 Homogenizer (Bertin

Technologies) set at 6500 revolutions per minute (rpm) for 40 sec at 4°C. Then, 200 µL

chloroform was added to the homogenate and shaken vigorously for 15 sec followed by

a 3-5 min incubation period at room temperature (RT). The homogenate was

centrifuged at 12000 g for 15 min at 4°C and the upper aqueous phase of the

suspension was transferred to new Eppendorf tube (Hamburg, Germany). Next, 600 µL

70% ethanol was added to the sample that was then transferred to a spin column and

centrifuged at 9600 g for 15 sec at RT. Buffer RW1 (350 µL) was added to the sample

and the mixture was centrifuged at 8000 g for 15 sec at RT. The flow through was

discarded, 80 µL DNase I stock solution (Qiagen) was added to column and incubated

for 15 min at RT. Another round of buffer RW1 was added to the sample and centrifuged again at 8000 g for 15 sec at RT. After discarding the flow through, RNA was washed twice by adding 500 µL buffer RPE. For elution of total RNA, 30 µL DNase- and DNase- and RNase-free water (Sigma-Aldrich, St. Louis, MO, USA) was added to the column, and then centrifuged at 8000 g for 1 min at RT. The RNA concentration was determined by absorbance at 260 nm using NanoDrop 2000 equipment (Thermo Scientific, Waltham, MA, USA) and samples were stored at -80°C until use.

2.2.3 Restriction Digestion, Purification, and Ligation

For restriction digestion, the following reagents were purchased from New England (NE) BioLabs (Ipswich, MA, USA): restriction enzymes BamHI, MfeI, NotI, and XbaI; 10X BSA; and 10X Universal buffer. Following the manufacturer's guidelines, a typical 100 µL reaction for restriction digestion of 1 µg DNA (pcDNA 3.1 plasmid or fGnRHR recombinant genes) included 40 U restriction enzyme, 10 µL buffer 2, 10 µL 10X BSA, and RNase-free water. After mixing, reactions were incubated at 37°C for 1 h in a cooling unit (VWR Sci., Hyclone, Logan, UT, USA).

Digested products were then purified using a QIAquick PCR Purification Kit (Qiagen). Five volumes of buffer PB was added to one volume of the digested DNA sample, placed in a spin column, and centrifuged at 17950 g for 1 min at RT to bind DNA to membrane. Flow through was discarded and the column was washed with 750 µL buffer PE followed by centrifugation. To elute DNA, 40 µL DNase- and RNase-free water was added to the column membrane, incubated for 3-5 min at RT, and the column

was centrifuged at 17950 g for 1 min at RT. DNA concentration was determined by absorbance at 260 nm using NanoDrop 2000 equipment and samples were stored at -20ºC until use.

Ligation of fGnRHR recombinant genes into the plasmid was performed in 120uL of reaction mixture which included the following reagents: 40 U T4 ligase and 10X T4 ligase buffer (NE BioLabs), 150 ng DNA insert, 600 ng pcDNA 3.1 vector (Invitrogen, Carlsbad, CA, USA), and DNase- and RNase-free water. The mixture was incubated for 14-16 h at 10ºC followed by a final purification step as described.

Integrity of all clones were verified via restriction enzyme digestion. Cloned vectors were sequenced at the Massachusetts General Hospital DNA Core (Boston, MA, USA) to confirm insertion of correct sequence.

2.2.4 Reverse transcriptase polymerase chain reaction (RT-PCR) and PCR

All primers were purchased from TIB MolBiol (Adelphia, NJ, USA). OneStep RT-PCR Kit (Qiagen) was used for reverse transcription and amplification of all total RNA samples. A typical 50µL reaction includes 10 µL OneStep RT-PCR buffer, 2µL dNTP mix; 2 µL enzyme mix; 50 pmol per primer; 500 ng RNA template; and *quantum satis* with DNase- and RNase-free water. RT-PCR was typically performed using a GeneAmp PCR 9700 machine (Applied Biosystems, Grand Island, USA) for 40 cycles under the following conditions:

- Reverse transcription - 50ºC for 30 min;

- Polymerase activation - 95ºC for 15 min;

- Denaturation - 94ºC for 30 sec;

- Annealing - 50ºC for 30 sec;

- Extension - 72ºC for 1 min 40 sec;

- Final extension - 72ºC for 10 min.

Amplification of all plasmid DNA from *Escherichia coli (E. coli)* colonies was performed using a Taq PCR Master Mix kit (Qiagen). First, a mixture of 525 µL Taq master mix, 50 pmol T7 forward plasmid primer; 50 pmol BGH reverse plasmid primer, and 512.4 µL water was aliquoted into 25µL reaction volumes. Then, a sample of each *E. coli* colony was added to each reaction as a template. Using a Hybaid PCR 9700 machine (AGS, Heidelberg, Germany), PCR for 40 cycles was performed under the following conditions (check settings):

- Polymerase activation - 94ºC for 3 min;

- Denaturation - 94ºC for 10 sec;

- Annealing - 50ºC for 30 sec;

- Extension - 72ºC for 1 min 30 sec;

- Final extension - 72ºC for 10 min.

Ten-microliter sample of PCR product was mixed with 2 µL 6X loading dye (New England BioLabs, Ipswich, MA, USA) and loaded onto a 0.8% agarose gel with ethidium bromide for electrophoresis using a PowerPac Basic Power Supply (BioRad, Hercules, CA, USA). Bands were visualized using a 312 nm ultra violet transilluminator (Fisher Scientific, Pittsburgh, PA) and images were captured using a D34 distant screen instant camera (Polaroid, Ridgefield Park, NJ, USA).

2.2.5 Cloning strategy

2.2.5.1   Construction of template plasmid encoding feline (f)GnRHR

To begin, a plasmid encoding fGnRHR (plasmid name: fGnRHr) was designed as a template for future plasmid constructs. First, the entire *fGnRHR* gene was amplified from total RNA with fGnRHR-specific primers. The forward primer incorporated an EcoRI restriction site, a Kozak sequence (for initiation of translation), and the first seventeen nucleotides of the fGnRHR sequence (Primer A, Table 2.1). The reverse primer included the last sixteen nucleotides of the *fGnRHR* gene and an XbaI restriction site (Primer B, Table 2.1). Once amplified, the *fGnRHR* gene was cloned into the EcoRI and XbaI restriction sites of a pcDNA3.1 vector (Fig. 2.1, Step 1).

2.2.5.2   Construction of template plasmid encoding Ubiquitin (Ub)

Next, a plasmid encoding Ub was constructed as a template for future plasmid constructs. First, the entire *Ub* gene was amplified from total RNA with Ub-specific primers. The forward primer contained sequences for EcoRI restriction site, a Kozak sequence, and the first twenty nucleotides of the *Ub* gene (Primer C, Table 2.1). The reverse primer included sequences for the last eighteen nucleotides of the *Ub* gene and NotI restriction site (Primer D, Table 2.1). Once amplified, the *Ub* gene was cloned into the EcoRI and NotI restriction sites of a pcDNA3.1 vector (Fig. 2.1, Step 1).

2.2.5.3   Construction of plasmid encoding Ub-fGnRHR

To begin construction of Ub-fGnRHR plasmid, two new primers were used to generate a recombinant *fGnRHR* gene. The forward primer incorporated a NotI

restriction site and the first nineteen nucleotides of the fGnRHR sequence (Primer E, Table 2.1). The reverse primer included the last eighteen nucleotides of *fGnRHR* gene, a six-histidine tag for protein detection via immunoblotting, a stop codon, and an XbaI restriction site (Primer F, Table 2.1). The *fGnRHR* gene was then amplified from the fGnRHR plasmid template and the fragment was cloned into NotI and XbaI restriction sites of a new pcDNA3.1 vector (Fig. 2.1, Step 2).

Next, the Ub sequence from the Ub plasmid was modified to replace the C-terminal glycine residue with alanine (G76A) to prevent premature cleavage of Ub from the target protein fGnRHR by C-terminal hydrolases in cells that will be transfected with plasmids [191]. To generate this modified Ub sequence, a new forward Ub primer was designed to include a BamHI restriction site, a Kozak sequence for initiation of translation, and the first eighteen nucleotides of the *Ub* gene (Primer G, Table 2.1). Also, a new reverse primer was generated and contained the last 25 nucleotides of Ub sequence (including codon for G76A modification) and NotI restriction site (Primer H, Table 2.1). Then, Primers G and H were used to amplify the desired sequence from the previously-constructed Ub plasmid. Finally, the Ub fragment was ligated into BamHI and NotI restriction sites of the vector encoding the recombinant *fGnRHR* gene, yielding a plasmid encoding Ub-fGnRHR (Fig. 2.1, Step 2).

2.2.5.4   Construction of plasmid encoding fGnRHR for vaccination purposes

To construct fGnRHR plasmid, the *fGnRHR* gene was amplified from the Ub-fGnRHR construct using two primers. A new forward primer was designed to include a

57

BamHI restriction site, a Kozak sequence, and the first nineteen nucleotides of the *fGnRHR* gene (Primer I, Table 2.1). This primer, along with primer F, was used to amplify the *fGnRHR* gene that was then cloned into the BamHI and XbaI sites of a new pcDNA3.1 vector (Fig. 2.1, Step 3).

2.2.6 Electroporation of *Escherichia coli* (*E. coli*) cells

For electroporation of bacteria, 40 µL TOP10 F′ Electrocomp *E. coli* cells (Invitrogen) were mixed in Eppendorf tube with 100 ng plasmid DNA and the suspension was transferred into an ice-cold 0.2 cm cuvette (BioRad). Electroporation was performed using a Gene Pulser Xcell Electroporation System (BioRad) under the following conditions: 2.5 kV, 25 µF, and 200 Ω. The pulse type was exponential decay for bacterial cells. Electroporated *E. coli* cells were incubated for 1 h with shaking at 220 rpm at 37⁰C. Then, 1 µL cells were added to 1 mL Super optimal broth (SOC) medium (Life Technologies, Grand Island, NY), and 100 µL of electroporated suspension were spread onto agar plates containing 0.1% ampicillin (Amresco, Solon, OH, USA) and incubated for 2-3 days at 37⁰C. To confirm successful transfection, 40 *E.coli* colonies were screened by PCR. Finally, PCR products were subjected to gel electrophoresis for the presence of the fGnRHR or Ub-fGnRHR amplicons at expected molecular weights.

2.2.7 Plasmid DNA isolation

In preparation for plasmid DNA isolation, *E.coli* clones with the correct molecular weight of the gene inserts were propagated for 12-15 h in 20 mL *Luria Bertani* broth

supplemented with 0.1% ampicillin (Amresco) with shaking at 200 rpm at 37ºC.

Plasmid DNA was isolated using a QIAfilter Plasmid Purification Midi Kit (Qiagen). To

harvest *E. coli* cells, cultures were transferred to an Oakridge tube and centrifuged at

6000 g for 15 min at 4ºC. After discarding the supernatant, cell pellets were re-

suspended in 4 mL ice-cold buffer P1. To lyse cells, 4 mL buffer P2 was added to the

suspension that was mixed and incubated for 5 min at RT. Then, 4 mL ice-cold buffer

P3 was added to lysate to precipitate non-plasmid DNA cellular components (e.g.,

genomic DNA, proteins, cell debris). The lysate was gently mixed and transferred to a

QIAfilter cartridge barrel and incubated for 10 min at RT. A QIAGEN-tip 100 column

was equilibrated with 4 mL buffer QBT. Once the column was empty, the lysate was

filtered through the equilibrated QIAGEN-tip to bind DNA, followed by washing of the

column with 10 mL buffer QC twice. To elute DNA, 5 mL QF was added to the column

and the flowthrough was collected into Nalgene tubes. DNA was precipitated by adding

3.5 mL RT isopropanol, vigorously shaking each tube, and then immediately subjecting

sample to centrifugation at 15000 g for 30 min at 4ºC. Supernatant was discarded, the

pellet was washed with 5 mL RT 70% ethanol, and then centrifuged at 15000 g for 10

min at 4ºC. After discarding the supernatant, the pellet was air-dried for 20 min. The

DNA pellet was re-dissolved with 300 µL RNA/DNA-free water, incubated on ice for 10

min, and centrifuged at 6000 g for 3 min at 4ºC. DNA concentration was determined

and plasmid isolates were stored at -20ºC until use.

2.2.8 Preparation of mammalian cell cultures for electroporation

Chinese hamster ovary (CHO)K1 cells (CCL-61, ATCC, Manassas, VA, USA) were cultured in 15 mL Ham's F-12K medium (Corning, Corning, NY, USA) with 10% fetal bovine serum (FBS; VWR) and 1% penicillin-streptomycin (P/S; Mediatech, Inc., Manassas, VA, USA) in 75 cm^2 flasks (Corning, Corning, NY, USA) for 2-3 days at 37ºC in an atmosphere of 5% CO_2. Human embryonic kidney (HEK293)T cells (CRL-11268, ATCC) were separately cultured in 15 mL Dulbecco's modified eagle medium (DMEM; Corning) with 10% FBS and 1% P/S in 75 cm^2 flasks. Once 80% confluency was reached, media was aspirated and cells were washed with 13 mL Hank's Balanced Salt Solution (HBSS; Corning) for 5 min at RT. HBSS was aspirated and the cells were incubated with 0.25% trypsin (Corning) for 10-15 min at 37ºC. Trypsinized cells were neutralized with 10% FBS, collected, and centrifuged at 300 g for 10 min at RT. Supernatant was aspirated, the cell pellet was suspended in 1 mL F12K or DMEM media. Ten microliters of cell suspension was added to 90 µL trypan blue (Sigma-Aldrich) and cells were counted using a hemocytometer.

2.2.9 Electroporation of mammalian cells

Aliquots of 5X10^5 cells were mixed with 1.5 µg plasmid DNA in a 100µL volume and the suspensions were transferred into an ice-cold 0.2 cm cuvette. Electroporation was performed under the following conditions: CHOK1: 250 V, 30 msec pulse length (PL); HEK293T: 110 V, 25 msec PL. The pulse type was square wave for all cell lines. After electroporation, 0.5 mL F12K or DMEM media with 10% FBS was immediately added to the cuvette, and the electroporated cells were transfer into a test tube that

remained at RT until all cells in all cuvettes were electroporated. Finally, electroporated cells were cultured in F12K or DMEM media with 10% FBS, and 1% P/S, and incubated at 37ºC in an atmosphere of 5% CO_2. Forty-eight hours later, geneticin G-418 sulfate (a neomycin-like antibiotic) with a concentration of 400 μg/mL (TEKnova, Hollister, CA, USA), was added to cell cultures as a selection agent for transfected cells. Cell cultures were maintained for two weeks with passage every 2-3 days depending on confluency.

2.2.10 Analysis of transcriptional expression of fGnRHR and Ub-fGnRHR in mammalian cells

HEK293T cells were transfected and cultured for 48 h as previously described. To confirm successful transfection and transcriptional expression of the recombinant genes, total RNA was extracted and used for amplification of fGnRHR mRNA using primers A and B, and Ub-fGnRHR mRNA was amplified with primers B and C via RT-PCR as previously described. As a positive control, RT-PCR was performed with total RNA isolated from feline pituitary gland to detect expression of fGnRHR transcript. Reactions with no reverse transcriptases were included as negative controls. Gel electrophoresis was performed to visualize PCR products with the approximate molecular weight of fGnRHR or Ub-fGnRHR. Images were captured using a Polaroid instant camera.

2.2.11 Analysis of translational expression of fGnRHR and Ub-fGnRHR in mammalian cells

2.2.11.1 Western blotting

2.2.11.1.1 Protein extraction

CHOK1 cells were transfected with plasmids encoding fGnRHR or Ub-fGnRHR, cultured for two weeks in media containing geneticin, and cryopreserved at -180ºC in a CryoMed CryoPlus III CryoFreezer (Thermo Scientific). Two months later, transfected CHOK1 cells were thawed and cultured for 2 days, harvested and counted using a hemocytometer. For protein extraction, $5X10^6$ cells were washed with 1 mL phosphate buffered saline (PBS; pH 7.4; Life Technologies), and centrifuged at 1503 g for 5 min at RT. After repeating this step, cells were re-suspended in 1 mL cell-lysing RIPA buffer (Thermo Scientific) supplemented with cOmplete® ULTRA protease inhibitor cocktail (Roche, Basel, Switzerland) that protect proteins from cleavage by serine, cysteine, aspartic, and metallo-based proteases. Re-suspended cells were homogenized in a Precellys 24 Homogenizer at 2348 g for 20 sec twice. To remove foam, homogenized samples were centrifuged at 1503 g for 3 min at RT. Finally, protein concentration was quantified via a Direct Detect spectrophotometer (Millipore, Billerica, MA, USA) that uses Fourier transform infrared spectroscopy to measure amide bonds in protein chains.

2.2.11.1.2 Protein detection

For electrophoresis, protein was denatured with Laemmli buffer (BioRad) at a 1:1 ratio and incubated at 100ºC for 10 min. Laemmli buffer was supplemented with β-

mercaptoethanol (5% v/v; Sigma-Aldrich) to reduce disulfide bonds. After cooling the

samples for 5 min at RT, 50 µg protein was loaded into a 10% Mini-PROTEAN TGX

precast polyacrylamide gel (BioRad). The loaded gel was placed into Tris/Glycine/SDS

running buffer (BioRad) and electrophoresis was performed at 100 V for 130 min. Then,

proteins were transferred onto nitrocellulose paper (BioRad) at 100 V for 90 min in

buffer containing Tris/Glycine buffer (BioRad) and methanol (20% v/v, Sigma-Aldrich).

After transfer, membranes were incubated with Ponceau stain (Sigma-Aldrich) for 5 min

to verify successful transfer of proteins. After washing membranes thrice with double-

distilled water, membranes were blocked with 5% blocker containing non-fat milk

powder and tris buffered saline (TBS) with 1% Tween 20 for 90 min at RT. Then,

membranes were incubated in primary antibody (Table 2.2) diluted with 5% blocker for

15-18 h at 4ºC. Primary antibody was removed and membranes were washed in cold,

double-distilled water for approximately 30 sec, and then washed in 0.1% TBS Tween

20 for 5 min three times with gentle shaking at RT. Membranes were incubated with

diluted secondary antibody (Table 2.3) for 90 min with gentle shaking at RT. The

secondary antibody was removed, and the 5-min washing step was repeated for times.

Finally, membranes were incubated in HyGLO Quick Spray chemiluminescent solution

(Denville Scientific, Holliston, MA) for 3 min, exposed membrane to x-ray films (Kodak,

Rochester, NY) for 1 min, and films developed and fixed in solution for 2 min each.

Films were scanned using an Epson 1500 scanner (Suwa, Japan).

2.2.11.2   Immunocytochemistry

CHOK1 cells (1X10^5) were transfected with the fGnRHR construct, and loaded into a Labtek chamber slide (Electron Microscopy Sciences, Hatfield, PA) with 1 mL F12K medium with 0.004% geneticin. As a control, untransfected CHOK1 cells were loaded into the chamber slide that was then incubated for 15-17 h at 37°C. Media was aspirated and cells were rinsed with 1 mL PBS twice for 5 min each at RT. Cells were then fixed with 1 mL 1% paraformaldehyde (PFA) for 10 min at RT. PFA was aspirated, cells were rinsed with 1 mL PBS twice for 2 min each, and then blocked with 500 µL 1% rabbit serum (RS) in PBS for 1 h at RT. Then, cells were incubated for 2 h at RT with 1 mL primary antibody (1:10 dilution in 1% RS; Santa Cruz SC-8682, Dallas, Texas, USA) against the first 20 amino acids of human (h) GnRHR that is 93% similar to fGnRHR sequence. After aspirating the primary antibody solution, cells were rinsed 5 times for 2 min each. Then, cells were incubated with secondary antibody Alexa Fluor 488 (Life Technologies) that was diluted (1:200) in 1% RS for 1 h in darkness at 4°C. Finally, cells were rinsed with 1 mL PBS 2 times for 5 min at RT. The grid was carefully removed and VectaShield® mounting medium (Vector Laboratories, Burlingame, CA, USA) with 4',6-diamidino-2-phenylindole (DAPI) was used to float a coverslip. Finally, images were captured using an Olympus fluorescence microscope (Shinjuku, Tokyo).

2.2.11.3   IP-One functional G-protein Coupled Receptor assay

Stimulation of cells expressing membrane-bound GnRHR with GnRH or GnRH agonists results in the activation of second messenger IP3 that has a very short half-

life before it is transformed into IP2 and then finally IP1 [192]. Because IP1 accumulates in cells exposed to lithium chloride (LiCl), it can be quantified and interpreted as a measure of GnRHR protein expression and functionality [192]. Using a homogenous time-resolved fluorescence (HTRF) IP-One terbium (Tb) assay kit (CisBio Bioassays, Bagnol sur Ceze, France), intracellular IP1 levels were measured in cells transfected with fGnRHR or Ub-fGnRHR constructs. First, HEK293T cells were transfected as described above and 48 h later the cells were diluted in stimulation buffer with 50 mM LiCl. Cells were seeded at 5×10^4 per well into Nunc white 384-well microplates (Thermo Scientific). Varying concentrations of GnRH analogue leuprolide (Tocris Bioscience, Bristol, UK) were added to each well. HEK293T cells were incubated for 45 min at 37ºC and then lysed by addition of 3 µL of the supplied conjugate-lysis buffer containing dye d2-labeled IP1, followed by 3 µL of conjugate-lysis buffer containing Tb cryptate-labeled anti-IP1 antibody that competes with both d2-labeled IP1 and native IP1 produced by cells. Both buffers were reconstituted according to the manufacturer's instructions. Standards and internal controls such as HEK cells not stimulated by leuprolide or cells not exposed to IP1-d2 were included in the assay. Plates were incubated for 1 h at RT and then placed at -20ºC for 4 h. The plate was shipped overnight to the Cisbio facility (Bedford, MA, USA) where a PHERAstar plate reader (BMG labtech, Ortenberg, Germany) was used to measure HTRF emissions at 337nm for excitation. Cryptate emission from the donor fluorophore was measured at 620 nm, and acceptor fluorophore emission was measured at 665 nm. A 620 nm:665 nm ratio was factored into calculations in order to reduce well-to-well variations as a result of photophysical interference [192]. The

specific signal is inversely proportional to the concentration of IP1 in the standard or in the cell lysate. Detection limit of IP1 is 5nM.

2.2.12 Statistical analysis

IP-One functional GPCR assay data are presented as the mean ± standard error of the mean. All *in vitro* experiments were performed on two separate and independent occasions. Data were analyzed by one-way analysis of variance with Scheffe *post-hoc* analyses (SPSS, IBM, Armonk, NY, USA). Differences of $P \leq 0.05$ were considered significant.

2.3 Results

2.3.1   Cloning of fGnRHR and Ub-fGnRHR

Here, the full-length *fGnRHR* gene was cloned into BamHI and XbaI restriction sites of pcDNA3.1 vector to obtain a fGnRHR construct that was subsequently transformed into *E. coli* cells. The release of approximately 1027 bp gene insert from the fGnRHR construct following digestion with BamHI and XbaI restriction enzymes confirmed the successful cloning of fGnRHR (Fig. 2.2). Also, clones with the correct molecular weight for fGnRHR inserts were propagated and then subjected to plasmid DNA purification and gene sequence verification. Similarly, Ub-fGnRHR was amplified and cloned into a pcDNA 3.1 vector. Restriction digestion of recombinant plasmid Ub-fGnRHR with BamHI and XbaI resulted in the release of a 1257 bp product and thus confirmed successful cloning (Fig. 2.3). Further, the cloned DNA sequence was verified

by sequencing the plasmid DNA from *E. coli* clones identified to have appropriate molecular weight of Ub-fGnRHR.

2.3.2 *In vitro* transcriptional expression of fGnRHR and Ub-fGnRHR

RT-PCR was performed to detect fGnRHR and Ub-fGnRHR mRNA and thus verify transcriptional expression of constructs electroporated into HEK293T cells. A 1027-bp PCR product was identified in cell cultures transfected with fGnRHR plasmid, but not in cells transfected with the empty plasmid (Fig. 2.4). Likewise, a 1257-bp PCR product was detected in Ub-fGnRHR-transfected HEK293T cells (Fig. 2.4). All products were sequenced and shown to be the full-length fGnRHR (Genbank accession number: NM_001287228.1) or Ub-fGnRHR coding sequence.

2.3.3 *In vitro* translational expression of fGnRHR and Ub-fGnRHR

2.3.3.1 Western blotting

In an attempt to identify GnRHR proteins expressed by transfected CHOK1 cells, Western blots were probed with primary antibodies purchased from six different manufacturers (Table 2.2). Using a Thermo Scientific 6XHIS antibody, a faint 90 kDa band was detected in untransfected CHOK1 cells and a strong band of the same molecular weight in Ub-fGnRHR-transfected cells (Fig. 2.5A). Western blots probed with an Abcam AB24095 antibody revealed strong bands at 90kDa, 65kDa, and 35kDa in untransfected and transfected CHOK1 cells (Fig. 2.5B). Abcam AB89266 antibody detected 70 and 35kDa bands in both transfected and untransfected CHOK1 cells (Fig. 2.5C). A Santa Cruz antibody produced poor immunostaining of 80kDa proteins from

fGnRHR-transfected and untransfected CHOK1 cells (Fig. 2.5D). A Fisher Scientific

antibody produced poor blots as well, with 68kDa bands in both transfected and

untransfected CHOK1 cells (Fig. 2.5E). As a final attempt to identify fGnRHR protein in

transfected CHOK1 cells, Western blots probed with a Pi Proteomics antibody revealed

a distinct, 90kDa band in fGnRHR-transfected and untransfected CHOK1 cells (Fig.

2.5F). Overall, detection of fGnRHR protein in CHOK1 cells via Western blotting with

different primary antibodies was unsuccessful, as there was no clear difference in

protein band patterns between untransfected and fGnRHR-transfected CHOK1 cells,

thus producing inconclusive results.

2.3.3.2   Immunocytochemistry

As an alternative to Western blotting, immunocytochemical staining was

employed in an effort to identify fGnRHR protein in transfected CHOK1 cells. Using a

primary antibody previously used for immunoblotting (Santa Cruz), immunocytochemical

examination of fGnRHR-transfected CHOK1 cells indicated GnRHR immunoreactivity

(Fig. 2.6A). However, similar immunoreactivity was detected in untransfected CHOK1

cells (Fig. 2.6B). Therefore, GnRHR protein expression was not validated in transfected

CHOK1 cells. Due to the equivocal outcomes of immunocytochemical studies, a

different approach was taken for *in vitro* identification of fGnRHR protein.

2.3.3.3   IP-One functional G-protein Coupled Receptor assay

A functional HTRF assay that measures GPCR-mediated IP1 accumulation was

used in an attempt to verify fGnRHR signaling pathway activation and thus receptor

protein expression in transfected HEK293T cells. No significant difference in IP1 accumulation was observed for the un-transfected cells exposed to increasing concentrations of leuprolide, a GnRH agonist ($P > 0.05$; Fig. 2.7A). The same outcome was observed for the fGnRHR-transfected cells ($P > 0.05$; Fig. 2.7B). Similarly, IP1 levels were unchanged in Ub-fGnRHR-transfected cells exposed to increasing leuprolide concentrations compared to cells incubated with 0 nM leuprolide ($P > 0.05$; Fig. 2.7C).

2.4 Discussion

The most effective fertility control product for feral catswould be stable in field conditions, can be produced at mass scale but for low cost, and has a duration of at least three to four years (i.e., the average lifespan of feral cats) [181]. Immunocontraceptive vaccines offer such desirable characteristics and have been shown to be promising for the management of companion animal species [193-195]. In addition to controlling reproduction, the ideal target for immunocontraception is one that has functional significance in the regulation of sex hormone-related behaviors in both males and females of all ages. As a counterpart to GnRH and a defining feature of pituitary gonadotropes, GnRHR is an important mediator of mammalian reproductive hormonal cascade in both sexes, and thus a suitable target for immunocontraceptive vaccine development.

The current objective was to construct and characterize an immunocontraceptive designed to target GnRHR for ablation of pituitary gonadotropic cells. DNA vaccination

69

has the capability to elicit cellular and humoral immune responses and subsequently induce long-term efficacy in animal hosts [127]. Invitrogen pcDNA3.1 was chosen as the vector for molecular cloning purposes because of the following features: a cytomegalovirus enhancer-promoter for high-level expression; bovine growth hormone polyadenylation signal and transcription termination sequence for enhanced mRNA stability; an ampicillin resistance gene; and pUC origin of replication sequence for selection and maintenance in *E. coli*. Such characteristics are desirable for a stable DNA-based vector.

Vaccination with DNA encoded to synthesize a heterologous antigen has been demonstrated to induce immune responses against various protein targets, including those involved in reproduction [186,187,196]. Therefore, fGnRHR was cloned into the BamHI and XbaI sites of the DNA vector for use in a proof-of-concept study in mice. As an additional mechanism for eliciting anti-self immunity to the receptor, Ub was fused to fGnRHR in a second vector in order to target the fusion protein to the UPS for degradation and subsequent antigen presentation. Studies have demonstrated successful use of a DNA vaccine composed of Ub fused to endogenous proteins. For example, aquaporin-1 (AQP-1) was artificially ubiquitinated to induce AQP-1-specific CTL killing of AQP-1-supported melanoma tumor cells in mice [189]. Strong IgG and CTL responses to hepatitis B virus core antigen (HBc-Ag) were elicited in BALB/c mice that were immunized with plasmid encoding Ub-fused HBc-Ag [169].

In order to exploit the UPS system to enhance antigen presentation and elicit the desired subsequent immune responses, it is important to confirm that the constructed DNA plasmids are capable of transcriptional and translational processes in mammalian cells. First, DNA sequencing was used to verify that fGnRHR and Ub-fGnRHR constructs contain the correct gene sequences. Then, RT-PCR was performed to validate mRNA expression in transfected HEK293T cells. Reactions using total RNA from cells transfected with fGnRHR yielded an expected 1027-bp PCR product. Likewise, a 1257-bp PCR product was detected in Ub-fGnRHR-transfected HEK cells. After performing RT-PCR on total RNA isolated from transfected cells over time, GnRHR mRNA expression was stable and no changes in the inserted fragment were found over time.

Western blotting is a technique commonly used to identify specific proteins from cell lysate [197]. Thus, immunoblotting was performed in an attempt to confirm expression of the fGnRHR or Ub-fGnRHR proteins in CHOK1 cells transfected with either of the corresponding recombinant DNA vectors. Both vectors were cloned with 6XHIS tag sequences for the sole purpose of using an anti-HIS tag antibody for target protein detection. Unfortunately, clear identification of the ubiquitinated receptor protein using this antibody was not the outcome for blotting assays. Alternatively, five other primary antibodies were used for numerous Western blots containing fGnRHR-transfected CHOK1 cell lysates. The variety of selected antibodies included those that are commercially available and directed against highly conserved (≥90%) epitopes of the human GnRHR (e.g., N terminus, third intracellular loop, and third extracellular

71

loop), and a custom-made fGnRHR antibody. However, neither fGnRHR nor Ub-fGnRHR proteins were clearly detected in transfected CHOK1 cells. Truncated (30-50kDa), mature (60-70kDa) and dimerized (>90-100kDa) GnRHR variants have been identified *in vitro* in different tissues in various mammalian species [198-201] and adds to the complexity of GnRHR protein detection. Transfection with other cell lines such as HEK293 cells (CRL-1573, ATCC) and African green monkey kidney (COS-7) cells (CRL-1651, ATCC) did not improve immunoblotting results (data not shown). Neither did the following changes to immunoblotting protocols: cell harvesting method; addition of triton X detergent to RIPA buffer; extended heating of proteins for further denaturation; varying SDS percentage in polyacrylamide gel; 5% BSA for blocking; varying primary or secondary antibody dilutions. Some of the immunoblotting results showed identical band patterns detecting multiple proteins of differing molecular weights in untransfected and fGnRHR-transfected cells (Fig. 2.5B, 2.5C). Similarly, unclear results were obtained following immunocytochemical staining of CHOK1 cells transfected with the fGnRHR construct. One would expect less or no immmunoreactivity in untransfected cells in comparison to transfected cells. Instead, similar immunoreactivity was detected in both fGnRHR-transfected and untransfected CHOK1 cells. One explanation for invalidation of *in vitro* fGnRHR protein expression is the lack of standardized primary antibodies against feline GnRHR on the market. This is related to the fact that fGnRHR protein sequence was not available to the public until the Samoylova group identified it in 2014 [202]. Second, most of the primary antibodies used for immunoblotting and staining were against the amino terminus of hGnRHR, the domain with the most variability in protein sequence compared to fGnRHR [202].

Because of this, an assay with high sensitivity and specificity was desired to detect fGnRHR protein expression in mammalian cell lines. Thus, an IP1 accumulation assay was used to confirm receptor protein expression in transfected HEK293T cells.

Artificially ubiquitinated fGnRHR should be directed to the proteasome and effectively degraded [189] and thus not available to activate the G_{q11}-mediated signaling pathway and subsequently increase intracellular IP1 levels. To confirm this scenario, IP1 accumulation was measured in Ub-fGnRHR-transfected HEK293T cells exposed to various concentrations of GnRH agonist leuprolide. There was no significant increase in IP1 concentrations in Ub-fGnRHR-transfected HEK293T cells (except at 100 nM) and untransfected cells. Leuprolide also failed to significantly increase IP1 levels in cells transfected with fGnRHR that is typically trafficked to the cell membrane [183,184]. Wide standard deviations clearly contributed to the inability to detect significant differences for each leuprolide concentration for fGnRHR-transfected cells. This outcome was unexpected, as our laboratory has demonstrated that leuprolide causes a dose-dependent increase in IP1 levels in HEK293T cells transfected with a DNA vector encoding mouse (m) GnRHR (data not shown). One reason for this conflicting outcome is that IP One Tb, an assay designed for high-throughput screening, was carried out by hand, and such a major change to assay execution may lead to variation in assay results. Also, irregular aggregation of electroporated HEK cells was observed while handling them, possibly resulting in inaccurate cell counts and plating for each independent experiment. An additional explanation for assay outcome may relate to expression and trafficking productivity of the fGnRHR (but not for mGnRHR) protein in

HEK293T cells. GPCR expression is typically low in transfected cell lines and poorly stable in detergents [203]. To remedy this, GPCR stabilization techniques are implemented, including truncations of the flexible regions and point mutations in receptor sequence [204]. Such engineering to the DNA sequence may be needed to improve *in vitro* fGnRHR protein expression.

Another possible reason for the inability to identify the fGnRHR-based proteins from the cloned vectors may be due to abnormal post-translational modification processes, especially for heterologous proteins. Indeed, functional membrane protein expression in mammalian cell systems is orchestrated by complex interactions between many factors. Such factors, which vary considerably between different expression systems, include the amount and stability of synthesized mRNA, folding of the nascent polypeptide chain in the ribosome, the efficiency of insertion into the membrane, the role of post-translational modifications (e.g. N-glycosylation), and molecular chaperones to facilitate folding [205]. Low heterologous membrane protein expression is a common problem with cell transfection procedures [206]. Engineering strategies for strengthening protein expression and trafficking are employed to improve heterologous protein production. For example, overexpression of Sec1/Munc18 protein Sly1p, a regulator of vesicle fusion from endoplasmic reticulum to Golgi, increases α-amylase production in yeast Saccharomyces cerevisiae [207]. Such strategies may be needed to improve fGnRHR protein expression for detection.

2.5 Conclusion

   In summary, a DNA plasmid encoding fGnRHR was engineered for study in mice for overcoming self-tolerance to the autologous protein receptor. In addition, a second DNA vector fusing Ub to fGnRHR was constructed in an effort to enhance degradation and antigen presentation and thus induce an immune response to the self-protein in mice. Although the DNA sequences and transcriptional expression of the constructs were confirmed, translational expressions of fGnRHR and Ub-fGnRHR were not validated via Western blotting, immunocytochemistry, or HTRF IP-One assays. Because fGnRHR may have low protein expression, optimization of protein detection assays might be necessary to improve receptor protein secretion. The next chapter covers generation and *in vitro* characterization of a novel nanoparticle system for *in vivo* delivery of these GnRHR, DNA-based constructs.

Table 2.1

Primers used for constructing plasmids encoding fGnRHR or Ub-fGnRHR

DNA Plasmid Name	Primer Name	Nucleotide Sequence (5' → 3')
fGnRHr	A	ACTCGAATTCGCCACCATGGCAAGTGCCCCTCC
	B	ACTCTCTAGATTACAGAGAGAGAAATACCCA
Ub	C	CGACTCGAATTCGCCACCATGCAGATCTTCGTGAAG
	D	GACTATGCGGCCGCCACCTCTCAGGCGAAGGACC
Ub-fGnRHR	E	TCTTTATGCGGCCGCATGGCAAGTGCCCCTCCTG
	F	ACTCTCTAGACTAGTGGTGATGGTGATGATGCAGAGAGAGAAATACCCATA
	G	ATACTCGGATCCGCCACCATGCAGATCTTCGTGAAG
	H	GACTATGCGGCCGCTCGCACCTCTCAGGCGAAGGACCAG
fGnRHR	I	ATACTCGGATCCGCCGCCACCATGGCAAGTGCCCCTCCTG

Abbreviations: fGnRHR, feline gonadotropin releasing hormone receptor; Ub, ubiquitin

76

Table 2.2

Primary Antibodies Used for Western Blotting and Immunocytochemistry

Antibody Name and Manufacturer	Catalog No.	Epitope	% Similarity to fGnRHR Sequence	Clonality	Isotype	Dilution	Figure No.
A. Thermo Scientific 6x-His Epitope Tag Antibody (Waltham, MA, USA)	MA1-21315	HHHHHH	0	Monoclonal	IgG2b	1:3000	1.4A
B. Abcam hGnRHR (Cambridge, UK)	AB24095	MANSASPEQNQHCSAINNSIPLMQGNLPY (AA1-29)	93	Monoclonal	IgG1	1:100	1.4B
C. Abcam hGnRHR (Cambridge, UK)	AB89266	VLHQDPHELQ LNQSKNNIPRARLKTLKMTV AFATSFTVCWTPYYVLGIWYWFDPEMLNRL (AA249-299)	90	Polyclonal	IgG1	1:1000	1.4C
D. Santa Cruz hGnRHR[1] (Dallas, Texas, USA)	SC8682	MANSASPEQNQNHCSAINNS (AA1-20)	90	Polyclonal	IgG	1:20* ; 1:50	1.4D
E. Fisher Scientific hGnRHR (Pittsburgh, PA, USA)	MS1139P1	MANSASPEQNQNHCSAINNSIPLMQGNLPY (AA1-29)	93	Monoclonal	IgG1	1:100	1.4E
F. Pi Proteomics Custom-made fGnRHR (Huntsville, AL, USA)	N/A	MASAPPEQNQNHCSAINNSIPLMQGNLP (AA1-28)	100	Polyclonal	IgG	1:500	1.4F

Abbreviations: fGnRHR, feline gonadotropin releasing hormone receptor; hGnRHR, human gonadotropin releasing hormone receptor. *Antibody and dilution used for immunocytochemistry.

Table 2.3

Secondary Antibodies Used for Western Blotting and Immunocytochemistry

Antibody Name	Catalog No.	Dilution	Figure No.
Jackson ImmunoResearch Goat Anti-mouse IgG-HRP	115-035-003	1:4000	1.4A
Santa Cruz Goat Anti-mouse IgG-HRP	SC-2005	1:2000	1.4B 1.4C 1.4E
Santa Cruz Mouse Anti-goat IgG-HRP	SC-2354	1:2000	1.4D
Jackson ImmunoResearch Goat Anti-rabbit IgG-HRP	111-035-003	1:4000	1.4F
Alexa Fluor 488-conjugated f(ab') rabbit anti-goat IgG *	A-11078	1:200	1.5A 1.5B

Abbreviation: HRP, horseradish peroxidase. * Antibody and dilution used for immunocytochemistry.

78
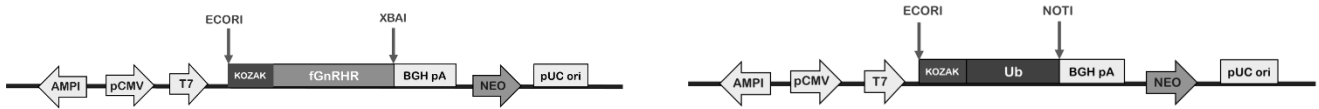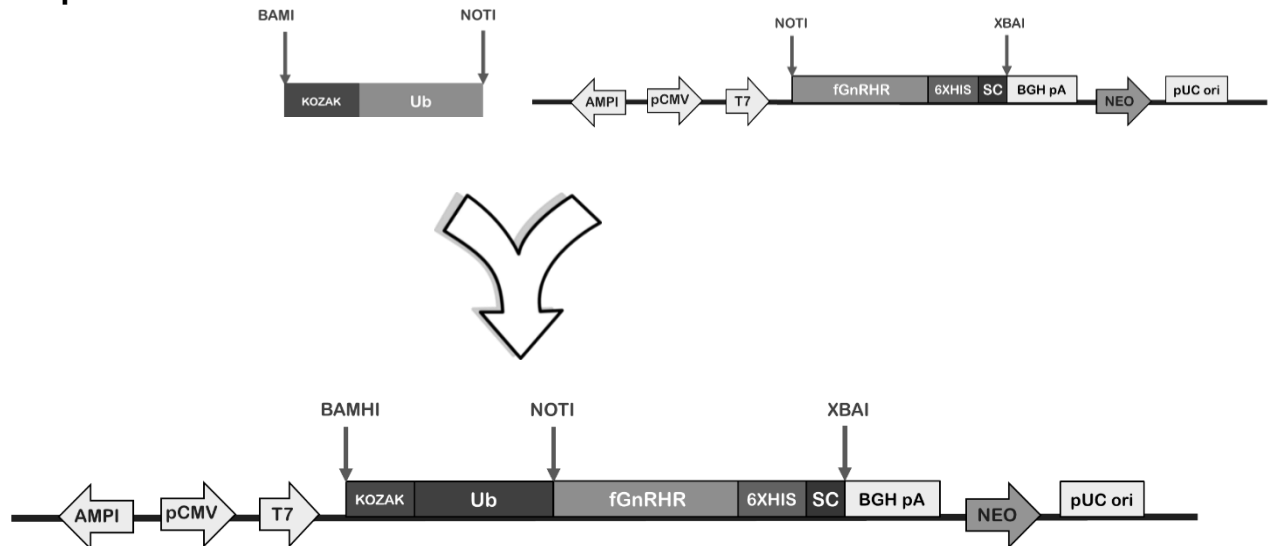
Step 1:

Step 2:

Step 3:

Figure 2.1: Construction strategy of plasmids encoding fGnRHR or Ub-fGnRHR.

Step 1: Plasmids encoding fGnRHR or Ub were constructed as templates for the plasmid-based vaccines.

Step 2: To construct a plasmid encoding Ub-fGnRHR, a modified murine *Ub* gene fragment was ligated into the BamHI and NotI restriction sites of a plasmid encoding fGnRHR (with the receptor gene inserted into NotI and XBaI restriction sites*).*

Step 3: To construct a plasmid encoding fGnRHR, the receptor gene was inserted into a pcDNA3.1 vector between restriction sites BamHI and XBaI.

Figure 2.2: Identification of fGnRHR plasmid insert by restriction endonuclease digestion.

Lane 1: 1kb DNA marker.

Lane 2: Undigested pcDNA3.1 plasmid (control).

Lane 3: Plasmid digested with BamHI restriction enzyme.

Lane 4: Plasmid digested with BamHI and XBaI restriction enzymes. The ~1 kb band represents the fGnRHR fragment.
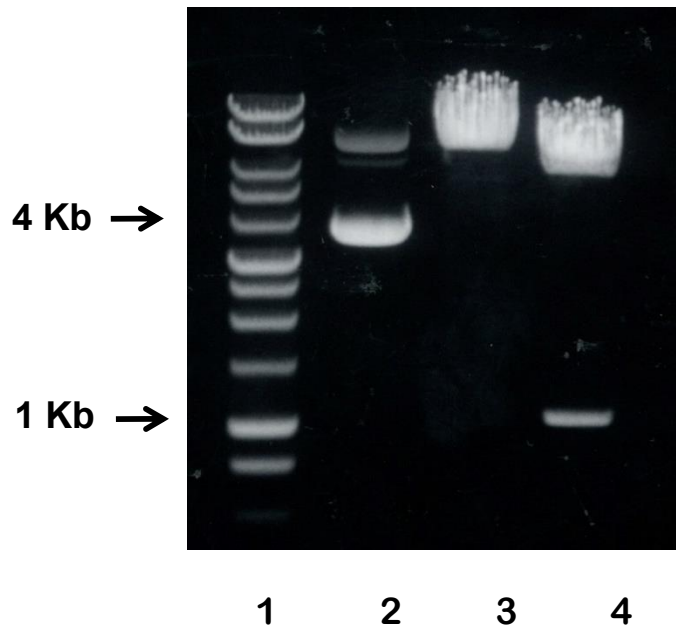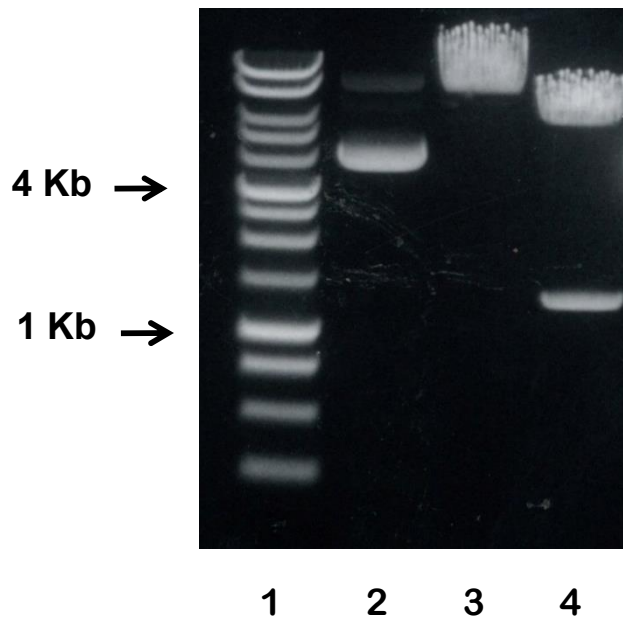
Figure 2.3: Identification of Ub-fGnRHR plasmid insert by restriction endonuclease digestion.

Lane 1: 1kb DNA marker.

Lane 2: Undigested pcDNA3.1 plasmid (control).

Lane 3: Plasmid digested with BamHI restriction enzyme.

Lane 4: Plasmid digested with BamHI and XBaI restriction enzymes. The ~1.3 kb band represents the Ub-fGnRHR fragment.
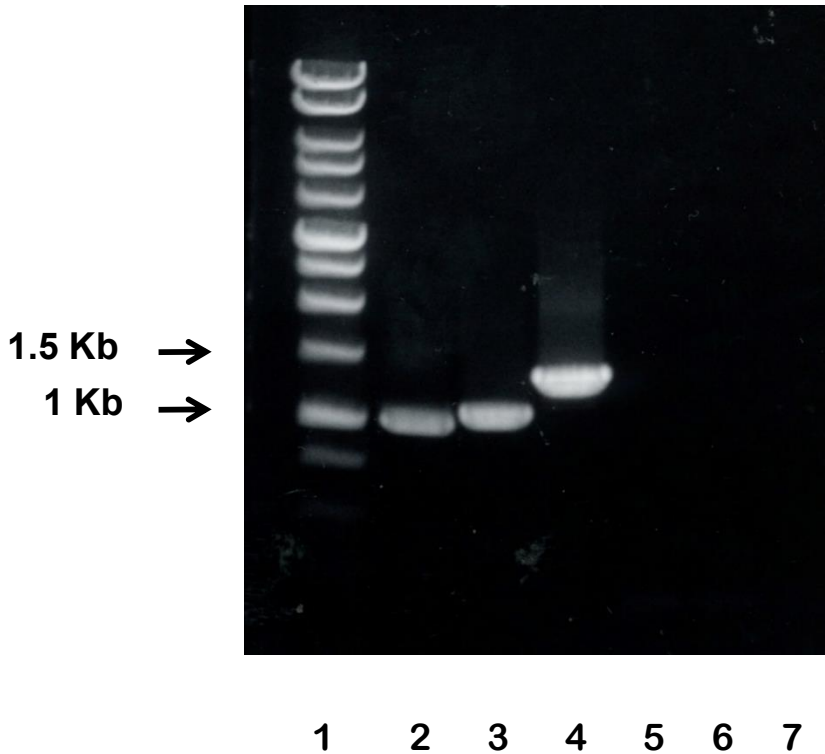
Figure 2.4: Transcriptional expression of fGnRHR or Ub-fGnRHR recombinant genes by HEK293T cells via RT-PCR.

Lane 1: 1kb DNA marker.

Lane 2: fGnRHR amplified from feline pituitary total RNA (positive control).

Lane 3: Plasmid encoding fGnRHR.

Lane 4: Plasmid encoding Ub-fGnRHR.

Lane 5: Empty plasmid (negative control).

Lane 6: Plasmid encoding fGnRHR (no reverse transcriptase control).

Lane 7: Plasmid encoding Ub-fGnRHR (no reverse transcriptase control).
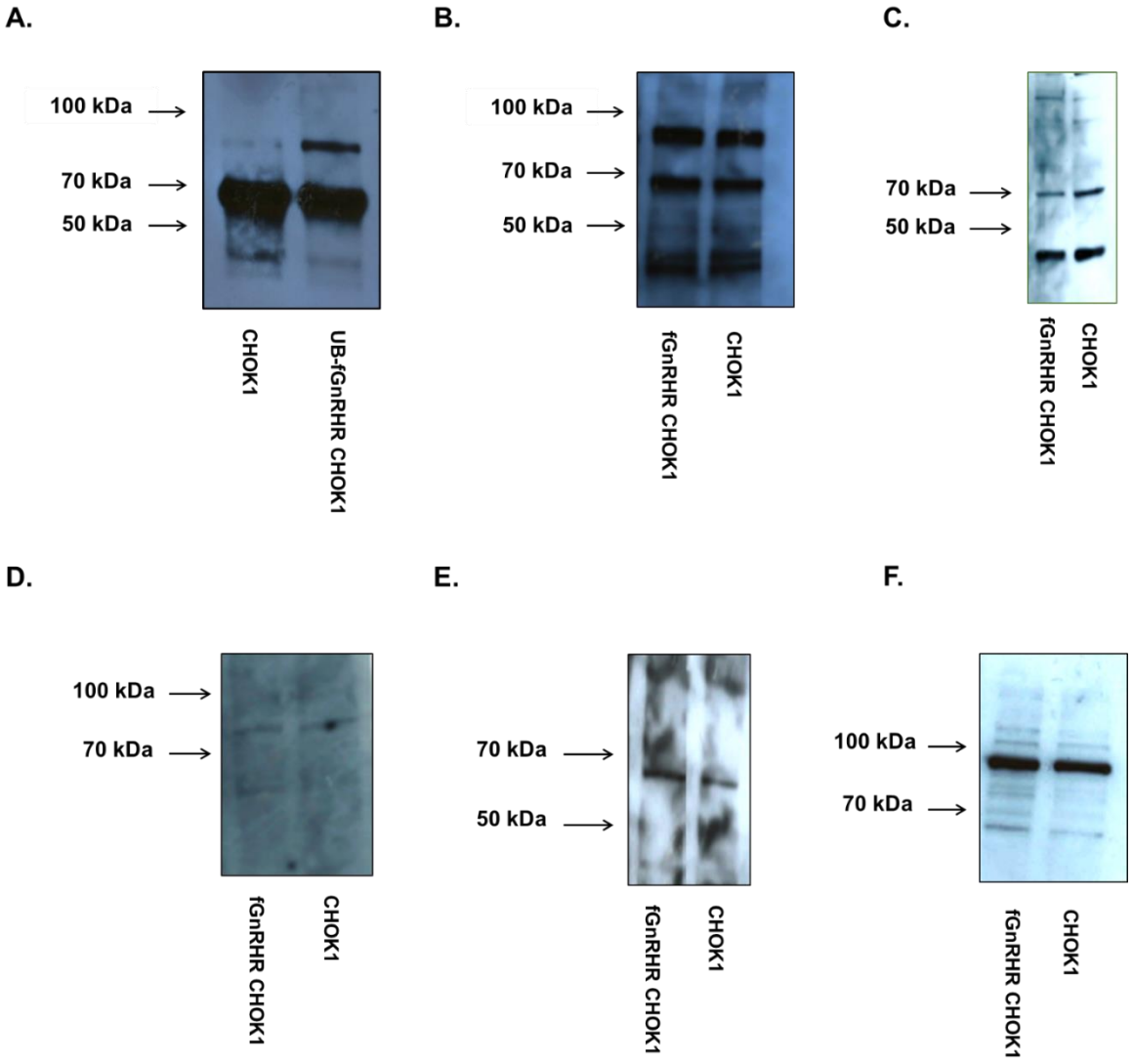
Figure 2.5: Immunoblotting for detection of fGnRHR or Ub-fGnRHR proteins in transfected CHOK1 cells. Membranes with protein from transfected cells were probed with the following primary antibodies:

A. Thermo Scientific 6XHIS;
B. Abcam hGnRHR (AA1-29);
C. Abcam hGnRHR (AA249-299);
D. Santa Cruz hGnRHR (AA1-20);
E. Fisher Scientific hGnRHR (AA1-29);
F. Custom-made Pi Proteomics fGnRHR (AA1-28).

After incubation with primary antibody, membranes were exposed to HRP-conjugated secondary antibodies. Membranes were exposed to x-ray films for visualization of proteins.

A.
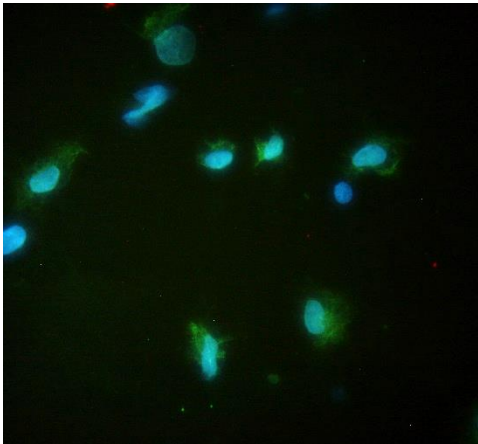
B.
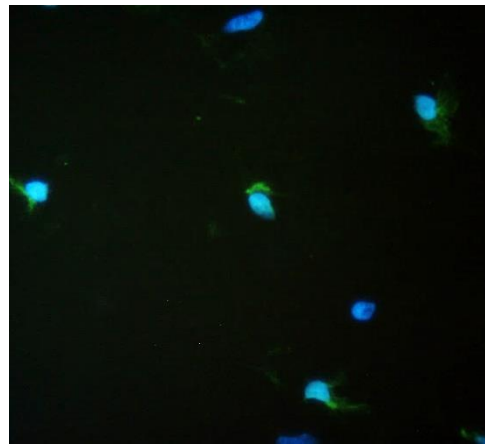
Figure 2.6: Feline (f)GnRHR immunoreactivity in transfected CHOK1 cells via immunocytochemistry. A primary antibody against the first 20 amino acids of human GnRHR was used with a green fluorophore-labeled secondary antibody to detect fGnRHR protein expression in transfected CHOK1 cells (A). Non-transfected CHOK1 cells were used as a negative control (B). Cells were exposed to mounting medium containing DAPI and immunoreactive CHOK1 cells visualized under a fluorescent microscope. No substantial difference is observed between the two representative images shown.

A.

B.
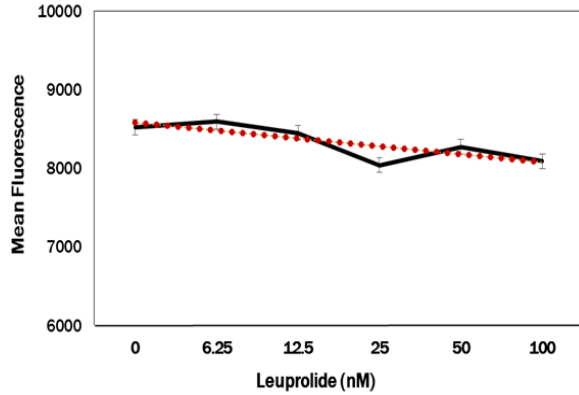
Non-tranfected HEK

fGnRHR-transfected HEK
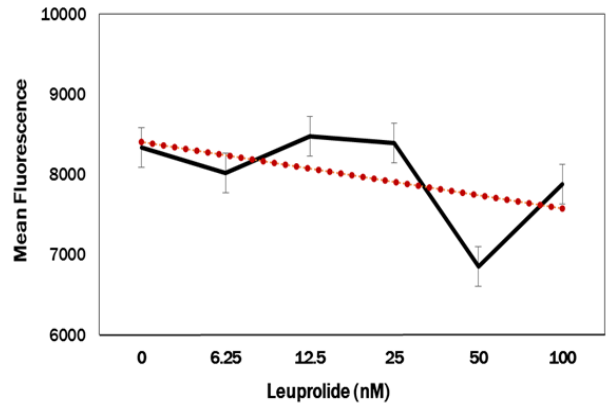
C.

Ub-fGnRHR-transfected HEK
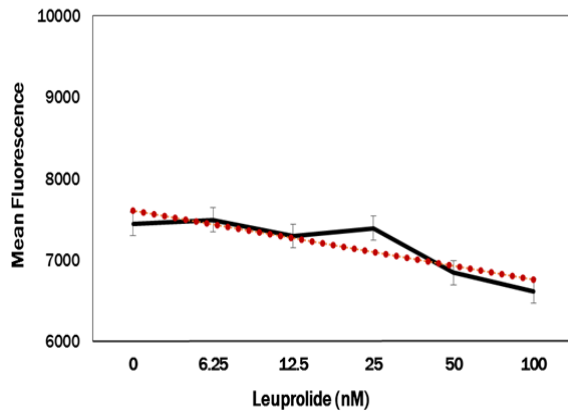
Figure 2.7: Leuprolide-induced IP1 accumulation in Human Embryonic Kidney (HEK) 293 cells transfected with fGnRHR or Ub-fGnRHR constructs. Untransfected HEK293T cells (A), or cells transfected with either fGnRHR plasmid (B) or Ub-fGnRHR plasmid (C) were treated with the different concentrations of leuprolide (GnRH agonist). Following treatments, cells were lysed and HTRF emissions were measured as a function of IP1 accumulation in cells. Results shown are the means ± SEM. * indicates a statistical difference ($P < 0.05$) compared to cells exposed to 0 nM leuprolide. Red dotted lines are trend lines.

CHAPTER 3

GENERATION AND *IN VITRO* CHARACTERIZATION OF
SUPERPARAMAGNETIC IRON OXIDE NANOPARTICLES
AS POTENTIAL DELIVERY SYSTEMS FOR DNA-BASED VACCINES

3.1 Introduction

DNA vaccination is an attractive and potentially effective strategy for eliciting

antigen-specific immune responses. However, an impediment to progress in DNA

vaccine development is low efficiency of inducing immune responses in vaccinated

animals. Factors contributing to this outcome include low cell transfection rates and

ineffective antigen expression [208]. Optimization of plasmid construction, careful

selection of an appropriate DNA-encoded protein, and the use of adjuvants are a few

examples of strategies commonly considered for improving the potency of DNA

vaccines.

One type of biocompatible delivery system that can be designed to stimulate the

immune system is based on nanoparticles. Nanoparticles are solid structures that can

be prepared from natural or synthetic polymers in various sizes less than one micron.

Because of their optical and magnetic capabilities [209,210], nanoparticles have

attracted much attention, especially in the field of drug delivery research. Indeed,

nanoparticles have the ability to deliver a wide range of small drugs, vaccines, and biological macromolecules to various areas of the body. Also, nanoparticles are capable of targeted administration to specific organs or cells for controlled drug delivery [211,212]. Studies have shown that nanoparticles delivered intramuscularly may act as an adjuvant. They stimulated increased antibody titres 6- to 10-fold in mice administered with inactivated avian influenza virus H5N2 compared to subjects administered the naked virus [213]. Intramuscular injections of nanoparticles are also known to significantly improve gene transfer [214]. Thus, coupling DNA plasmids to nanoparticles is a good strategy to enhance the immunogenicity of DNA-based vaccines.

Nanoparticles come in a variety of formulations, including poly-lactic glycolic acid particles, silica particles, gold particles, etc. One type is superparamagnetic iron oxide nanoparticles (SPIONs) containing iron oxide cores, usually magnetite, Fe_3O_4, or maghemite, γ-Fe_2O_3. Due to their composition, SPIONs have magnetic properties that allow the particles to target a specific area under the influence of external magnets. This unique physical property can be exploited for magnetofection, a principle that is associated with the application of a magnetic field to cells in order to transfect them with nucleic acids [215]. Magnetofection has been demonstrated to significantly improve the transfection rate of DNA in African monkey kidney (COS-7), hepatocellular carcinoma (HepG2), and Madin–Darby Canine Kidney (MDCK) cells without cytotoxic side effects [216,217]. With the additional benefits of inexpensive manufacturing costs and safety in animals [218,219], SPIONs represent a practical approach to enhancing intracellular delivery of DNA vaccine.

The physiochemical characteristics of SPIONs are essential to drug delivery and therefore must be considered when designing a delivery system. For example, particle shape directly influences uptake into cells, as rod-shaped particles show the highest phagocytotic rates, followed by spheres, cylinders, and cubes [220]. Although they may not have the most efficient cell internalization, spherical SPIONs provide a uniform surface area for coating or complexation of therapeutic agents. Research findings of Huang *et al.* indicated that silica nanoparticles with spherical morphology accumulated in the liver, whereas long, rod-shaped particles localized to the spleen [221]. The morphology of ferric oxide nanoparticles can be affected by several factors, including nanoparticle exposure to chemicals and conditions of the reactions performed to synthesize the polymer. In particular, amine-based surfactants with bulky hydrocarbon chains can exert steric hinderance that ultimately affects the shape of iron oxide particles during their synthesis [222]. Another important characteristic of nanoparticles is the hydrodynamic diameter, or size. The techniques most commonly employed for measuring the size of SPIONs are transmission electron microscopy and dynamic light scattering, the latter of which is based on the dispersion of the light caused by the Brownian motion of the particles [223]. SPION size greatly impacts their half-life in circulation. For example, particles greater than 200 nm in diameter concentrate in the spleen or are ingested by phagocytic cells [224]. In contrast, SPIONs smaller than 10 nm are primarily removed by renal clearance [224]. Maximizing DNA loading on SPIONs is important for their successful utilization in gene therapy applications. Thus, it is important to synthesize particles that satisfy loading capacity needs. Another

physiochemical property of SPIONs is zeta (ζ) potential, or the charge of the particle's

outermost layer of ions that originate from the dispersion medium. This parameter is

widely used to estimate the surface charge of a particle and can be measured via

dynamic electrophoretic scattering. Zeta potential is an important feature of particles

because it gives an indication of particle stability in homogenous ferrofluids. Zeta

potential also plays an important role in SPION distribution in the body, specifically

target cell internalization of nanoparticles. When dispersed in a physiological medium,

molecules absorbed onto SPION surfaces can influence the stability of the

nanoparticles. Therefore, it is important to design particles that possess a zeta potential

optimal for biological solutions. SPIONs with highly cationic or anionic zeta potentials

(i.e., ±30 mV or greater) show dispersion stability and thus do not aggregate under

normal storage conditions [225].

Surface modifications are another important parameter affecting particle behavior

in biological solutions. Indeed, nanoparticle surface chemistry greatly influences cell

recognition, biodistribution and immune response [226,227]. Magnetic iron oxide

nanoparticles lacking a surface coating have the propensity to aggregate because of the

exposed hydrophobic surfaces with large surface area to volume ratios [159]. Therefore,

the ideal surface modification must possess good biocompatibility, biodegradation and

colloid stability [228]. Accordingly, selection of surface molecules for nanoparticle

modification is important for optimal functionality in living systems. Various types of

organic or inorganic materials provide good stability in physiological buffers and

biocompatibility and thus can be utilized as surface molecules for nanoparticles

89

[144,229-231]. For example, carbohydrate-based surface coating (e.g., starch) is common for SPIONs because of its inherent affinity to iron oxide and its ability to protect the particles from the surrounding environment [232]. Also, SPIONs may be coated with starch to simulate glycoprotein-like characteristics in biological systems [232]. Low molecular weight polyethylene glycol (PEG) can be anchored on SPION surfaces to improve their viability and stability [233]. In fact, PEGylation of biocompatible drug delivery systems can enhance *in vitro* APC uptake and presentation [234,235]. SPIONs that are modified with hydrophilic polymers like PEG or biomaterials containing hydroxyl or amino functional groups, may evade *in vivo* phagocytosis by circulating macrophages, thus having better therapeutic efficacy [236]. At physiological conditions, nucleic acids are negatively charged because of the presence of phosphate groups [131]. Therefore, in order to be suitable for gene delivery, SPIONs must be modified with cationic polymers that mediate interactions with anionic nucleotides and plasma membranes. Chitosan, poly(lactic acid), dextran, dimethyldidodecyl-ammonium bromide and polyethylenimine (PEI) have all proven to be effective candidates for this purpose [237-240]. SPIONs modified with amine groups have also produced strongly cationic particles for DNA plasmid adsorption [241].

This chapter describes the synthesis of SPIONs modified with positively charged amine groups or PEG, *in vitro* characterization of SPIONs, and evaluation of their potential application as a model delivery system for DNA-based contraceptive vaccines.

3.2 Materials and Methods

3.2.1 Synthesis of aminated and PEGylated SPIONs

To begin the process of synthesizing aminated SPIONs, 2 mL of starch-coated SPION platforms (fluidMAG-D, Chemicell, Berlin, Germany) were incubated with 3 mL 5 N NaOH (VWR Sci., Hyclone, Logan, UT, USA) for 15 min at room temperature (RT). Then, 1.3 mL epichlorohydrin (VWR) was added to the SPIONs and the mixture was incubated for 24 h with shaking at RT in order to cross-link the starch coating on the nanoparticles and thus covalently strengthen particle stability. To purify SPIONs, the cross-linked product was then dialyzed five times over a 48-h period at RT against deionized water (DI H2O) using a 10 kDa float-a-lyzer G2 dialysis device (Spectrum Laboratories, Rancho Dominguez, CA, USA). The purified product was incubated with 2 mL concentrated NH_4OH (30% ammonia; VWR) for 24 h at 25ºC with shaking. After a final dialysis step, the cross-linked, aminated product was concentrated by applying the particles to a Dynal magnetic separator (Life Technologies, Carlsbad, CA) for 48 h at 4ºC and then aspirating 4 mL of supernatant.

Aminated-based, PEGylated SPIONs were generated using N-Hydroxysuccinimide (NHS) chemistry. First, 3 mL of aminated SPIONs (concentration: 322.18 mg Fe/mL) were added to a mixture of 1.35 mL dimethyl sulfoxide (DMSO; VWR), 1.35 mL phosphate buffer saline (PBS; pH: 8.01; Corning, Corning, NY, USA) and 67.5 mg 5kDa methoxyl (m)PEG-NHS (Nanocs, Boston, MA, USA). NHS-functionalized mPEG is an amino reactive PEG derivative that can be used to modify surfaces with available amino groups. The mixture was incubated at RT for 4 h with

91

shaking. At the completion of the synthesis, the reaction mixture was diluted with 2 mL

DI H2O, and then placed on a magnetic separator for 48 h at 4ºC. Finally, the

PEGylated SPIONs were washed four times with fresh DI H2O.

3.2.2 Characterization of Aminated and PEGylated SPIONs

3.2.2.1 Measurement of iron content in aminated and PEGylated SPIONs

A standard ferrozine assay was used to quantitatively characterize the iron

content of aminated and PEGylated SPIONs. The assay included 0.0075, 0.02, 0.05,

0.1, 0.15, 0.2, and 0.25 mg/mL of iron standard (Sigma-Aldrich, St. Louis, MO, USA) to

create a standard curve for interpolating data from the SPION samples. Triplicate

samples of aminated and PEGylated SPION stock suspensions were diluted 1:4000

with 10 mM HCl and 200 µL were aliquoted into a Fluotrac 24-well plate (Sigma-

Aldrich). Then, 200 µL 50 mM NaOH were added to each well. Next, equal parts 4.5%

$KMnO_4$ and 1.4 M HCl were combined and 200 µL of the mixture were added to all

wells. The plate was vortexed for 1 min at 650 revolutions per minute (RPM) at RT,

sealed with aluminum foil, incubated for 2 h at 60ºC, followed by cooling the plate to RT

for 10 min. Then, 9.95 mg ferrozine, 5.12 mg neocuproine (Thermo Scientific, Waltham,

MA, USA), 578 mg ammonium acetate (Alfa Aesar, Ward Hill, MA, USA), 528 mg

ascorbic acid (BDH Chemicals, Poole Dorset, UK), and 3 mL deionized water was

mixed together and 60 µL of the ferrozine-based solution was added to each well. After

incubating the plate for 30 min at RT, 280 µL sample from each well was transferred

into a 96-well plate (Sigma-Aldrich) that was inserted into a SpectraMax i3 plate reader

(GE, Fairfield, CT, USA) for measurement of fluorescence at 400/460 nm.

3.2.2.2   Measurement of amine content in aminated and PEGylated SPIONs

A standard fluorescamine assay was used to quantitatively characterize the amine content of aminated and PEGylated SPIONs. The assay included 0.1, 0.2, 0.4, 0.8, and 1.25 mM of ethanolamine (Alfa Aesar) to create a standard curve for interpolating data from the SPION samples. Triplicate samples of aminated and PEGylated SPION stock suspensions were diluted to 0.25 mg Fe/mL and 250 µL of each SPION type were aliquoted into a black, 96-well plate (Sigma-Aldrich). Then, 50 µL fluorescamine (concentration: 3 mg/mL in dimethyl sulfoxide) were added to each SPION and standard well. After brief mixing, the plate was incubate for 10 min at RT. Samples were transferred into light-blocking, 1.5 mL Eppendorf tubes that were centrifuged for 24 min at 14000 RPM at RT. Finally, 200 µL of the supernatant from each tube was transferred into a new black, 96-well plate that was inserted into a SpectraMax i3 plate reader for measurement of fluorescence signals at a setting of 400/460 nm.

3.2.2.3   Size distribution and zeta potential of aminated and PEGylated SPIONs

The intensity-weighted size (or hydrodynamic diameter) distributions and zeta potential of aminated and PEGylated SPIONs were measured by dynamic light scattering using a Malvern ZetaSizer Nano ZS90 particle-sizing instrument (Malvern, Worcestershire, UK). First, SPION suspensions were diluted (1 µL SPIONs in 999 µL DI H_2O) and the 1 mL sample was applied to a DTS1070 folded capillary cell (Malvern). Capillary cells were placed into the particle-sizer and SPION size distribution and measurements were taken in triplicate under the following parameter settings: material:

iron oxide nanoparticles (refractive index: 2.42; absorption: 0.05); measurement: 173º

backscatter; number of classes: 300; lower limit: 0.4; upper limit: 1000; equilibration

time: 0 sec. Zeta potential measurements were taken in triplicate under the following

new or changed parameter settings: equilibration time: 120 sec; minimum number or

runs: 10; maximum number or runs: 10.

3.2.2.4   Transmission electron microscopic imaging of aminated and PEGylated

SPIONs

A Zeiss 10A conventional transmission electron microscope (tem; Jena,

Germany) was used to capture images of aminated and PEGylated SPIONs. In

preparation for TEM analysis, 300 mesh, formvar-carbon copper grids (Ted Pella,

Redding, CA) were placed onto pieces of parafilm and 7 µL diluted, aminated or

PEGylated SPION dispersions were applied to the grids. After 15 min of ambient drying,

SPION-loaded grids were placed into sample holder, which was then paired with the

specimen stage. Images were captured on the electron microscope operating at an

accelerating voltage of 200 KV and a magnification of 160K.

3.2.3 DNA plasmid loading capacity of aminated and PEGylated SPIONs

To determine the loading capacity of SPIONs with plasmid DNA, pcDNA3.1

vector (Invitrogen, Carlsbad, CA, USA) was immobilized to the surface of SPIONs. In a

1.5mL Eppendorf tube (Hamburg, Germany), 4 mg aminated or PEGylated SPIONs

were incubated with 400 µg pcDNA3.1 vector (10:1 ratio). After suspensions were

quantum satis to 400 µL with PBS, samples were mixed via rotation for 35 min at RT.

Then, DNA-nanoparticle preparations were subjected to magnetic separation for 6 h at RT. A 2 µL sample of the resulting supernatant was evaluated for the concentration of unadsorbed DNA determined by absorbance at 260 nm using NanoDrop 2000 equipment (Thermo Scientific, Waltham, MA, USA). The plasmid DNA loading capacity of SPIONs was calculated from the depletion of DNA from the supernatant after adsorption and magnetic separation.

3.2.4 *In vitro* study of DNA release from aminated and PEGylated SPIONs

The *in vitro* release of DNA was estimated by incubating the aminated or PEGylated SPIONs with pcDNA3.1 vector (1:7 ratio) in PBS. Once the DNA loading capacity of SPION formulations at day 0 was determined, suspensions were incubated at 37ºC. At time points day 1, 3, 7, 14 and 21, and 30, SPIONs were applied to a magnetic separator at 37ºC for 6 h. After magnetic separation at each time point, a 2 µL sample of the resulting supernatant was evaluated for the concentration of unadsorbed DNA. The amount of DNA that remained absorbed to SPIONs was calculated from the depletion of DNA from the supernatant after adsorption and magnetic separation.

3.2.5 Viability of human embryonic kidney (HEK)293 cells exposed to aminated or PEGylated SPIONs

The effects of aminated and PEGylated SPIONs on HEK 293 cell viability were explored using an MTT [3-(4,5-dimethylthiazol-2-yl)-2,5-diphenyltetrazolium bromide] colorimetric assay. First, HEK293T cells (CRL-11268, ATCC) were cultured for 48 h at 37ºC in 15 mL Dulbecco's modified eagle medium (DMEM; Corning) with 10%

fetal bovine serum (FBS; VWR) and 1% penicillin-streptomycin (P/S; Mediatech, Inc.,

Manassas, VA, USA) in 75 cm^2 flasks (Corning). Once 80% confluency was reached,

media was aspirated and cells were washed with 13 mL Hank's Balanced Salt Solution

(HBSS; Corning) for 5 min at RT. HBSS was aspirated and the cells were incubated

with 0.25% trypsin (Corning) for 15 min at 37ºC. Trypsinized cells were neutralized with

10% FBS, collected, and centrifuged at 300 g for 10 min at RT. Supernatant was

aspirated, the cell pellet was suspended in 1 mL DMEM media. Ten microliters of cell

suspension was added to 90 µL trypan blue (Sigma-Aldrich) and cells were counted

using a hemocytometer.

HEK293 cells (5X10^3) were seeded into a clear, 96-well plate (Corning) with 100

µL DMEM supplemented with 1% P/S. Twenty-four hours later, media was replenished

and cells were incubated with 0, 2.5, or 4 mg aminated or PEGylated SPIONs for 60 h

at 37ºC. HEK293 cells exposed to apoptotic agent staurosporine (10% v/v) were also

included in the assay as a positive control. Next, cells were incubated with 20 µL MTT

(5 mg/mL, VWR) for 6 h at 37ºC. Then the MTT treatment was aspirated and cells were

incubated with 150 µL DMSO for 30 min at RT with shaking. Finally, absorbance was

measured at 550nm using a Biotek plate reader and cell viability percentage was

calculated. Untreated cells served as 100% cell viability.

3.2.6   Statistical analysis

Data are presented as the mean ± standard error of the mean. Zeta potential,

hydrodynamic diameter, DNA concentration measurements, and MTT assay

absorbance measurements were performed in triplicate. MTT assay data were analyzed by one-way analysis of variance followed by Tukey test for multiple group comparisons (SPSS, Inc.). Differences of $P \leq 0.05$ were considered significant.

3.3 Results

Starch-coated, magnetic nanoparticles were cross-linked and then modified with cationic amine groups for surface tethering of DNA. Using a ferrozine assay, the iron content of the amino-modified particles was measured as 322.17 ± 11.65 mg Fe/mL (Table 3.1). An ethanolamine assay measured the amine concentration as 0.098 ± 0.0003 mM (Table 3.1). Dynamic light scattering technology determined that the average hydrodynamic diameter of aminated SPIONs was 178.27 ± 2.91 nm (Table 3.1, Fig. 3.1A). The mean zeta potential of these SPIONs was measured as 28.30 ± 1.71 mV (Table 3.1, Fig. 3.1B). TEM images revealed that the aminated SPION magnetite cores have spherical morphology and the core-shell nanostructures typically contained approximately twenty Fe_3O_4 particles encapsulated within the starch shell (Fig. 3.1C). Also, minor aggregation and colloidal instability was observed for aminated SPIONs. Incubation of aminated SPIONs with DNA plasmid increased the average hydrodynamic diameter to 203.0 ± 2.53 nm (Table 3.1, Fig. 3.2A). The augmented particle size and the drastic shift in average zeta potential from a cationic value to a strongly anionic value of -45.40 ± 1.96 mV both indicate successful DNA absorption on the particles (Table 3.1, Fig. 3.2B). The DNA loading capacity for the aminated SPIONs was measured as 50.77 ± 0.15 µg per mg of SPIONs (Table 3.1). Micrographs indicated that post DNA vector adsorption and magnetic separation treatments, particle morphology was preserved but

97

particle aggregation was exacerbated into irreversible agglomeration and thus colloidal instability was observed (Fig. 3.2C).

NHS chemistry was performed to synthesize 5 kDa PEGylated SPIONs from aminated particle precursors. The iron concentration of the PEGylated nanoparticles was measured as 148.46 ± 9.27 mg Fe/mL and the amine content was determined as 0.092 ± 0.0002 mM (Table 3.1). PEGylation of the aminated SPIONs resulted in slightly larger particles with a lower positive charge, as the hydrodynamic diameter and zeta potential averaged 185.0 ± 0.54 nm and 19.7 ± 2.08 mV, respectively (Table 3.1; Fig. 3.3A, 3.3B). Transmission electron micrographs indicated that PEGylated SPIONs magnetite cores have spherical morphology (Fig. 3.3C). In addition, observations of nanoparticles in suspension and consistent hydrodynamic diameter over a 30-day period indicated colloidal stability. PEGylated SPION hydrodynamic diameter increased to 212.6 ± 0.17 nm after incubation with plasmid DNA (Table 1, Fig. 3.4A). In addition, the average zeta potential of these DNA-treated particles dramatically decreased to -46.0 ± 1.52 mV (Table 1, Fig. 3.4B). The DNA loading capacity of the PEGylated SPION preparation was determined as 43.99 ± 0.28 µg per mg of SPIONs (Table 3.1). Surface tethering of DNA had no impact on magnetite core morphology (Fig. 3.4C), particle size, or colloidal stability.

Cumulative *in vitro* release rates of plasmid DNA from PEGylated and aminated SPIONs were measured at various time points over a 30-day period (Fig. 3.5). Studies of aminated particles indicated that approximately 1.7% of DNA was released by day 1.

There was less than a 1% increase in released DNA over the following 29 days, resulting in only 2.6 ± 0.03 % of DNA released from the aminated particles over the 30-day period. In contrast, approximately 15.5% of DNA was released from PEGylated SPIONs by day 1. There was only a 1% increase in released DNA by day 3 compared to day 1. The amount of plasmid DNA release between day 3 and 14 was no more than 0.05%. However, an additional 3% of DNA was released from PEGylated SPIONs by day 21. From day 21 through 30, 5% of additional DNA was release from the particle surfaces. Overall, 24.2 ± 0.73 % of plasmid DNA was released from PEGylated SPIONs within a 30-day period.

It was important to assess the cytotoxic capabilities of the synthesized SPIONs, as iron accumulation in cells can lead to iron toxicity. The effects of aminated or PEGylated SPION exposure to HEK293 cell survival was determined by MTT assay (Fig. 3.6). Percentages of viable cells incubated with 2.5 mg/mL, 10 mg/mL, or 40 mg/mL PEGylated SPIONs were similar to untreated cells (P > 0.05). The same outcome was observed for HEK293 cells treated with the same concentrations of aminated SPIONs (P > 0.05). Cells treated with cytotoxic agent staurosporine were used as a positive control.

3.4 Discussion

The ideal delivery vehicle for DNA-based vaccines would possess biocompatible and biodegradable properties, the capability for controlled delivery of DNA for accumulation in specific tissues or cells, and adjuvant-like effects to enhance and

prolong antigen-specific immune responses [242]. Nanoparticles have these characteristics and, therefore, are being widely explored as carriers of plasmid DNA. In particular, SPIONs have drawn considerable attention in nuclei acid biotherapeutic delivery research because their unique magnetic properties are suitable for substrate-mediated cellular internalization of immobilized DNA.

Here, SPIONs were characterized for their potential as nanocarriers of pcDNA3.1 vector, the platform for immunocontraceptives described in the previous chapter of this work. The hydroxyl functional groups from the starch coating on the SPION platforms provide for additional modifications and have been demonstrated to be useful for drug targeting [243-245]. Positively-charged amine groups were conjugated to cross-linked SPIONs for binding of DNA. It was important to assess the physiochemical properties of the aminated SPIONs, as they are essential to nanoparticle interaction with biological systems and thus influence DNA delivery outcomes. Aminated SPIONs were characterized as having an average zeta potential of ~ +28 mV, a value close to that of strongly cationic nanoparticles (i.e., zeta potential > +30 mV) [246]. The mean hydrodynamic diameter of the aminated SPIONs (~ 178 nm) was on the lower end of typical nanoparticle size spectrum (50 nm-700 nm) but suitable for DNA immobilization, deep penetration into tissues, and efficient uptake by cells [247]. Successful DNA loading of the aminated SPIONs was confirmed by a drastic shift to a strongly anionic zeta potential of -45 mV and increased particle size to 203 nm. Anionic particles are a favorable characteristic for APC uptake, as SPIONs with high surface charge (positive or negative) are more likely phagocytosed than neutrally-charged SPIONs [225]. It is

known that positively-charged scavenger receptors on macrophages recognize negatively-charged particles [248]. Thus, anionic and spherical particles can potentially bind to available cationic sites on macrophage surfaces [248]. The loading capacity of amino-modified SPIONs for DNA plasmid was measured as 50.81 µg mg^{-1}. Reports of adsorption capacities for polymers vary greatly and include 6.04 µg per mg 25 kDa PEI-conjugated poly(lactic-co-glycolic acid) microparticles [249], and 89 µg per mg amino-modified, silica-coated magnetic nanoparticles [250]. DNA immunization of companion animals usually does not exceed microgram dosage, as vaccine research studies commonly vaccinate cats and dogs with 400 µg DNA total [51,251]. The reason for the high dosage of DNA is most likely due to estimations that less than 0.01% of plasmid injected into muscle is taken up by and expressed in muscle cells [252-254]. This is due to the fact that the majority of injected "naked" plasmid is degraded by extracellular nucleases and/or removed from muscle via the lymphatic system and thus only nanograms of DNA is intracellularly delivered [255]. Because cationic polymers can facilitate plasmid DNA uptake and transfection *in vitro* and *in vivo*, the synthesized aminated SPIONs are expected to deliver micrograms of DNA to target cells [256].

Nanoparticles having high positive or negative zeta potential show consistent dispersion stability in suspension [257]. This was the case for pre- and post-DNA-loaded aminated SPIONs. However, the colloidal stability of the aminated SPIONs was poor when the particles were suspended in PBS and subjected to magnetic separation. Particle aggregates or agglomerates formed followed by irreversible sedimentation as a result of these treatments. Further, TEM images confirmed that aminated SPIONs are

inclined to cluster post-magnet treatments and suspension in PBS. On a molecular level, aggregates result from the formation of strong bonds between nanoparticles [258]. Aggregates differ from agglomerates in that the latter are loose bonds between individual nanoparticles or aggregates acting under weak forces such as van der Waals forces [258]. Further, aggregates and agglomerates occur in suspensions when the van der Waals attractive forces between particles are larger than the electrostatic repulsive forces [258]. Most nanoparticles tend to aggregate in biological solutions such as blood, saliva, and cell culture media, thus increasing their overall size [258]. In particular, amine groups, whether as lone functional groups or as part of amino acids, have been shown to cause particle aggregation [259-261]. Nanoparticles that aggregate prior to binding to the membranes of APCs have endocytotic patterns that differ from those of individual nanoparticles [258,262,263]. Indeed, aminated SPIONs with a hydrodynamic diameter significantly greater than the size of dendritic cells and macrophages make phagocytosis impossible. Furthermore, the surface chemistry of nanoparticles dictates their behavior in biological media, as biomolecules dynamically attach and detach to the nanoparticle surface [258]. In particular, sodium chloride (NaCl), a common component of cell culture media and PBS solutions, can stabilize electrostatic forces on nanoparticle surfaces, causing van der Waals forces to drive the formation of agglomerates or aggregates [258]. Thus, in the current study, the aggregation of aminated particles in PBS suspension may be due to interactions with NaCl.

Molecular interactions between the vector and the polymer determine vector binding or release from delivery vehicles [250]. Specifically, negatively-charged nucleic

acids interact with polymeric biomaterials through nonspecific mechanisms, including hydrophobic, electrostatic, and van der Waals interactions [250]. In this study, aggregation patterns were exacerbated after DNA loading. This was an unexpected observation, as DNA has been shown to reduce ionic strength, thereby stabilizing particles and preventing them from aggregation or agglomeration in the biological solutions [258]. With a macromolecule like DNA, there is the potential for a single molecule to bind to the surface of more than one particle and thus promote agglomeration. Adjusting DNA concentrations can counter this undesired effect. In this work, studies of cumulative *in vitro* release rate of plasmid DNA from aminated SPIONs determined that approximately 2.6% of DNA was released over a 30-day period. This low DNA release rate is very likely a consequence of the aminated SPION aggregates that potentially trapped DNA inside the complexes and, thus, interfered with its release. The aggregation properties and extremely low DNA release rate of aminated SPIONs are undesirable for vaccine applications. Indeed, a DNA-based immunocontraceptive coupled to a SPION delivery system should have a higher DNA release rate than ~3% per month in order to have an immediate effect on reproductive capabilities of an animal. Thus, it was important to synthesize alternative particles that have better colloidal stability and DNA delivery properties.

Aminated SPIONs were modified with 5 kDa PEG to mask some of the surface charge, improve particle stability, and possibly enhance the plasmid DNA release rate. Although PEGylated SPIONs were characterized as having a less cationic zeta potential (~ +20 mV) and a slightly larger hydrodynamic diameter (~ 178 nm) than aminated

103

particles, these properties are suitable for immobilization of negatively-charged DNA. In the absence of any treatment, PEGylated SPIONs maintained good dispersion and colloidal stability in PBS suspension. Although PEGylated particles form aggregates after subjected to an external magnetic field, the aggregates were reversible after gentle vortexing or trituration. This outcome was expected, as pre-coating of nanoparticle surfaces with stabilizing molecules such as PEG or albumin has been utilized to increase steric stabilization and thus prevent nanoparticles from aggregation in biological solutions [241,258].

DNA length, salt concentration, particle size, surface modification, and charge density play crucial roles in the complexation of DNA to positively charged nanoparticles [264]. In addition, DNA spatial conformation is influential to its adsorption to nanoparticles [264]. In aqueous solutions, DNA molecules conform to an elongated coil due to the strong repulsion between negatively charged phosphate groups [250]. The length of the commonly used vector DNA (e.g., plasmid) and genomic DNA is at least several hundred nanometers long, while the diameters of nanoparticles are generally much smaller than 300nm. Consequently, combining plasmid DNA with magnetic nanoparticles results in DNA molecules wrapping around the particle, thus occupying most of the surface binding sites on a single nanoparticle or stretching out to associate with several nanoparticles. As a result, there is a limited number of DNA molecules that can be absorbed on each nanoparticle. It is important to note that regardless of mechanism, there is always a limit to a particle's loading capacity that is determined by surface area. Further, PEGylation of nanoparticle surfaces would reduce the loading

capacity, since PEG requires some space as well. PEGylation, however, may improve

other properties. It is important to maximize particle surface especially for transfection

applications, where DNA loading capacity is directly related to therapeutic outcomes.

Also, it is critical to consider techniques, such as particle PEGylation, for enhancing

DNA loading capacity during complexation on positively charged SPIONs. Similar to

aminated particles, successful DNA loading of PEGylated SPIONs was confirmed by a

drastic shift to a strongly anionic zeta potential (~ -45 mV) and increased particle size (~

212 nm). The DNA loading capacity of PEGylated particles was determined as 43.99 µg

mg^{-1}, an absorption value lower than that of amino-modified SPIONs. This was

expected for particles with a lower positive charge. Studies have shown that the DNA

absorption capacity of amino-modified magnetic nanoparticles can be greatly improved

if DNA is pre-treated with condensing agents, such as PEG, prior to incubation with

particles. This pre-treatment causes the conformation of DNA molecules to transition

from an elongated coil state to a highly dense and compact state with a globular shape

[265,266]. Thus, the anionic phosphate groups that comprise DNA are considerably

shielded, making fewer sites available for cationic nanoparticle binding. Further, this

eliminates DNA coiling around the nanoparticle surface. Instead, only a small portion of

each DNA globule has electrostatic interactions with the SPIONs; this allows several

DNA globules to potentially be adsorbed, thus enhancing overall DNA loading capacity

for particles. One study taking advantage of the physiochemical properties of PEG-

treated DNA demonstrated that the loading levels of amino-modified, silica-coated

magnetic nanoparticles with condensed DNA four times greater than that of elongated,

coiled DNA, with final loading capacity of 385 µg mg^{-1} [250]. Application of this

105

technique may improve the DNA absorption of SPION platforms and DNA release profile while preserving particle colloidal stability observed with PEGylated SPIONs.

Release rate studies showed that within a 30-day period, 24.2% of immobilized DNA complexes was released from PEGylated SPIONs surfaces, with 15.5% of DNA released by day one. Studies by Segura's group had similar outcomes, as 25% of plasmid DNA were released over an eight-day period, with approximately 15% released within the first 24 h [267,268]. The capability of the PEGylated particles to revert back to homogenous suspensions most likely played a role in the higher plasmid DNA release rate from PEGylated SPIONs compared to aminated particles. It is important to emphasize that approximately a quarter of loaded plasmid DNA was released from the PEGylated SPIONs. Having most of the DNA continue to be bound to the nanoparticles may be a beneficial characteristic for vaccine delivery systems. First, efficient uptake of SPIONs by DCs facilitates increased transfection of these cells with plasmid DNA. Second, the release of the remaining plasmid DNA from the PEGylated SPIONs at a later time may have a booster effect, thereby making a multiple vaccination schedule unnecessary. This is valuable for vaccinating feral animals that allow very few opportunities to be captured and treated. Also, a DNA vaccine delivery system with a built-in, 2-in-1 boostering capabilities is useful for animals in shelters with restrictive financial budgets.

3.5 Conclusion

In essence, aminated SPIONs and PEGylated SPIONS were synthesized, loaded with plasmid DNA, and evaluated for their potential use as delivery systems for DNA-based vaccines. Characterization of both SPIONs suggests that PEGylated SPIONs are preferred candidates for plasmid DNA delivery. Thus, studies evaluating the contraceptive potentials of DNA-based contraceptive vaccines loaded onto PEGylated SPIONs for *in vivo* delivery were warranted.

Table 3.1

Characterization of aminated and PEGylated SPIONs

SPION Type	[Fe] (mg/mL)	[NH2] (mM)	Hydrodynamic Diameter (nm)		Zeta Potential (mV)		DNA Loading Capacity (µg mg^{-1})	DNA Released (% Total)
			- DNA	+ DNA	- DNA	+ DNA		
Aminated	322.17 ± 11.65	0.098 ± 0.0003	178.27 ± 2.91	203.0 ± 2.53	28.30 ± 1.71	-45.40 ± 1.96	50.77 ± 0.15	2.6 ± 0.03
PEGylated	148.46 ± 9.27	0.092 ± 0.0002	185.0 ± 0.54	212.6 ± 0.17	19.7 ± 2.08	-46.0 ± 1.52	43.99 ± 0.28	24.2 ± 0.73

Abbreviations: PEG, polyethylene glycol; SPION, superparamagnetic iron oxide nanoparticles

A.
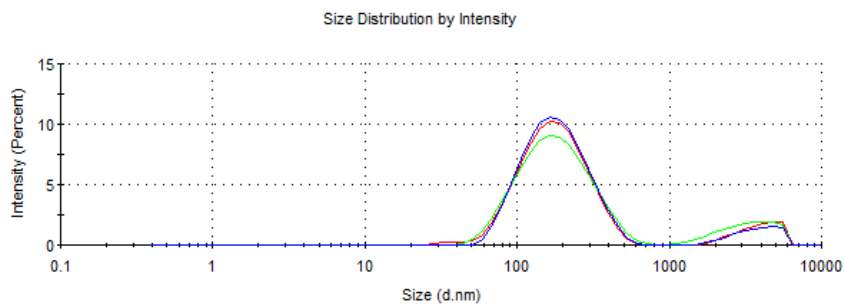
B.
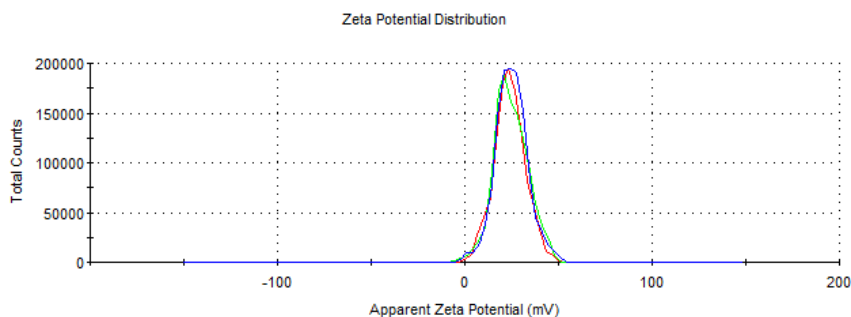
C.

Figure 3.1: Characterization of aminated SPIONs. Hydrodynamic diameter and zeta potential measurements (mean ± SEM) were taken in triplicate from very dilute SPION suspensions in deionized water. SPION size averaged 178.27 ± 2.91 nm (A) and the mean zeta potential was measured as 28.30 ± 1.71 mV (B). Transmission electron micrographs indicated SPION morphology in PBS suspension (C, magnification: 160K).

A.

B.

C.

Figure 3.2: Characterization of aminated SPIONs loaded with plasmid DNA. Hydrodynamic diameter and zeta potential measurements (mean ± SEM) were taken in triplicate from very dilute SPION suspensions in deionized water. DNA-loaded, aminated SPION size averaged 203.3 ± 2.53 nm (A) and particle charge was measured as -45.40 ± 1.96 mV (B). Transmission electron micrographs indicated DNA-SPION morphology in a PBS suspension (C, magnification: 160K).
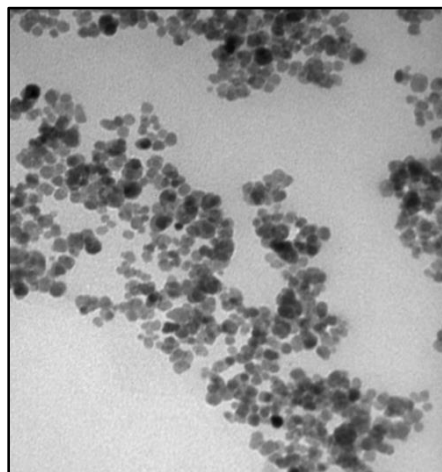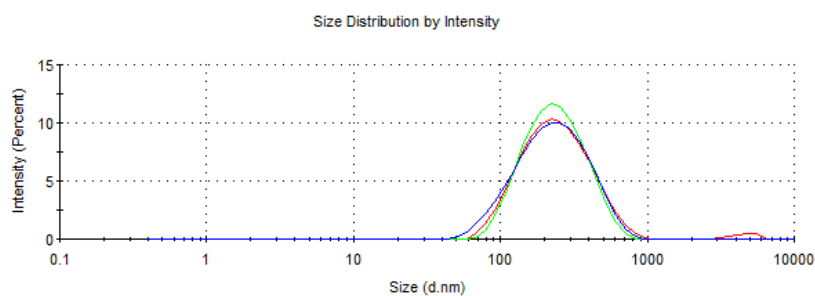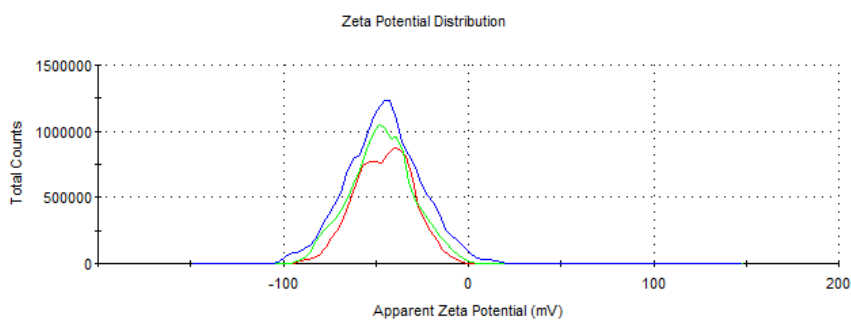
A.
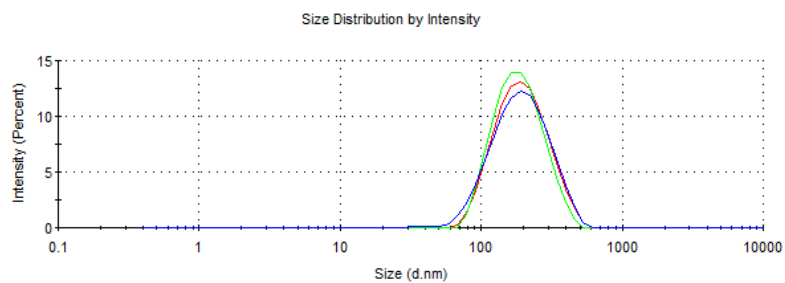
B.
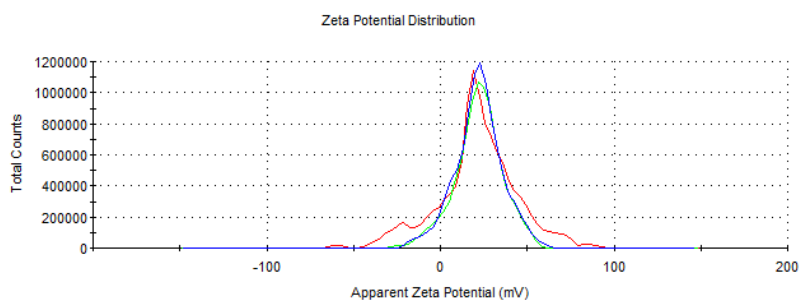
C.
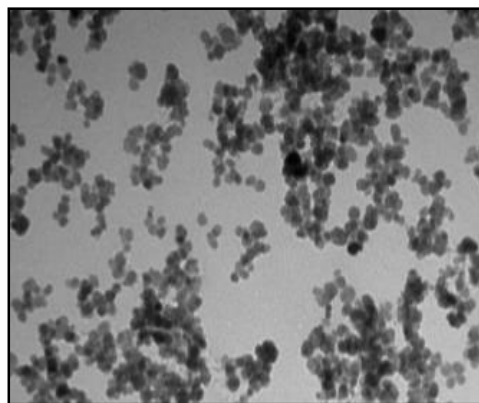
Figure 3.3: Characterization of PEGylated SPIONs. Hydrodynamic diameter and zeta potential measurements (mean ± SEM) were taken in triplicate from very dilute SPION suspensions in deionized water. SPION size averaged 185.0 ± 0.54 nm (A) and particle charge was measured as 19.70 ± 2.08 mV (B). Transmission electron micrographs indicated SPION morphology in PBS suspension (C, magnification: 160K).
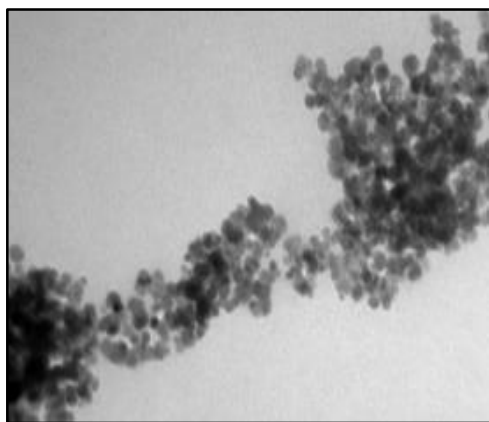
A.
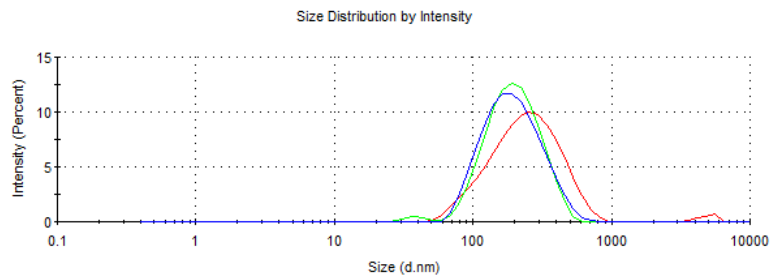
B.
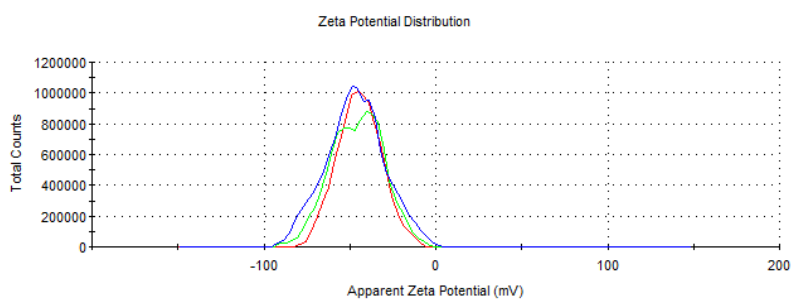
C.
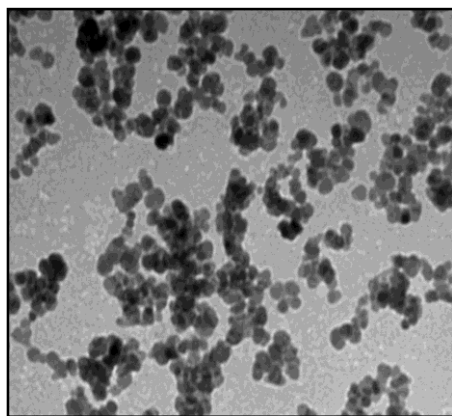
Figure 3.4: Characterization of PEGylated SPIONs loaded with plasmid DNA. Hydrodynamic diameter and zeta potential measurements (mean ± SEM) were taken in triplicate from very dilute SPION suspensions in deionized water. DNA-loaded, PEGylated SPION size averaged 212.6 ± 0.17 nm (A) and particle charge was measured as -46.0 ± 1.42 mV (B). Transmission electron micrographs indicated SPION morphology in PBS suspension (C, magnification: 160K).
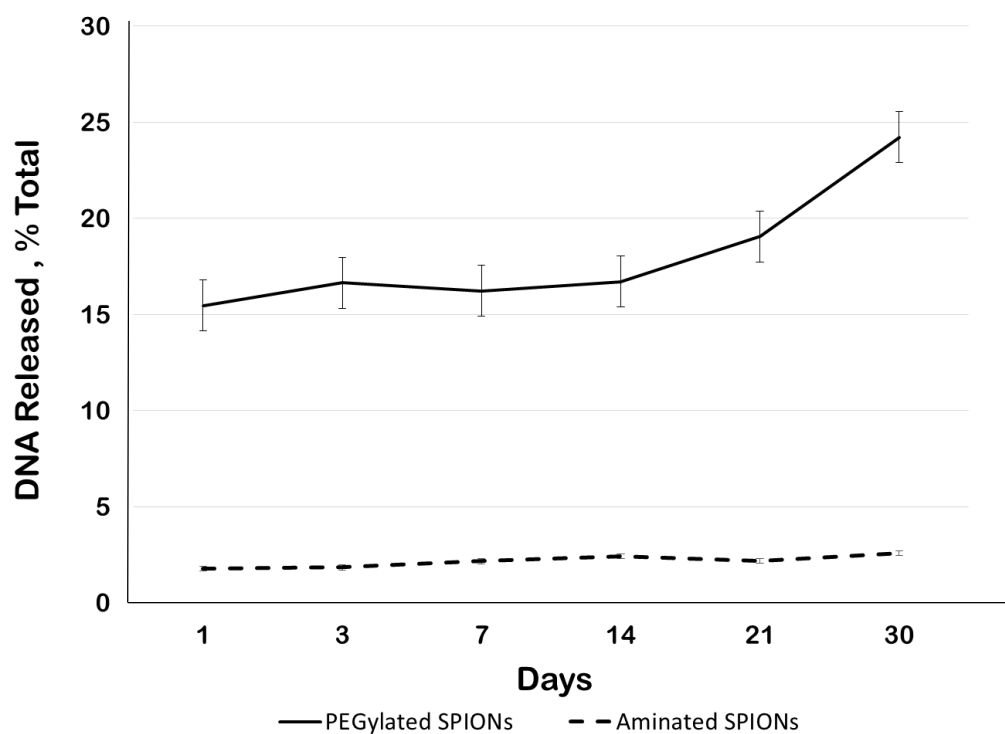
Figure 3.5: Cumulative *in vitro* release rate of plasmid DNA from aminated and PEGylated SPIONs. SPIONs were loaded with DNA and suspensions were incubated at 37ºC. At different time points, SPIONs were applied to a magnetic separator and the resulting supernatant was evaluated for DNA content. Over a 30-day period, 2.6% plasmid DNA was released from aminated SPIONs and 24.2% plasmid DNA was released from PEGylated SPIONs.
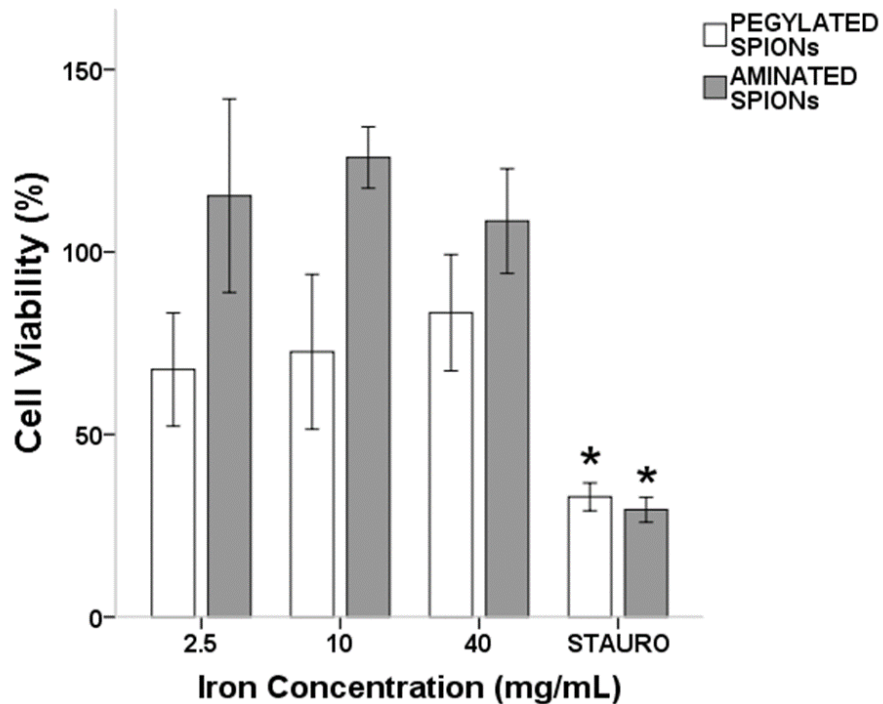
Figure 3.6: Effects of aminated and PEGylated SPION exposure on HEK293 cell survival. Cell viability was determined by MTT assay after incubation with each type of SPION at different iron concentrations for 60 hours. Data are expressed as means ± standard error mean. Untreated HEK cells were considered to have a cell viability of 100 %. * indicates a statistical difference (P < 0.05) compared to untreated HEK cells within the aminated or PEGylated SPION group.

CHAPTER 4

IN VIVO CHARACTERIZATION OF DNA-BASED VACCINES DIRECTED AGAINST
GONADOTROPIN-RELEASING HORMONE RECEPTOR IN MICE

4.1 Introduction

DNA vaccines can be delivered to various tissues by different methods, with intramuscular (IM) injection as the most conventional route of administration. Following immunization by this method with a needle and syringe, the DNA is either directly taken up by cells in the skeletal muscle, or enters blood or lymph circulation to the draining lymph nodes or spleen where APCs are transfected, resulting in immune system activation. IM vaccination has some limitations as a route for in vivo gene delivery. First, large amounts of DNA (e.g., 300-400 µg DNA) are typically needed to induce an immune response due to inefficient uptake of DNA by non-professional antigen-presenting muscle cells [51,251]. Further, directly transfected myocytes lack the co-stimulatory molecules required by professional APCs for T cell activation [269-272]. Also, a low number of professional APCs reside in muscle tissue, although they may be recruited to muscle in response to the local inflammation associated with the needle injection [273-275]. An additional drawback to nucleic acid-based immunization via IM injections is the lack of widespread distribution of DNA within the inoculated tissue [276]. Thus, strategies for optimizing gene transfection by IM injection are of great necessity.

115

Over the last few decades, magnetic nanoparticles have been collectively implemented as a physical gene delivery technology to optimize delivery of DNA vectors [277-279]. Nanoparticles with magnetic cores are loaded with DNA and then coupled with a magnetic field gradient to induce magnetic force-assisted transfection of target tissues [280]. This phenomenon, known as magnetofection, can provide accelerated vector accumulation at target sites. Internalization of genetic material via magnetofection normally occurs through endocytotic processes and is dependent on cell type [281,282]. Typical components of a functional magnetic nanoparticle suitable for magnetofection and biomedical application includes the magnetic core, protective coating, organic linker, and the active molecule to be delivered to target sites. While the electromagnetic properties of metallic nanoparticles make them attractive candidates as gene delivery systems, iron oxide nanoparticles are more fitting for biomedical applications since magnetite cores are superparamagnetic and can be metabolized by living biological systems [281,282]. Cathryn Mah and colleagues were among the first research groups to demonstrate targeted delivery of DNA using magnetic particles. In their groundbreaking study, conjugation of adeno-associated virus, encoded with green fluorescent protein, to the surface of magnetic particles resulted in increased transduction efficiency *in vivo* following IM injection of 129/svJ mice [283]. While magnetofection has demonstrated successful substrate-mediated delivery of DNA, there are limitations to implementing this gene delivery technology. First, combining all major components of a functional magnetic particle into a nanometer-scale space is a challenge and requires special attention to particle design and synthesis in order to avoid one component deactivating the function of another. Therefore, conditions

116

required for nanoparticle preparation (e.g., pH) must be carefully controlled to achieve desired outcomes such as consistent particle size. Also, it is important for magnetic particles to maintain colloidal stability during magnetofection, as the size of transfection agents dramatically influences their endocytotic and phagocytotic rates and the magnetic force of attraction, crucial factors contributing to enhancement of gene transfections [284,285]. Another drawback to magnetofection is providing adequate magnetic field strength for achieving particle penetration and subsequent gene delivery to target sites deep within the subject. Finally, the cost of anesthesia must be considered because *in vivo* magnetofection requires immobilization of the subject in order to carry out the recommended minimum external magnetic field application time of 30 minutes. Nevertheless, the application of magnetic nanoparticles as a physical delivery system for DNA is worthy of consideration for enhancing transfection efficiency of nucleic acid-based vaccines.

The skin contains high concentrations of professional APCs, and is thus a site capable of inducing potent immune responses [286]. The skin is comprised of many layers and each layer contains a subset of resident and transient immune cells. First, the epidermis is the outermost layer (0.05–0.2 mm thick) and primarily composed of epithelial cells in addition to melanocytes, Langerhans cells, and Merkel cells [286]. Beneath the epidermis is the dermis, a thicker layer (1.5–3 mm) mainly consisting of a collagen fiber network. Cells of the innate and adaptive system, including macrophages, mast cells, Langerhans cells, and dermal dendritic cells (DCs), reside in or circulate through the dermis [286]. APCs in the skin process incoming antigens, and in turn

activate the immune system or immune tolerance to self-antigens [287]. Thus, gene delivery to the epidermis or dermis may result in greater immunological responses compared to other anatomical sites such as muscle [287-289]. Also, because of the higher population of professional APCs (e.g., DCs and macrophages), delivery of a smaller quantity of vaccine antigen to the skin could also stimulate a robust immune response. Indeed, such mechanisms could prove to be beneficial for improving immune responses in hard-to-treat groups (e.g., cats) or lowering the cost of vaccine antigens. Common dermal immunization methods include gene gun technology, electroporation, and intradermal injections.

Beginning with gene gun vaccination, also known as particle-mediated, ballistic or biolistic immunization, the technique uses compressed helium to propel plasmid DNA-coated, gold microparticles through the stratum corneum, where the particles lodge in the epidermal and dermal layers of the skin [290]. The gold particles permeate plasma membranes and subsequently transfect a variety of cells, including Langerhans cells in the stratum spinosum that is below the stratum corneum [290], dermal DCs, keratinocytes in the dermis, follicular epithelium [291,292], and, to a lesser extent, dermal macrophages [293]. Minor necrosis and mild tissue damage caused by the gold particles may be interpreted as maturation and stimulation signals for dermal DCs and Langerhans cells, the latter of which migrates through the skin and drains into the lymph nodes [293]. Advantages of gene gun immunization include targeting of a variety of immune cells, use of smaller quantities of DNA (1-5 µg DNA per shot) with 10-100-fold more expression of the DNA-encoded protein than IM vaccinations [294-296], and

upregulation of APC activation by gold beads alone [297]. A major disadvantage to ballistic vaccination is expenses for the gene gun apparatus itself and gold particles, both of which may be cost prohibitive for worldwide immunocontraceptive vaccination programs in underdeveloped countries. Another limitation is the high frequency of inoculation required to elicit immune responses. This is especially unfavorable for application in feral animal populations that that provide rare opportunity for capture. Lastly, conflicting data indicates that gene gun technology may predominantly induce a Th2 response [298]. In the case of eliciting an immune response against self-antigens, a strong Th1 response that perpetuates autoimmune responses is desired over a Th2 response.

Since the early 1980s, electroporation has been used as a molecular research tool for *in vitro* cell transfection [299,300]. Briefly, electroporation involves the application of short, controlled electric pulses to target tissues. This method of gene delivery has been shown to significantly improve the transfection rate of skin cells. Also, the applied electric field increases cell membrane permeability by forming transient, aqueous pathways that allow DNA molecules to enter the cell without losing its integrity [299]. Thus, DNA enters cells directly as an alternative to the less effective route of endocytosis. The benefits of DNA vaccination via electroporation is demonstrated by the observed 2-3-fold increase in protein expression in muscle [301,302] and robust stimulation of immune responses [301]. In another study, compared to naked DNA injection, skin electroporation increased protein expression by 83 orders of magnitude along with increased antibody and Th1 responses [303]. However, there are some

119

drawbacks to this technique for dermal immunization. First, electroporation has been shown to augment DNA expression in skin and muscle cells, but no enhancement of professional APC transfection [303]. Another disadvantage of electroporation is poor DNA stability. Fortunately, this is easily remedied by using DNase inhibitors that increase transfection and expression of the gene of interest [303]. Also, compared to gene gun application, a large quantity of DNA per immunization is required for adequate protein expression. Lastly, electroporation is potentially painful, an undesirable side effect for the recipient.

Compared to gene delivery via gene gun technology and electroporation, intradermal (ID) needle injections simply place DNA at the edge of the dermis and in contact with keratinocytes and professional APCs [304]. This technique circumvents the stratum corneum by injecting the DNA into the dermis and, to a lesser extent, into the epidermis. The needle injection may puncture and therefore directly transfect only a few cells. Alternatively, endocytosis is the main mechanism of cell transfection via ID injection. Similar to IM injections, a major advantage to utilizing this technique for dermal immunization is the inexpensive materials needed for ID needle injections. Also, compared to IM immunization, gene delivery to the dermis makes DNA accessible to Langerhans cells and thus less DNA is required for inoculation [297]. However, one disadvantage to ID vaccination is lower efficiency of cell transfection when compared to gene gun and electroporation techniques. Also, ID injections tend to limit exposure of DNA to the area immediately surrounding the injection site and possible negligence of nearby lymphatic or circulation systems. To offset this, gene delivery to the dermal layer

of the ear pinna, a targeted site with a high population of professional APCs (specifically DCs) and nearby major superficial cervical draining lymph nodes, will induce immune responses to DNA vaccination. The effectiveness of ID injections via the ear pinna has been demonstrated in cats [305] and dogs [306,307]. Furthermore, Forg *et al.* has shown superiority of the ear pinna over muscle tissue as a site for DNA immunization [308].

In the current study, CD-1 mice were vaccinated once with DNA encoding feline GnRHR alone (fGnRHR) or the receptor fused to ubiquitin (Ub-fGnRHR). The following methods were used for gene delivery: IM immunization, IM immunization via magnetofection, and ID immunization. Objectives were to evaluate the effects of DNA immunization against GnRHR and the administration method on immune response induction and reproductive parameters at 4, 8, and 12 weeks after vaccination.

4.2 Materials and Methods

4.2.1 Housing

All animal procedures were performed according to a protocol approved by the Institutional Animal Care and Use Committee of Auburn University. Six-week old, outbred CD-1 male mice, purchased from Charles River Laboratories (Willington, MA, USA) and weighing approximately 25-30 g, were allowed three days to acclimate in the housing facility of the Department of Laboratory Animal Health, College of Veterinary Medicine at Auburn University. Mice were housed two per cage in a standard plastic cages (length, 0.47 m; width, 0.25 m; height, 0.22 m) containing wood chip bedding

(Lab Products, Rockville, MD, USA) and plastic water bottles. Animals were housed under constant controlled lighting (12-hour light: 12-hour dark) and temperature (20-23°C) with free access to pelleted food (Prolab RMH 1000, St. Louis, MO, USA) and water.

4.2.2 Preparation of plasmid DNA

Chapter 1 describes the construction of DNA-based vaccines encoding fGnRHR or Ub-fGnRHR and the electroporation of plasmids into *Escherichia coli (E. coli)* cells. In preparation for mass production of plasmid DNA, *E.coli* clones with the correct molecular weight of the gene inserts were propagated for 12-15 h in 20 mL *Luria Bertani* (LB) broth supplemented with 0.1% ampicillin (Amresco, Solon, OH, USA) with shaking at 200 rpm at 37ºC. Then, 1 mL of cultured broth was added to 1 L LB broth supplemented with 0.1% ampicillin and propagated for 12-15 h with shaking at 200 rpm at 37ºC. Then, plasmid DNA was isolated using a QIAfilter Plasmid Purification Maxi Kit (Qiagen, Germantown, MD, USA). To harvest *E. coli* cells, cultures were transferred to 250 mL Oakridge tubes and centrifuged at 6000 g for 15 min at 4ºC. After discarding the supernatant, cell pellets were re-suspended in 60 mL ice-cold buffer P1. To lyse cells, 60 mL buffer P2 was added to the suspension that was mixed and incubated for 5 min at RT. Then, 60 mL ice-cold buffer P3 was added to lysate to precipitate non-plasmid DNA cellular components (e.g., genomic DNA, proteins, cell debris). The lysate was gently mixed and transferred to a QIAfilter cartridge barrel that was attached to a 45 mm-neck, 500mL glass bottle connected it to a vacuum source. After a 10-minute incubation period at RT, the lysate was filtered through the QIAfilter cartridge barrel to

bind DNA. The vacuum was switched off and 50 mL Buffer FWB2 was added to the barrel. The precipitate was gently stirred and the vacuum source was switched on until the liquid was pulled through completely. Next, 35mL Buffer QBT was added to a QIAGEN-tip 2500 and then, once column was empty, 100mL filtered lysate was applied to the previously equilibrated QIAGEN-tip 2500. Then, the column was washed with 100 mL buffer QC twice. To elute DNA, 35 mL QF was added to the column and the flowthrough was collected into two Nalgene tubes. DNA was precipitated in each tube by adding 12.25 mL RT isopropanol, vigorously shaking each tube, and then immediately subjecting samples to centrifugation at 15000 g for 30 min at 4ºC. Supernatant was discarded, the pellet was washed with 5 mL RT 70% ethanol, and then centrifuged at 15000 g for 10 min at 4ºC. After discarding the supernatant, the pellet was air-dried for 20 min. The DNA pellet was re-dissolved with 600 µL RNA/DNA-free water, incubated on ice for 10 min, and centrifuged at 6000 g for 3 min at 4ºC. DNA concentration was determined and plasmid isolates were stored at -20ºC until use.

4.2.3 Endotoxin removal from plasmid DNA

All plasmids were purified by EndoFree Plasmid Mega Kit (Qiagen) that provides anion-exchange-based, endotoxin-free plasmid DNA purification. First, 46 mL 3-(N-morpholino)propanesulfonic acid (MOPS) buffer and 4.8 mL ER buffer were added to 2 mL plasmid DNA samples. After the DNA solution was mixed ten times and incubated on ice for 30 min, the DNA solution was applied to a QIAGEN-tip 2500 column that was previously equilibrated with 35 mL QBT buffer. Then, the column was washed with 100 mL buffer QC twice. To elute DNA, 35 mL QN was added to the column and the

flowthrough was collected into two Nalgene tubes. DNA was precipitated in each tube by adding 12.25 mL RT isopropanol, vigorously shaking each tube, and then immediately subjecting samples to centrifugation at 15000 g for 30 min at 4ºC. Supernatant was discarded, the pellet was washed with 5 mL RT 70% ethanol, and then centrifuged at 15000 g for 10 min at 4ºC. After discarding the supernatant, the pellet was air-dried for 20 min. The DNA pellet was re-dissolved with 600 µL RNA/DNA-free water, incubated on ice for 10 min, and centrifuged at 6000 g for 3 min at 4ºC. DNA concentration was determined and plasmid isolates were stored at -20ºC until use.

4.2.4   Preparation of vaccination formulations

4.2.4.1   DNA vaccines

Each plasmid DNA construct stock solution was diluted with phosphate buffered saline (PBS) to a concentration of 1 mg/mL. Then, 50-µL aliquots were made using U-100 insulin syringes (Becton Dickinson, Franklin Lakes, NJ, USA) with 28 or 30 gauge (G) X 1/2" needles (Covidien, Mansfield, MA, USA).

4.2.4.2   Preparation of PEGylated SPIONs as DNA delivery systems

Nanoparticles were spread onto agar plates and observed for 48 h to confirm sterility. The plasmid DNA loading capacity of PEGylated SPIONs was determined as 43.99 µg mg^{-1}, as in Chapter 2. Therefore, to immobilize plasmid DNA onto nanoparticle surfaces, 10 mg PEGylated SPIONs were mixed with 1 mg DNA vaccine constructs in a 1.5mL Eppendorf tube (Hamburg, Germany). Then, the DNA-SPION preparation was

diluted with PBS and 50 µL were aliquoted into U-100 insulin syringes with 28G X 1/2"
needles.

4.2.5   Animal Studies

4.2.5.1   DNA administration via intramuscular needle injections

Mice (N = 8 per group) were randomized into the following control and treatment
groups: (1) empty pcDNA 3.1 plasmid; (2) plasmid DNA encoding fGnRHR; and (3)
plasmid DNA encoding Ub-fGnRHR. Each animal was intramuscularly immunized with
100 µg of the respective DNA construct (50 µg DNA per quadriceps femoris muscle) in
100 µL of total injection volume (50 µL per limb). Mice were observed daily post
vaccination to detect any adverse responses to the treatment.

4.2.5.2   DNA administration via magnetofection

Mice (N= 8 per group) were randomized into the following treatment groups: (1)
SPIONs adsorbed with plasmid DNA encoding fGnRHR; and (2) SPIONs adsorbed with
plasmid DNA encoding Ub-fGnRHR. Prior to vaccination, mice were subcutaneously
injected with sterile isotonic saline fluid at 2-3% body weight (BW) to replace any fluid
loss during the procedure, and eyes were lubricated with sterile ophthalmic ointment.
Four animals were anesthetized with a cocktail of xylazine (15 mg/kg) and ketamine
(100 mg/kg). Due to observed intolerance to the anesthesia, the remaining four animals
were maintained on isoflurane inhalant anesthesia via an induction chamber (1-3% +
0.5-1 L/min oxygen) during magnetofection. Subjects were intramuscularly vaccinated
with 100 µg of the respective DNA construct (50 µg DNA per quadriceps femoris
muscle) in 100 µL of total injection volume (50 µL per limb). Following immunization, a
neodymium magnet (K&J Magnets, Pipersville, PA, USA) was taped to the caudal

aspect of the thighs (opposite the injection sites) of each subject for 30 min. At the completion of the procedure, isoflurane was discontinued and all mice were maintained on 100% oxygen via face mask until they regained consciousness, followed by full recovery (e.g., upright posture with normal ambulatory ability) in a cage with thermal support.

4.2.5.3   DNA administration via intradermal needle injections

Mice (N= 8 per group) were randomized into the following treatment groups: (1) empty pcDNA 3.1 plasmid; (2) plasmid DNA encoding fGnRHR; and (3) plasmid DNA encoding Ub-fGnRHR. Prior to vaccination, mice were subcutaneously injected with sterile isotonic saline fluid at 2-3% BW to replace any fluid loss during the procedure. Each animal was anesthetized via intraperitoneal (IP) injection with a cocktail of ketamine (75 mg/kg) and dexmedetomidine (0.5 mg per BW) and eyes were lubricated with sterile ophthalmic ointment. Then, each ear pinna was spread on the tip of a forefinger covered with a metallic protection guard, and 50 µg of the respective DNA construct was injected into the dermis of each ear pinna (100 µg DNA per animal) for a total injection volume of 100 µL (50 µL DNA-PBS preparation per pinna). Post-immunization, all animals were monitored until they regained full recovery from anesthesia.

4.2.6 Blood and tissue collection

Blood samples (0.2 mL) were collected in capillary tubes via lateral tail vein puncture one week prior to DNA immunization. Additional tail vein blood draws were performed at four and eight weeks post vaccination. At twelve weeks post vaccination,

all mice were placed under surgical anesthesia with IP injections of ketamine (75 mg/kg) and dexmedetomidine (0.5 mg per BW) before being subjected to intracardiac puncture for terminal blood collection. Animals were euthanized via cervical dislocation. After blood collection, specimens were centrifuged and sera were stored at -20ºC until assayed. Testes were collected, weighed, and stored in 4% phosphate buffered formalin for histopathological evaluation. Pituitaries were collected and stored at -20ºC until assayed. Major organs were grossly examined for evidence of pathology.

4.2.7 Measurement of serum testosterone levels via enzyme-linked immunosorbent assay (ELISA)

Serum concentrations of testosterone in mice were measured by using a mouse/rat testosterone ELISA assay kit (ALPCO, Salem, MA) according to the manufacturer's instructions. First, serum samples were thawed to RT. Then, 10 µL of duplicate serum samples, calibrator, and control were dispensed into appropriate wells. Then, 100 µL of incubation buffer were added to each well, followed by 50 µL of enzyme conjugate. After the assay plate was incubated with shaking for 1 h at RT, contents were discarded and the plate was washed four times with 300 µL of tris buffer saline (TBS) wash solution. After removal of the wash buffer, 200 µL of substrate solution was added to each well and the plate was incubated in aluminum foil for 30 minutes at RT. To discontinue the reaction, 50 µL of stop solution was added to each well. Finally, absorbance was measured at 450nm. All plates were loaded with internal quality control rat sera (ALPCO). The sensitivity of hormone detection was 0.066 ng/mL. The intra assay coefficient of variation was calculated as 8.4%. The inter assay

coefficient of variation was calculated as 25.5% using the optical density (OD) values generated from assaying the rat control sera.

4.2.8   ELISA for detection of anti-GnRHR antibodies in murine sera

Detection of IgG antibodies against GnRH receptor was carried out by ELISA. This assay included customized GnRHR-based peptides synthesized by Pi Proteomics (Huntsville, AL). First, a 96-well plate (Corning, Corning, NY, USA) was coated with 80 µL streptavidin (Amresco, Solon, OH, USA) diluted in TBS (200 µg streptavidin per well) for 4 h at RT. Then, each well was washed thrice with 150 µL TBS solution, followed by incubation for 15 h at 4ºC with 80 µL solution containing feline GnRHR peptide (amino acids 1-28; 500 ng peptide per well) biotinylated at the carboxyl-terminus. The peptide solution was discarded and each well was washed thrice with 150 µL TBS solution supplemented with 1% bovine serum albumin (BSA) and 0.05% Tween 20. Next, serum samples from vaccinated mice were diluted 1:3200 with TBS/1% BSA solution and added to the plate in duplicate (80 µL per well). After incubating the plate for 2 h at 37ºC, the serum was discarded and each well was washed thrice with 150 µL TBS/0.05% Tween 20 solution. Then, horseradish peroxidase-conjugated rabbit anti-mouse IgG antibody (Jackson Immunoresearch Laboratories, West Grove, PA, USA) was diluted 1:2000 in TBS/1% BSA/0.05% Tween 20 solution and added to the plate (80 µL per well). After incubating the plate for 1 h at RT, the secondary antibody was discarded and each well was washed four times with 150 µL TBS solution supplemented with 0.05% Tween 20. Forty milligrams of chromogenic substrate o-phenylenediamine dihydrochloride (Acros Organics, Waltham, MA, USA) and 13.7 µL

128

30% H_2O_2 were dissolved in 20 mL phosphate-citrate buffer and then aliquoted at 80 µL

per well for an 8-min incubation period at RT. Finally, the reactions were stopped by

adding 80 µL of 8.0 N sulfuric acid to each well, and the plate absorbance was read at

490 nm. All plates were loaded with negative control serum from rabbits and positive

control serum collected from rabbits vaccinated with fGnRHR peptide AA1-28. The intra

assay coefficient of variation was calculated as 8.7%. The inter assay coefficient of

variation was calculated as 16.7% using the optical density (OD) values generated from

assaying the positive and negative control rabbit sera.

4.2.9   Transcriptional expression of GnRHR in pituitaries from immunized mice

4.2.9.1   RNA isolation

Total RNA was isolated from each pituitary collected from vaccinated animals

using an RNeasy Lipid Tissue Mini Kit (Qiagen) according to the manufacturer's

instructions. First, each frozen pituitary was added to a 1.5 mL Eppendorf tube with 1

mL QIAzol Lysis reagent and then homogenized for 1 min using a pestle. Then, 200 µL

chloroform was added to the homogenate and shaken vigorously for 15 sec followed by

a 3-5 min incubation period at RT. The homogenate was centrifuged at 12000 g for 15

min at 4°C and the upper aqueous phase of the suspension was transferred to new

Eppendorf tube (Hamburg, Germany). Next, 450 µL 70% ethanol was added to the

sample that was then transferred to a spin column and centrifuged at 9600 g for 15 sec

at RT. Buffer RW1 (350 µL) was added to the sample and the mixture was centrifuged

at 8000 g for 15 sec at RT. The flow through was discarded, and 80 µL DNase I stock

solution (Qiagen) was added to column and incubated for 15 min at RT. Another round

of buffer RW1 was added to the sample and centrifuged again at 8000 g for 15 sec at RT. After discarding the flow through, RNA was washed twice by adding 500 µL buffer RPE. For elution of total RNA, 30 µL DNase- and RNase-free water (Sigma-Aldrich, St. Louis, MO, USA) was added to the column, and then centrifuged at 8000 g for 1 min at RT. The RNA concentration was determined by absorbance at 260 nm using NanoDrop 2000 equipment (Thermo Scientific, Waltham, MA, USA). Then, RNA samples were diluted with RNase-free water to a concentration of 10 ng/µL and the RNA concentration was re-evaluated. Finally, the 10 ng/µL samples were diluted with RNase-free water to a concentration of 1 ng/µL and used for Reverse transcriptase polymerase chain reaction (RT-PCR).

4.2.9.2   RT-PCR

All primers were purchased from TIB MolBiol (Adelphia, NJ, USA). OneStep RT-PCR Kit (Qiagen) was used for reverse transcription and amplification of all total RNA samples. A typical 50µL reaction includes 10 µL OneStep RT-PCR buffer, 2µL dNTP mix; 2 µL enzyme mix; 50 pmol primer; 1 ng RNA template; and *quantum satis* with DNase- and RNase-free water. No reverse-transcriptase reactions were included as negative controls. RT-PCR was typically performed using a GeneAmp PCR 9700 machine (Applied Biosystems, Grand Island, USA) for 35 cycles under the following conditions:

- Reverse transcription - 50ºC for 30 min;

- Polymerase activation - 95ºC for 15 min;

- Denaturation - 94ºC for 30 sec;

- Annealing - 58ºC for 30 sec;

- Extension - 72ºC for 1 min;

- Final extension - 72ºC for 10 min.

PCR products were mixed with 8.33 µL 6X loading dye (New England BioLabs, Ipswich, MA, USA) and 8 µL samples were loaded onto a 0.8% agarose gel with ethidium bromide for electrophoresis using a PowerPac Basic Power Supply (BioRad, Hercules, CA, USA). Bands were visualized using a 312 nm ultra violet transilluminator (Fisher Scientific, Pittsburgh, PA) and images were captured using a D34 distant screen instant camera (Polaroid, Ridgefield Park, NJ, USA).

4.2.10 Statistical analysis

All ELISAs were performed on at least two separate and independent occasions. Differences of $P \leq 0.05$ were considered significant. All data are presented as the mean ± standard error of the mean. Heterogeneity of variances (i.e., violation of Levene's Test of Equality of Variances with $P \leq 0.05$) were detected in the serum testosterone datasets associated with the following groups: mice intradermally vaccinated with empty plasmid DNA; mice intradermally vaccinated with DNA encoding fGnRHR; mice subjected to magnetofection after intramuscular administration with DNA encoding Ub-fGnRHR. Therefore, these datasets were subjected to natural log transformation prior to statistical analysis. GnRHR antibody data were analyzed by a general linear model repeated measures analysis of variance with Scheffe *post-hoc* analyses (SPSS, IBM, Armonk, NY, USA). Serum testosterone data were analyzed using a mixed model

repeated measures analysis of variance and least squares means (SAS version 9.3, The SAS Institute, Cary, NC, USA). The following model was analyzed:

- Dependent variable: serum testosterone levels

- Independent variables (including interactions):

  1. DNA construct (C; pcDNA, fGnRHR, Ub-fGnRHR)

  2. Route of administration (R; IM, IM followed by magnetofection, ID)

  3. Time (T; 0, 4, 8, or 12 weeks post-immunization)

  4. Experimental animals (A)

- Fixed Effects, Random Effects and Interactions (with error terms)

Source	Error Term
R	A(R X C)
C	A(R X C)
R X C	A(R X C)
A(R X C)	Residual
T	Residual
R X T	Residual
C X T	Residual
R X C X T	Residual

Graphs of 95% confidence interval (CI) of the mean were constructed to determine the range of mean pre-immunization testosterone levels for all mice involved in the current studies (Excel, Microsoft, Redmond, WA, USA). Further, the 95% CIs

were used to plot the average 12-week testosterone concentrations measured in each treated mouse relative to the CI. If the mean 12-week testosterone value for individuals in the same treatment group falls above or below the 95% CI, the value is truly representative of a change in testosterone levels at the twelve-week time point. In contrast, testosterone values that scatter within and around the CI are not truly representative of a change in testosterone levels at the twelve-week time point compared to pre-treatment values.

4.3 Results

4.3.1 Body and testicular weights of mice vaccinated against GnRHR

The average pre-immunization BWs of animals immunized via IM injections were similar between groups, measuring 29.0 ± 0.63 g in the control plasmid group, 27.0 ± 0.48 g in the fGnRHR group, and 28.7 ± 0.64 g in the Ub-fGnRHR group (P > 0.05; Table 4.1). Mean BWs at twelve weeks post-immunization (or necropsy) were similar between groups, measuring 49.1 ± 2.52 g in the pcDNA group, 47.0 ± 2.87 g in the fGnRHR group and 48.2 ± 2.50 g in the Ub-fGnRHR group (P > 0.05; Table 4.1). At the same time point, average testes weights were similar between groups, measuring 0.25 ± 0.01 g in the control group, 0.21 ± 0.01 g in the fGnRHR group, and 0.23 ± 0.01 g in the Ub-fGnRHR plasmid group (P > 0.05; Table 4.1). There was no difference between mean testes to BW ratios 12 weeks post-immunization, as ratio percentages measured 0.51 ± 0.02% in the pcDNA group, 0.49 ± 0.02% in the fGnRHR group, and 0.48 ± 0.03% in the Ub-fGnRHR group (P > 0.05; Table 4.1).

Mean pre-immunization BWs of animals immunized via magnetofection were similar between groups, measuring 30.0 ± 0.70 g in the fGnRHR group and 28.7 ± 0.28 g in the Ub-fGnRHR group (P > 0.05; Table 4.1). Average BWs at twelve weeks post-immunization were similar between groups, measuring 46.0 ± 2.91 g in the fGnRHR group and 44.1 ± 2.16 g in the Ub-fGnRHR group (P > 0.05; Table 4.1). At the same time point, average testes weights were similar between groups, measuring 0.25 ± 0.01 g in the fGnRHR group and 0.23 ± 0.00 g in the Ub-fGnRHR plasmid group (P > 0.05; Table 4.1). There was no difference between mean testes to BW ratios 12 weeks post-immunization, as ratio percentages measured 0.55 ± 0.05% in the fGnRHR group and 0.52 ± 0.03% in the Ub-fGnRHR group (P > 0.05; Table 4.1).

The average pre-immunization BWs of animals immunized via ID injections were similar between groups, measuring 26.5 ± 0.40 g in the control plasmid group, 27.4 ± 0.42 g in the fGnRHR group, and 27.2 ± 0.47 g in the Ub-fGnRHR group (P > 0.05; Table 4.1). Mean BWs at twelve weeks post-immunization were similar between groups, measuring 46.0 ± 1.90 g in the pcDNA group, 44.8 ± 1.77 g in the fGnRHR group and 48.8 ± 2.45 g in the Ub-fGnRHR group (P > 0.05; Table 4.1). At the same time point, average testes weights were similar between groups, measuring 0.22 ± 0.00 g in the control group, 0.23 ± 0.00 g in the fGnRHR group, and 0.22 ± 0.01 g in the Ub-fGnRHR plasmid group (P > 0.05; Table 4.1). At 12 weeks post-immunization, there were no differences between mean testes to BW ratios between the pcDNA group (0.49 ± 0.02%) and the fGnRHR group that averaged 0.53 ± 0.02% (P > 0.05; Table 4.1). Similarly, mean testes to BW ratios in the Ub-fGnRHR group (0.46 ± 0.03%) were

statistically similar to the average ratio percentages in the control group (P > 0.05; Table 4.1).

4.3.2 Serum testosterone concentrations in mice vaccinated against GnRHR

An ELISA was used to measure testosterone levels in serum samples from subjects immunized via IM needle injections. In mice vaccinated with negative control pcDNA plasmid, mean serum testosterone concentrations at each post-vaccination time point were similar to pre-immunization levels, measuring 8.09 ± 3.33 ng/mL before treatment, 8.48 ± 2.92 ng/mL at 4 weeks, 4.73 ± 1.59 ng/mL at 8 weeks, and 9.56 ± 6.88 ng/mL at 12 weeks (P > 0.05; Fig. 4.1A). The same outcome was also observed in mice immunized with plasmid DNA encoding fGnRHR, with serum testosterone values measuring 6.85 ± 2.08 ng/mL prior to inoculation, 11.31 ± 2.80 ng/mL at 4 weeks, 9.92 ± 5.11 ng/mL at 8 weeks, and 6.14 ± 3.17 ng/mL at 12 weeks (P > 0.05; Fig. 4.1B). In comparison to serum testosterone levels prior to IM injection with the Ub-fGnRHR construct (9.84 ± 3.30 ng/mL), animals had similar hormone levels 4, 8, and 12 weeks after vaccination, measuring at 5.94 ± 1.86 ng/mL, 8.28 ± 3.91 ng/mL, and 9.99 ± 3.93 ng/mL, respectively (P > 0.05; Fig. 4.1C).

In the group of subjects vaccinated with fGnRHR construct immobilized to PEGylated SPIONs, four of the eight mice died due to anesthesia complications. Therefore, an ELISA was used to measure testosterone levels in serum samples from only the eight mice immunized with Ub-fGnRHR immobilized to nanoparticles. Mean testosterone levels measured 4 and 8 weeks after magnetofection with SPIONs

conjugated to Ub-fGnRHR (8.78 ± 2.51 ng/mL and 4.54 ± 1.35 ng/mL, respectively) did not change significantly compared to pre-immunization testosterone levels of 9.14 ± 0.95 ng/mL, respectively ($P > 0.05$; Fig. 4.2). Similarly, at 12 weeks post-immunization, mean serum testosterone concentrations in the Ub-fGnRHR-SPION group was not statistically different (19.73 ± 3.71 ng/mL for Ub-fGnRHR) compared to the pretreatment values ($P > 0.05$; Fig. 4.2). Further analysis indicated that the mean 12-week testosterone values for Ub-fGnRHR-SPION mice were scattered within and outside of the 95% CI, as five mice were above, two mice were below, and one mouse was within the 95% CI of the pre-immunization mean (Fig. 4.4A).

Blood was collected from mice treated with DNA via ID injection and sera were assayed for testosterone concentrations. In mice vaccinated with negative control pcDNA plasmid, mean serum testosterone concentrations at each post-vaccination time point were no different from pre-immunization values, measuring 5.26 ± 2.19 ng/mL before treatment, 4.84 ± 2.64 ng/mL at 4 weeks, 6.48 ± 1.71 ng/mL at 8 weeks, and 13.08 ± 6.10 ng/mL at 12 weeks ($P > 0.05$; Fig. 4.3A). The same outcome was also observed in mice that received dermal immunization with plasmid DNA encoding fGnRHR, measuring 11.18 ± 3.59 ng/mL prior to inoculation, 17.18 ± 6.23 ng/mL at 4 weeks, 13.27 ± 3.66 ng/mL at 8 weeks, and 6.73 ± 5.83 ng/mL at 12 weeks ($P > 0.05$; Fig. 4.3B). After ID vaccination with plasmid encoding ubiquitinated fGnRHR, mean testosterone concentrations measured at 4 and 8 weeks (5.32 ± 1.74 ng/mL and 6.79 ± 2.67 ng/mL, respectively) were similar to pretreatment values of 11.32 ± 4.07 ng/mL ($P > 0.05$; Fig. 4.3C). In contrast, at 12 weeks post-dermal immunization, mean serum

testosterone concentrations in the Ub-fGnRHR group were significantly lower (1.29 ± 0.49 ng/mL) compared to pre-immunization levels ($P < 0.05$; Fig. 4.3C). Further, the mean 12-week testosterone values for each mouse intradermally-injected with Ub-fGnRHR was below the lower limit of the 95% CI for the pre-immunization mean (Fig. 4.4B).

4.3.3 Effects of administration method on serum testosterone concentrations in vaccinated mice

Mixed model repeated measures analysis of variance indicated that changes in serum testosterone levels was due to route of DNA administration, specifically IM and ID needle injection (Table 4.2; $P < 0.05$). Also, the mixed ANOVA determined that changes in serum testosterone levels reflect the interaction between the administration route and DNA construct (Table 4.2; $P < 0.05$). In addition, the P value for interaction between DNA construct and time approached significance (Table 4.2; $P = 0.0699$). No relationship between serum testosterone levels and all other fixed effects, random effects, or interactions was observed in the mixed ANOVA (Table 4.2; $P > 0.05$). To determine which combination of DNA construct and administration route had a significant impact on serum testosterone levels at the 12-week time point, mean testosterone concentrations from vaccinated mice were compared based on administration routes IM injection or ID injection (Fig. 4.5). Serum testosterone levels were similar in mice vaccinated with sham DNA via IM or ID injection ($P > 0.05$; Fig. 4.5A). The same outcome was observed in mice vaccinated with fGnRHR DNA via the same routes of administration ($P > 0.05$; Fig. 4.5A). Contrastingly, mice immunized with

137

Ub-fGnRHR DNA via ID injection had significantly lower serum testosterone concentrations (1.28 ± 0.31 ng/mL) than animals vaccinated via intramuscular injection (P < 0.05; Fig. 4.5C).

4.3.4   Serum anti-GnRHR antibody production in mice vaccinated against GnRHR

Sera collected from immunized mice were assayed for anti-GnRHR antibodies via ELISA. In all mice involved in the study, no anti-GnRHR antibodies were detected in serum samples taken prior to immunization (Fig. 4.6-4.8). Mice administered IM had poor responses to treatments, indicated by the similar mean absorbance values in the pcDNA (0.071 ± 0.003), fGnRHR construct (0.060 ± 0.001), and Ub-fGnRHR construct (0.060 ± 0.003) groups 12 weeks post-immunization (P > 0.05; Fig. 4.6). The same outcome was observed for mice subjected to magnetofection as a method of fGnRHR (0.058 ± 0.002) or Ub-fGnRHR (0.068 ± 0.003) DNA delivery (P > 0.05; Fig. 4.7). Animals immunized with the fGnRHR construct via ID injections had absorbance values (0.075 ± 0.002) similar to mice in the control pcDNA group that had a mean absorbance value of 0.071 ± .001 (P > 0.05; Fig. 4.8). In contrast, GnRHR antibodies were detected in sera collected 12 weeks after mice received ID injections with the Ub-fGnRHR construct, as absorbance values in the treated group were significantly higher (0.116 ± 0.002) compared to the pcDNA control group (P < 0.05; Fig. 4.8).

4.3.5 GnRHR mRNA expression in pituitaries collected from mice vaccinated against GnRHR

GnRHR mRNA was amplified from total RNA isolated from pituitaries collected at necropsy (i.e., 12 weeks post-immunization) from vaccinated subjects. GnRHR mRNA expression was similar in pituitaries from all mice immunized via IM injection (Fig. 4.9). Also, there was no difference in *GnRHR* gene expression in pituitaries from animals subjected to IM magnetofection (Fig. 4.10). In contrast, GnRHR mRNA expressions in pituitaries appeared lower in mice vaccinated with Ub-fGnRHR via ID injection compared to the control or fGnRHR counterparts (Fig. 4.11). Amplification of *ACTB* housekeeping gene indicated similar mRNA expression in all mice involved in the study (Fig. 4.9-4.11).

4.4 Discussion

In this novel, proof-of-concept study, eight-week old, CD-1 male mice were each vaccinated once with 100 µg DNA designed to target GnRHR in an attempt to ablate anterior pituitary gonadotropic cells and thus achieve contraceptive effects. An outbred strain of mouse was chosen because its genetic heterozygosity mimics that of the feral cat population, the target species in need of a safe, permanent, and cost-efficient contraceptive. Here, DNA plasmids were constructed to encode a heterologous feline GnRHR protein that elicited immune responses in mice. In addition, mice were immunized with DNA encoding fGnRHR fused to Ub. Theoretically, such a fusion protein is degraded by the proteasome and presented to circulating naïve T cells more rapidly than a non-ubiquitinated protein. Mice were immunized via IM needle injection,

magnetofection, or ID needle injection to determine the effects of administration method on immunogenicity of DNA-based immunocontraceptives. Serum testosterone levels, anti-GnRHR antibody production, and pituitary GnRHR mRNA expression were measured in order to evaluate the biological impact of DNA-based immunocontraceptives targeted against GnRHR on reproductive potential in murine subjects.

Mice vaccinated with sham plasmid, fGnRHR plasmid, or Ub-fGnRHR plasmid via IM injection had similar serum testosterone concentrations 12 weeks post-immunization compared to pretreatment values. Also, no difference was detected in testes to body weight ratios and pituitary GnRHR mRNA expression 12 weeks after mice were vaccinated with control or fGnRHR-encoding DNA. Heterologous antigens are commonly used to induce immunity against autologous proteins. For example, immunization with DNA encoding a self-tumor antigen human tyrosinase-related protein (TRP), but not the self-protein, induced both antibody and T cell responses to self TRP, leading to protection from B16F10 tumor growth in mice [309]. In another study involving a murine model, auto-antibodies were generated in experimental autoimmune myasthenia gravis following immunization with the *Torpedo californica* (Pacific electric ray) acetylcholine receptor antigen [310]. Ubiquitination of proteins also has been successful in inducing immune responses against self-proteins. For instance, DNA immunization of mice with plasmid encoding ubiquitinated TRP-2 broke tolerance and induced protective immunity to melanoma [311]. Since no changes in testosterone were observed in mice immunized either with fGnRHR or Ub-fGnRHR via IM administration in

140

our study, the route of administration may account for lack of expected testosterone suppression. No significant impairment to testosterone levels in vaccinated subjects might be explained by the fact that direct needle injection into muscle only transfects a small portion of myocytes at the administration site. This low transfection efficiency typically results in low expression of the target protein and thus no effect on biological function. Therefore, it was important to investigate the effects of an advanced method of delivering DNA to muscle in mice.

In vivo magnetofection is a method commonly used for efficient, intramuscular DNA delivery by using plasmid-loaded magnetic particles for magnetic force-assisted transfection of target tissues [312]. Here, mice were injected in their quadriceps with PEGylated SPIONs loaded with DNA vaccines against GnRHR, followed by application of an external magnetic field on the opposite side of the injection site. There was no difference in serum testosterone levels in mice vaccinated with SPIONs loaded with Ub-fGnRHR at 4 or 8 weeks post-magnetofection. The mean 12-week testosterone value for Ub-fGnRHR-vaccinated mice were randomly scattered on the 95% CI graph. Such erratic scattering raises the question of whether or not the average 12-week testosterone levels for the entire Ub-fGnRHR-SPION group are truly different from pre-treatment values. Further, the measured testosterone levels were not accompanied by changes in other immunological, neuroendocrine, or reproductive parameters such as presence of GnRHR antibodies, pituitary GnRHR mRNA expression, or testes-to-body weight ratios in treated mice. No effects of magnetic force-assisted transfection on testosterone concentrations was an unexpected outcome in mice vaccinated with Ub-

fGnRHR-loaded SPIONs, as other studies have demonstrated successful use of

magnetic particles for DNA delivery and biological effects on target tissues. For

example, magnetofection of murine mammary adenocarcinoma with plasmid DNA

encoding interleukin-12 using SPIONs resulted in a significant antitumor effects in mice

[313]. In this study, mice were unresponsive to magnetically-assisted delivery of DNA

directed against GnRHR possibly due to aggregation of PEGylated SPIONs post-

magnetofection. It is also possible that the external magnets used for magnetofection

did not exert an adequate force to draw SPIONs into the thick quadriceps muscle. As

the magnetic field strength falls off rapidly, sites deeper within the body become more

difficult to target, thus preventing deep penetration and widespread distribution of the

loaded plasmid DNA. Some groups have recently proposed a way around this problem

by implanting magnets near the target site within the body [314]. However, this strategy

is impractical for the feral cat population, the target species for immunocontraception.

Another approach to improving magnetofection techniques is to expose DNA-loaded

SPIONs to professional APCs. Specifically, mature DCs, which play a major role in

inducing immune responses to foreign materials, would be an appropriate target for

DNA-loaded nanocarriers. Indeed, DNA vaccines delivered directly to DCs has been

identified as an essential mechanism for efficacious antigen presentation and

subsequent induction of cytotoxic T lymphocyte (CTL) responses [292,315,316].

Further, immature (i)DCs use pinocytosis and phagocytosis to spontaneously internalize

SPIONs over an extended incubation time [317]. For example, using confocal

microscopy, location of fluorescent dye-loaded nanoparticles treated with DCs

confirmed internalization of these biomaterials by DCs [318]. Also, studies indicate that

exposure of iDCs to the surface area of nanoparticles induces maturation of iDCs by increasing expression of costimulatory molecules (e.g., CD40, CD80, CD83, CD86) and major histocompatibility complex (MHC) class II molecules (HLA-DR and HLA-DQ) [319], DC markers also upregulated in mature DCs by lipopolysaccharides [320]. Thus, targeting plasmid DNA to a high population of professional APCs, with or without SPIONs, may be a strategy for eliciting an immune response against GnRHR and ultimately pituitary gonadotropic cells.

The skin is an attractive site for DNA vaccine administration because its layers, particularly the dermis, are rich in professional APCs [286]. Thus, as the third route tested for administration of plasmid DNA, mice were vaccinated with DNA encoding fGnRHR alone or fused to Ub via an ID needle injection into the dermis of the ear pinna. Serum testosterone concentrations measured 12 weeks post-inoculation were similar in animals immunized with negative control pcDNA plasmid or fGnRHR plasmid compared to pre-treatment values. In contrast, in mice intradermally vaccinated with DNA encoding Ub-fGnRHR, testosterone levels significantly diminished 12 weeks after inoculation. These observations were further validated via the 95% CI analysis, as all testosterone values from Ub-fGnRHR-vaccinated mice were well below the lower confidence limit. It is important to note that mice dermally-injected with DNA encoding mouse GnRHR fused to Ub had similar serum testosterone levels to control animals (data not shown), indicating that feline GnRHR encoding sequence in Ub-fGnRHR construct was crucial for impairment to testosterone production.

DNA vaccines applied intradermally is mostly taken up by keratinocytes [321]. However, these cells are unable to initiate primary T cell responses. Thus, it is likely that activated DCs were involved in priming naïve T cells after immunization with the Ub-fGnRHR DNA construct. Specifically, ID needle injection directly transfected dermis-residing professional APCs that expressed, processed, and presented the chimeric protein and then migrated to draining lymph nodes where they interact with naïve T cells. DNA vaccines are extremely efficient in eliciting cytotoxic T cell activity due to vaccine immunogen presentation to and subsequently activation of CD8+ CTLs. Although induction of GnRHR-specific CTLs was not directly investigated in this study, the presence of these cytotoxic immune cells and their targeting of gonadotropes is possibly indicated by the abatement of GnRHR mRNA expression in pituitaries isolated from Ub-fGnRHR mice compared to sham-treated animals. Measurement of serum gonadotropin levels and pituitary histological analysis may provide additional clues in determining disruption of gonadotrope function and *pars anterior* architecture.

Successful DNA vaccination also induces antibody response against the target antigen. Many factors have been reported to have an effect on the efficacy of the DNA-elicited antibody response such as the administration method and the form of the DNA-encoded antigen [322]. Here, anti-GnRHR antibodies were produced in mice intradermally vaccinated with the Ub-fGnRHR construct and not in subjects vaccinated the same route with the pcDNA control plasmid. In this case, the Ub-fGnRHR protein produced in the DC cytoplasm, is the main target of immune surveillance in the context of MHC II molecules on DCs, which migrate to the lymph nodes and present it to naïve

144

CD4+ T cells. Reports have demonstrated that DNA inoculations by ID routes predominantly stimulate T helper (Th) 1 cells that are involved in the development of cytotoxic T cells, activate phagocytic cells and assist B cells to make IgG2a antibody [322]. Most likely, in mice intradermally vaccinated with the Ub-fGnRHR construct, Th1 cells activated mature B cells that produced anti-GnRHR antibodies. These GnRHR-specific antibodies may travel through the hypophyseal portal system and bind to GnRHR-expressing gonadotropes, a signal to natural killer cells that are subsequently activated and kill the antibody-coated cells. Activated CD+4 T cells migrate to the spleen, where memory T cells have been shown to persist for up to a year in the absence of a source of persistent antigen [323]. This property is desirable in the feral population of cats that are difficult to catch more than once for boosters.

The Ub-fGnRHR DNA construct was designed to target and ablate cells expressing GnRHR in murine subjects. At necropsy, gross examination of major organs (heart, lungs, kidneys, liver) from mice dermally-vaccinated with this construct yielded normal findings. This may indicate that this vaccination strategy can have a negative effect on reproductive parameters such as testosterone without causing major, non-reproductive side effects.

4.5 Conclusion

In summary, our experiments were designed to determine the effects of DNA immunization against GnRHR and the route of administration on immune responses, reproductive parameters, and gonadotrope ablation in a murine model. Vaccination with

145

control, fGnRHR, or Ub-fGnRHR plasmids via IM injection or magnetofection did not result in significant changes of these parameters. Similar observations were noted in mice vaccinated with control or fGnRHR constructs via ID injection at all time points. In contrast, at 12 weeks post-dermal immunization, mean serum testosterone concentrations in the Ub-fGnRHR group were significantly lower (1.28 ± 0.31 ng/mL) compared to pre-immunization levels of 9.46 ± 2.27 ng/mL ($P < 0.05$). Moreover, unlike in control animals, anti-GnRHR IgG antibodies were detected in sera from mice dermally vaccinated with Ub-fGnRHR construct. Also, GnRHR mRNA expression estimated by RT-PCR was lower in this group than in control animals. The outcome of these parameters indicated induction of a proper immunological responses which, most likely, affected pituitary gonadotropes and lead to testosterone suppression. To demonstrate immunocastration, additional long-term studies are needed to achieve complete ablation of gonadotrope cells.

Table 4.1

Body weights of mice prior to immunization and at necropsy and testes weights of mice at necropsy

Administration Method	Vaccine Construct	Body Weight (g)		Testes Weight (g)	Testes/Body Weight Ratio (%)
		Pre-immunization	Necropsy	Necropsy	Necropsy
Intramuscular Injection	pcDNA	29.0 ± 0.63	49.1 ± 2.52	0.25 ± 0.01	0.51 ± 0.02
	fGnRHR	27.0 ± 0.48	47.0 ± 2.87	0.21 ± 0.01	0.49 ± 0.02
	Ub-fGnRHR	28.7 ± 0.64	48.2 ± 2.50	0.23 ± 0.01	0.48 ± 0.03
IM Magnetofection	fGnRHR	30.0 ± 0.70	46.0 ± 2.91	0.25 ± 0.01	0.55 ± 0.05
	Ub-fGnRHR	28.7 ± 0.28	44.1 ± 2.16	0.23 ± 0.00	0.52 ± 0.03
Intradermal Injection	pcDNA	26.5 ± 0.40	46.0 ± 1.90	0.22 ± 0.00	0.49 ± 0.02
	fGnRHR	27.4 ± 0.42	44.8 ± 1.77	0.23 ± 0.00	0.53 ± 0.02
	Ub-fGnRHR	27.2 ± 0.47	48.8 ± 2.45	0.22 ± 0.01	0.46 ± 0.03

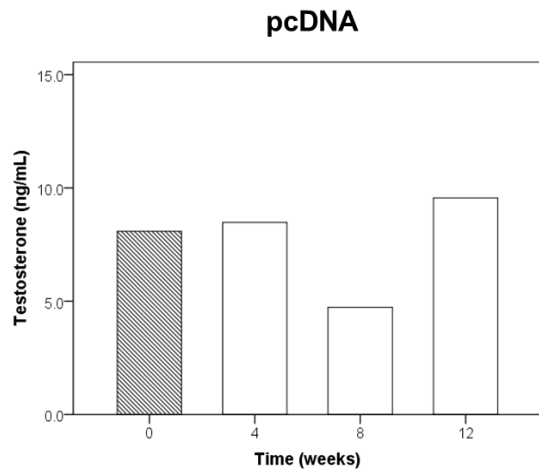Legend: pcDNA: empty plasmid; fGnRHR: plasmid encoding fGnRHR; Ub-fGnRHR: plasmid encoding Ub-fGnRHR.

Table 4.2

Tests of Fixed Effects, Random Effects, Interactions on Serum Testosterone Levels in Vaccinated Mice
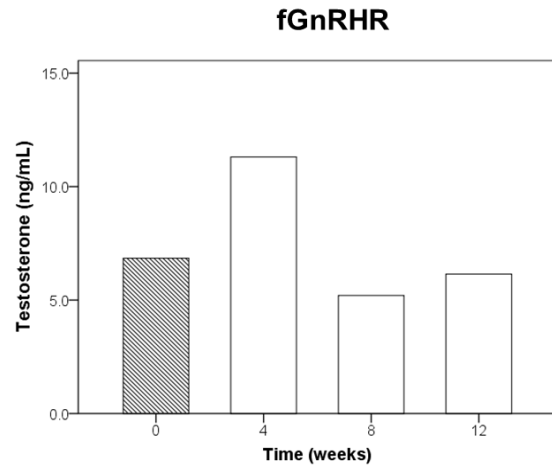
Effect	P Value
R	0.0459*
C	0.8208
R X C	0.0096*
A(R X C)	0.4578
T	0.2066
R X T	0.0949
C X T	0.0699
R X C X T	0.1749

* P < 0.05

A.

pcDNA

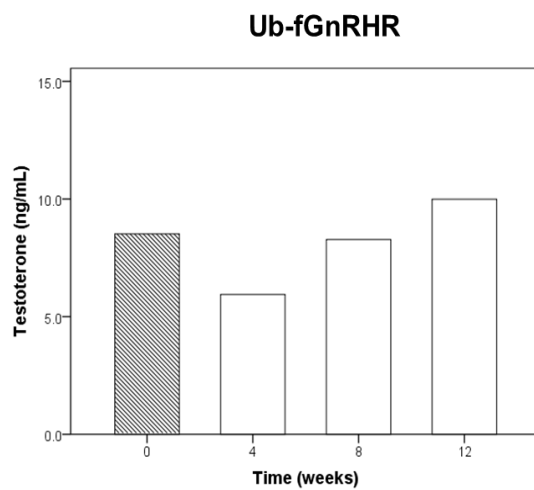**B.**

fGnRHR

C.

Ub-fGnRHR

Figure 4.1: Testosterone in sera collected from mice immunized via intramuscular injection. The following DNA constructs were administered in quadriceps muscle via needle injection:

(A) empty pcDNA plasmid;
(B) plasmid encoding fGnRHR;
(C) plasmid encoding Ub-fGnRHR.

Blood was collected prior to immunization (day 0) and then at weeks 4, 8, and 12 post-immunization. Testosterone was detected using mouse/rat testosterone ELISA kit. Data are shown as means with an SEM of 0.035.

Ub-fGnRHR

Figure 4.2: Testosterone in sera collected from mice immunized via magnetofection. Animals were vaccinated with plasmid encoding Ub-fGnRHR immobilized on PEGylated superparamagnetic iron oxide nanoparticles (SPIONs). Immediately following immunization, a magnet was applied to the injected limb. Blood was collected prior to immunization (day 0) and then at weeks 4, 8, and 12 post-immunization. Testosterone was detected using mouse/rat testosterone ELISA kit. Data are shown as means with an SEM of 0.035.
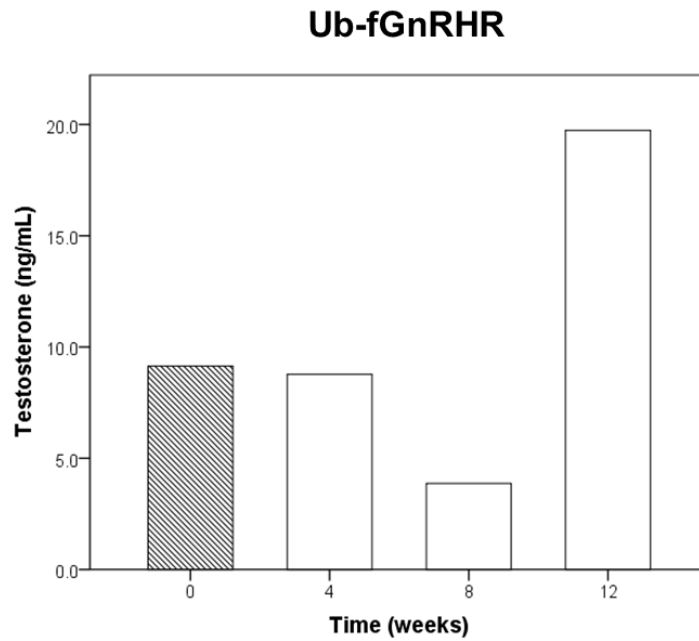
Figure 4.3: Testosterone in sera collected from mice immunized via intradermal injection. The following DNA constructs were administered in the ear pinna dermis via needle injection:

(A) empty pcDNA plasmid;
(B) plasmid encoding fGnRHR;
(C) plasmid encoding Ub-fGnRHR.

Blood was collected prior to immunization (day 0) and then at weeks 4, 8, and 12 post-immunization. Testosterone was detected using mouse/rat testosterone ELISA kit. Data are shown as means with an SEM of 0.035. * $P < 0.05$ represents statistical difference compared to day 0.
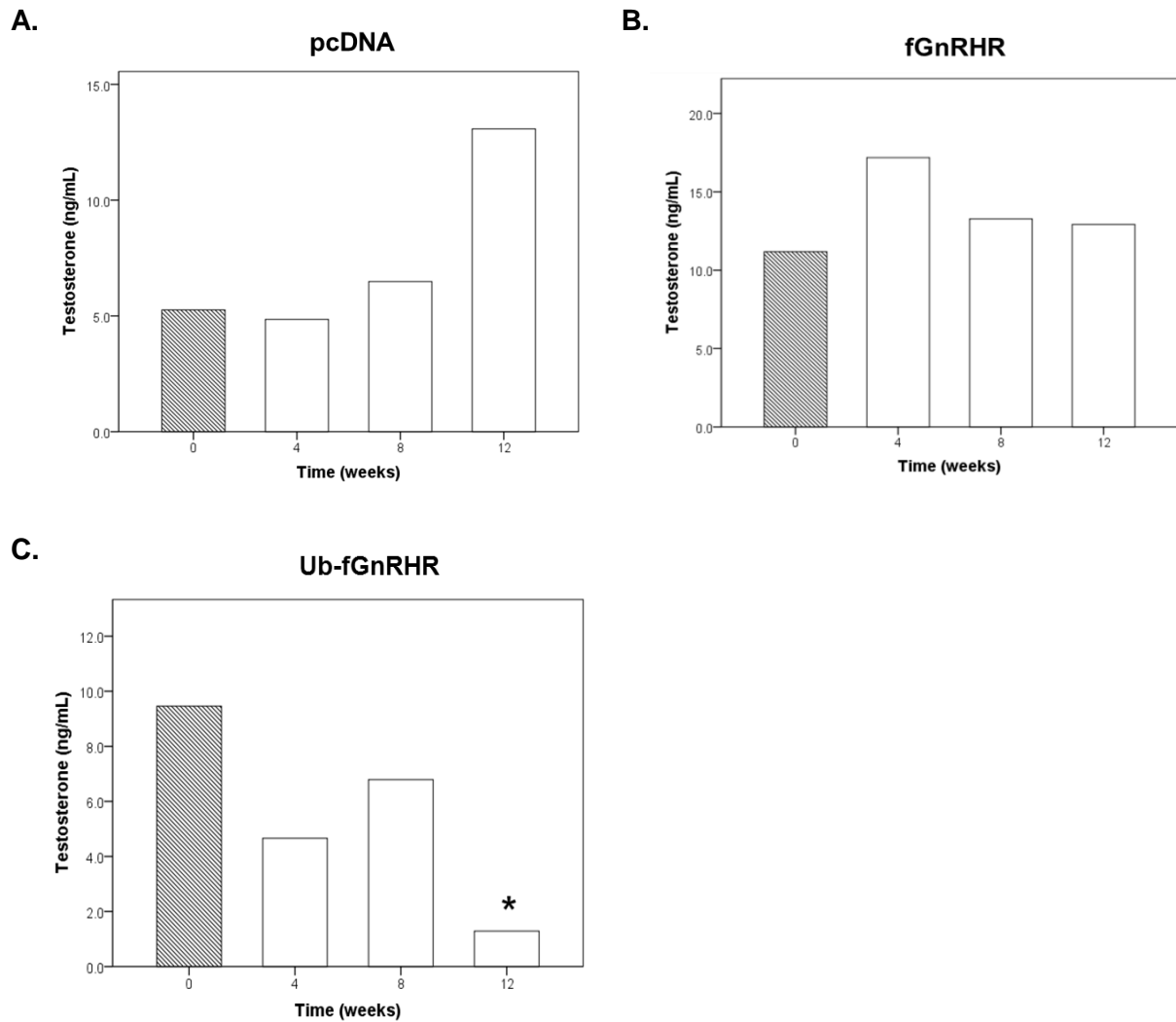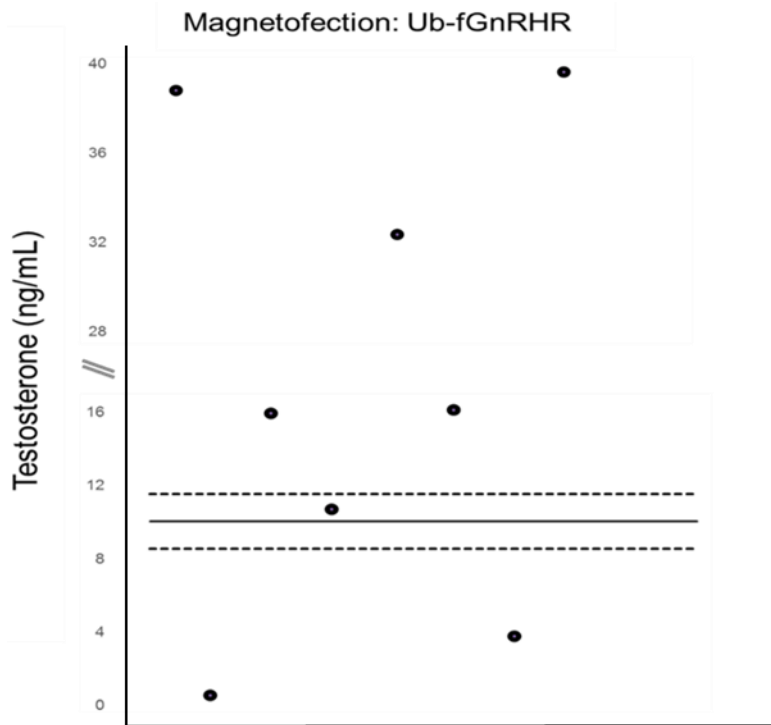
A.

Magnetofection: Ub-fGnRHR

B.

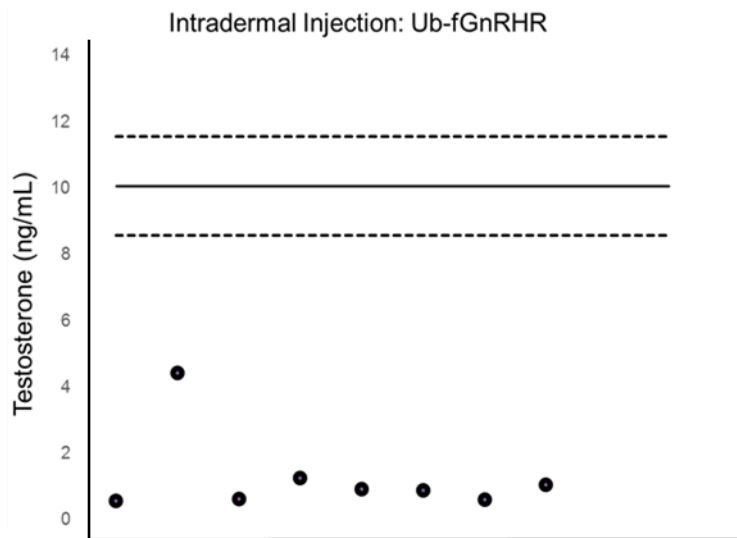Intradermal Injection: Ub-fGnRHR

Figure 4.4: Testosterone in individual mice twelve weeks after vaccination relative to confidence interval calculated for mean testosterone for all mice prior to vaccination. The average testosterone levels for all mice involved in the current study was measured as 10.06 ng/mL, as indicated by the solid line. The 95% confidence interval for the true population mean ranged from 8.57 ng/mL to 11.55 ng/mL, as indicated by the lower and upper dashed line, respectively. Each black dot represents the mean testosterone value for an individual mouse vaccinated with the Ub-fGnRHR construct via magnetofection (A) or intradermal needle injection (B).

A.

pcDNA

B.

fGnRHR

C.
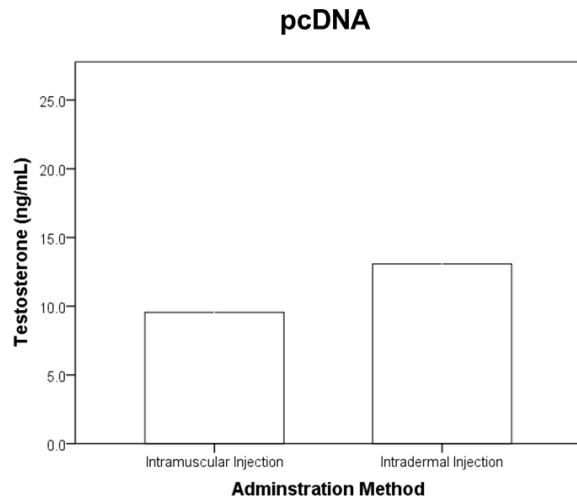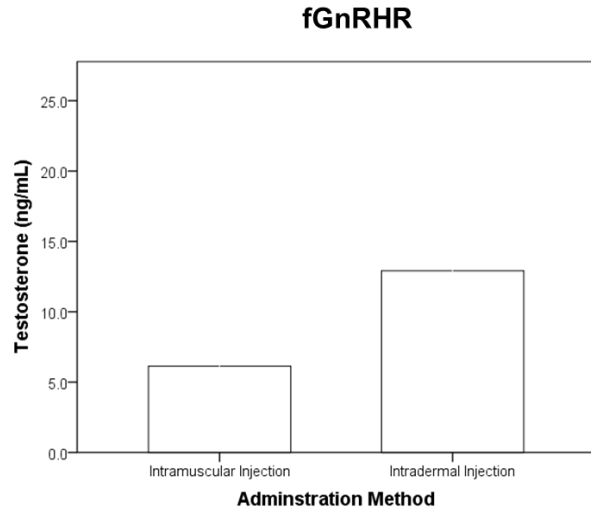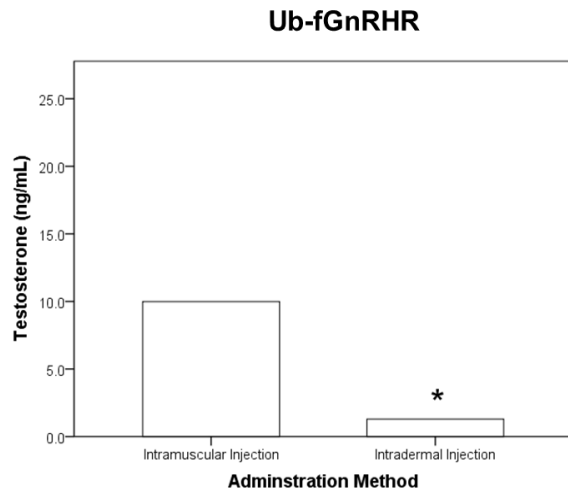
Ub-fGnRHR

Figure 4.5: Testosterone in sera collected from mice immunized via intramuscular injection or intradermal injection. Mice were vaccinated with either empty plasmid DNA (A), plasmid encoding fGnRHR (B), or plasmid encoding Ub-fGnRHR (C). Blood was collected at 12 weeks post-immunization. Testosterone was detected using mouse/rat testosterone ELISA kit. Data are shown as means with an SEM of 0.035. * indicates statistical difference (P < 0.05).

A.

Pre-immunization

B.

Post-immunization
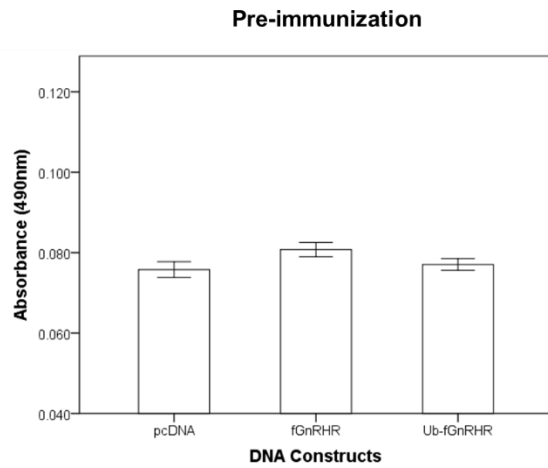
Figure 4.6: Anti-GnRHR antibodies in sera collected from mice immunized via intramuscular injection. The following DNA constructs were administered in the quadriceps muscle via needle injection:

(A) empty pcDNA plasmid;
(B) plasmid encoding fGnRHR;
(C) plasmid encoding Ub-fGnRHR.

Blood was collected prior to immunization (A) and then at 12 weeks post-immunization (B). GnRHR antibodies were detected via ELISA with GnRHR-derived peptide (AA1-28) as a detector molecule. Data are shown as means ± SEM.

154

A. **B.**
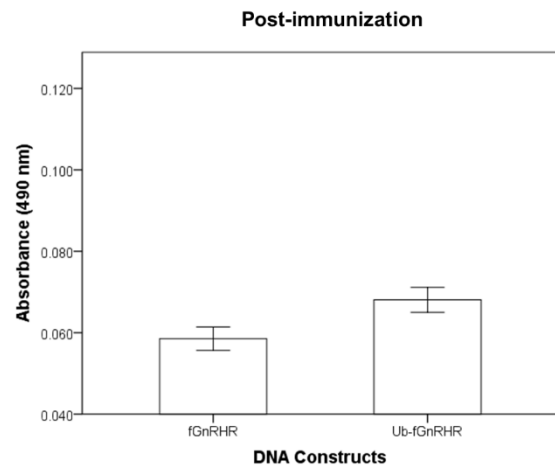
Figure 4.7: Anti-GnRHR antibodies in sera collected from mice immunized via magnetofection. Animals were vaccinated with the following DNA constructs immobilized on PEGylated superparamagnetic iron oxide nanoparticles (SPIONs):

(A) plasmid encoding fGnRHR;
(B) plasmid encoding Ub-fGnRHR.

DNA constructs were administered in quadriceps muscle via needle injection followed by application of a magnet to the injected limb. Blood was collected prior to immunization (A) and then at 12 weeks post-immunization (B). GnRHR antibodies were detected via ELISA with GnRHR-derived peptide (AA1-28) as a detector molecule. Data are shown as means ± SEM.
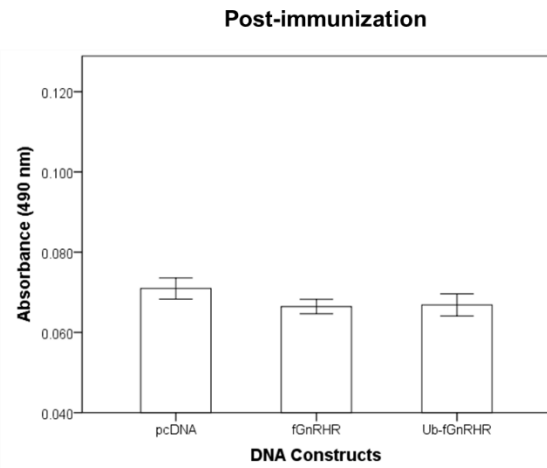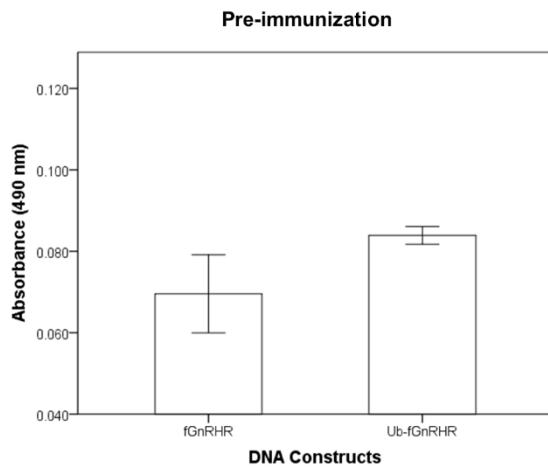
Figure 4.8: Anti-GnRHR antibodies in sera collected from mice immunized via intradermal injection. The following DNA constructs were administered in the ear pinna dermis via needle injection:

(A) empty pcDNA plasmid;
(B) plasmid encoding fGnRHR;
(C) plasmid encoding Ub-fGnRHR.

Blood was collected prior to immunization (A) and then at 12 weeks post-immunization (B). GnRHR antibodies were detected via ELISA with GnRHR-derived peptide (AA1-28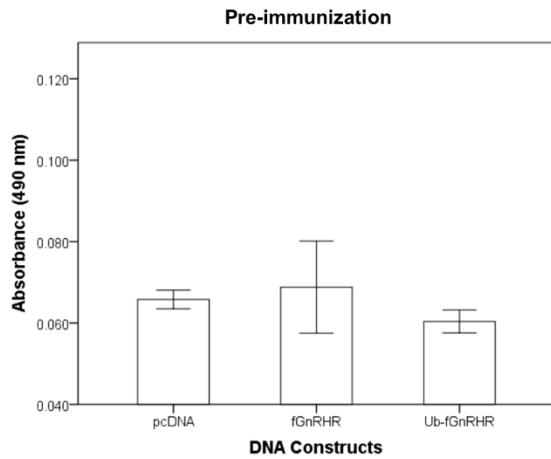) as a detector molecule. Data are shown as means ± SEM. * $P < 0.05$ represents statistical difference compared to mice vaccinated with empty plasmid.
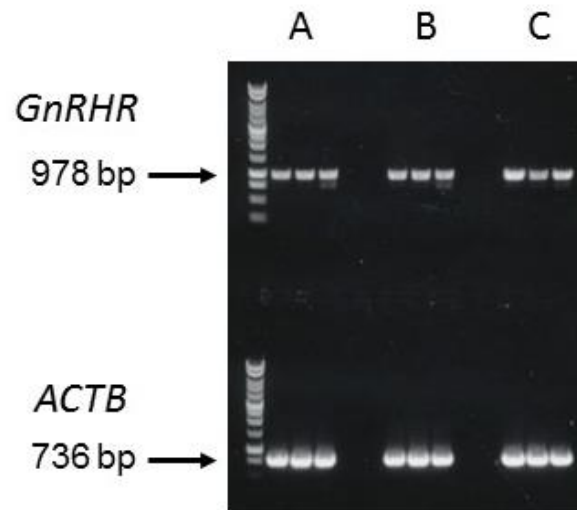
Figure 4.9: GnRHR mRNA expression in pituitary glands collected from mice immunized via intramuscular injection. The following DNA constructs were administered in the quadriceps muscle via needle injection:

(A) empty pcDNA plasmid;
(B) plasmid encoding fGnRHR;
(C) plasmid encoding Ub-fGnRHR.

Pituitaries were collected at necropsy (or 12 weeks post-immunization). Total RNA was isolated from pituitary glands and RT-PCR was performed for *GnRHR* gene and *ACTB* (housekeeping) gene expression.
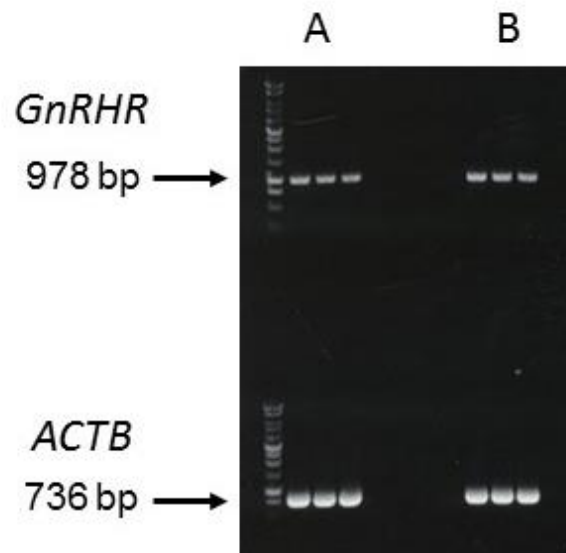
Figure 4.10: GnRHR mRNA expression in pituitary glands collected from mice immunized via magnetofection. Animals were vaccinated with the following DNA constructs immobilized on PEGylated superparamagnetic iron oxide nanoparticles (SPIONs):

(A) plasmid encoding fGnRHR;
(B) plasmid encoding Ub-fGnRHR.

DNA constructs were administered in quadriceps muscle via needle injection followed by application of a magnet to the injected limb. Pituitaries were collected at necropsy (or 12 weeks post-immunization). Total RNA was isolated from pituitary glands and RT-PCR was performed for *GnRHR* gene and *ACTB* (housekeeping) gene expression.
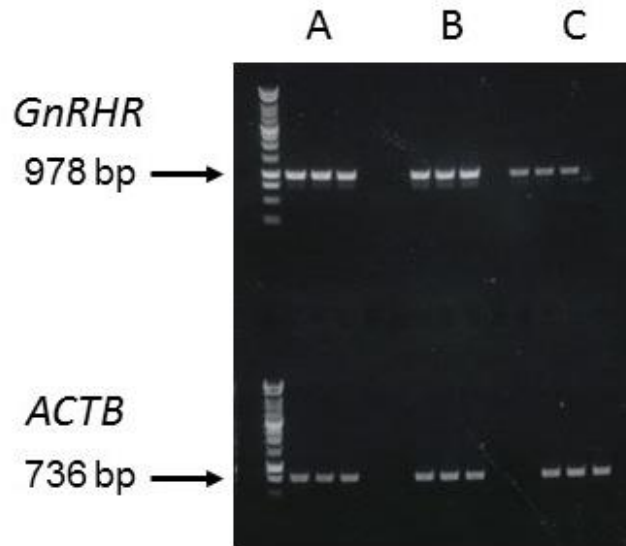
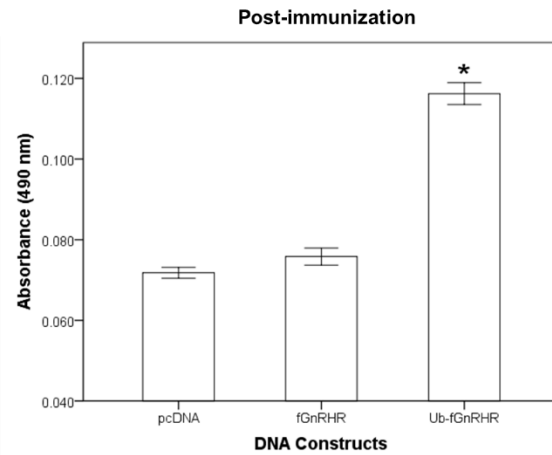**Figure 4.11:** GnRHR mRNA expression in pituitary glands collected from mice immunized via intradermal injection. The following DNA constructs were administered in the ear pinna dermis via needle injection:

(A) empty pcDNA plasmid;
(B) plasmid encoding fGnRHR;
(C) plasmid encoding Ub-fGnRHR.

Pituitaries were collected at necropsy (or 12 weeks post-immunization). Total RNA was isolated from pituitary glands and RT-PCR was performed for *GnRHR* gene and *ACTB* (housekeeping) gene expression.

CONCLUSIONS

The fecundity of cats has prompted efforts towards the development of long-term or permanent contraception as an approach to controlling the feral feline population. Indeed, fertility control products for feral cats are of great need considering the welfare of cats and their impact on environment and public health. The actively growing feral cat population, despite global spay/neuter campaigns and programs, is another indication of the necessity for reliable contraceptive agents. The history of fertility control agents designed for cats is extensive and includes various targets explored to prevent gamete production, function, or outcome. Many contraceptive modalities aim at disrupting GnRH function, the main regulator of the hypothalamic-pituitary-gonadal axis and thus reproductive function in mammals. Therefore, it was only a matter of time that its receptor, GnRHR, would garner interest as a target for contraception. This work describes the contraceptive potential of DNA-based vaccines designed to target GnRH receptor as a strategy to ablate GnRHR-expressing pituitary gonadotropic cells in a murine model. Herein, one-time, intradermal vaccination of male CD-1 mice with DNA plasmid encoding feline GnRHR fused to ubiquitin induced anti-GnRHR antibody production, impaired GnRHR mRNA expression in the pituitary, and significantly decreased serum testosterone levels three months post-immunization. Based on these observations, GnRH receptor appears to be a viable option for inducing an immune response against pituitary gonadotropic cells resulting in contraception in animals. Considering the limited number of publications detailing *in vivo* experiments focused on

the contraceptive potential of GnRHR in mammals, the present study is a novel

approach to immunocontraception. In essence, development of a DNA-based

immunocontraceptive vaccine targeting GnRHR for gonadotropic cell ablation may

result in a valuable alternative to controlling the feral cat population.

REFERENCES

1. Moldave K, Rhodes L, Aza C, Briggs J. Contraception and Fertility Control in Dogs and Cats: A Report of the Alliance for Contraception in Cats & Dogs (ACC&D). Alliance for Contraception in Cats & Dogs; 2013

2. Levy JK. Contraceptive vaccines for the humane control of community cat populations. Am J Reprod Immunol 2011; 66:63-70

3. Office of Environment and Heritage. *Feral Cats*. 2015; Retrieved from http://www.environment.nsw.gov.au/pestsweeds/FeralCats.htm

4. Rupprecht CE. Rabies: reemergence of the disease. Compend Contin Educ Vet 2002; 24 57-60

5. Blanton JD, Palmer D, Rupprecht CE. Rabies surveillance in the United States during 2009. J Am Vet Med Assoc 2010; 237:646-657

6. Elmore SA, Jones JL, Conrad PA, Patton S, Lindsay DS, Dubey JP. Toxoplasma gondii: epidemiology, feline clinical aspects, and prevention. Trends Parasitol 2010; 26:190-196

7. Lee SE, Kim NH, Chae HS, Cho SH, Nam HW, Lee WJ, Kim SH, Lee JH. Prevalence of Toxoplasma gondii infection in feral cats in Seoul, Korea. J Parasitol 2011; 97:153-155

8.   Lee AC, Schantz PM, Kazacos KR, Montgomery SP, Bowman DD. Epidemiologic and zoonotic aspects of ascarid infections in dogs and cats. Trends Parasitol 2010; 26:155-161

9.   McElroy KM, Blagburn BL, Breitschwerdt EB, Mead PS, McQuiston JH. Flea-associated zoonotic diseases of cats in the USA: bartonellosis, flea-borne rickettsioses, and plague. Trends Parasitol 2010; 26:197-204

10.   Chomel BB, Boulouis HJ, Breitschwerdt EB. Cat scratch disease and other zoonotic Bartonella infections. J Am Vet Med Assoc 2004; 224:1270-1279

11.   Maggi RG, Mozayeni BR, Pultorak EL, Hegarty BC, Bradley JM, Correa M, Breitschwerdt EB. Bartonella spp. bacteremia and rheumatic symptoms in patients from Lyme disease-endemic region. Emerg Infect Dis 2012; 18:783-791

12.   Nutter FB, Levine JF, Stoskopf MK. Reproductive capacity of free-roaming domestic cats and kitten survival rate. J Am Vet Med Assoc 2004; 225:1399-1402

13.   Liberg O. Food Habits and Prey Impact by Feral and House-Based Domestic Cats in a Rural Area in Southern Sweden. Vol 65.

14.   Coleman JS, Temple SA. How many birds do cats kill? . *Wildlife Control Technology* Vol Jul/Aug1995:44

15.   Coleman JS, Temple SA, Craven SR. Cats and wildlife: a conservation dilemma. Madison, Wisconsin: University of Wisconsin-Madison;1997

16.   Jessup DA. The welfare of feral cats and wildlife. J Am Vet Med Assoc 2004; 225:1377-1383

17. Pimentel D LL, Rodolfo Z, and Morrison D. Environmental and Economic Costs of Nonindigenous Species in the United States. Bioscience 2000; 50:53-65

18. Hatley PJ. Feral Cat Colonies in Florida: The Fur and Feathers are Flying. Paper presented at: 9th Annual Public Interest Environmental Conference: "Florida's Final Frontiers: Saving What's Left" 2003; University of Florida

19. Bibb K, Hughes P. Lower Keys Marsh Rabbit 5-Year Review: Summary and Evaluation. Vero Beach, Florida: U.S. Fisheries and Wildlife Service; 2007

20. LaFever DH, Schmidt PM, Perry ND, Faulhaber CA, Lopez RR, Silvy NJ, Forys EA. Use of a population viability analysis to evaluate human-induced impacts and mitigation for the endangered Lower Keys marsh rabbit. Human-Wildlife Conflicts 2008; 2:260-269

21. Chomsky N. 2003 AVMA Membership Directory & Resource Manual.

22. Kutzler M, Wood A. Non-surgical methods of contraception and sterilization. Theriogenology 2006; 66:514-525

23. Pesavento PA, Murphy BG. Common and emerging infectious diseases in the animal shelter. Vet Pathol 2014; 51:478-491

24. Hurley KE, Pesavento PA, Pedersen NC, Poland AM, Wilson E, Foley JE. An outbreak of virulent systemic feline calicivirus disease. J Am Vet Med Assoc 2004; 224:241-249

25. Highland MA, Byrne BA, Debroy C, Samitz EM, Peterson TS, Oslund KL. Extraintestinal pathogenic Escherichia coli-induced pneumonia in three kittens and fecal prevalence in a clinically healthy cohort population. J Vet Diagn Invest 2009; 21:609-615

26.   Neville P, Remfry J. Effect of neutering on two groups of feral cats. Vet Rec 1984; 114:447-450

27.   Levy JK, Gale DW, Gale LA. Evaluation of the effect of a long-term trap-neuter-return and adoption program on a free-roaming cat population. J Am Vet Med Assoc 2003; 222:42-46

28.   Nutter FB, Stoskopf MK, Levine JF. Time and financial costs of programs for live trapping feral cats. J Am Vet Med Assoc 2004; 225:1403-1405

29.   University of Florida College of Veterinary Medicine. *Operation Catnip.* 2015; Retrieved from http://www.vetmed.ufl.edu/extension-outreach/operation-catnip/

30.   Hughes KL, Slater MR, Haller L. The Effects of Implementing a Feral Cat Spay/Neuter Program in a Florida County Animal Control Service. J Appl Anim Welf Sci 2002; 5:285-298

31.   Natoli E, Maragliano L, Cariola G, Faini A, Bonanni R, Cafazzo S, Fantini C. Management of feral domestic cats in the urban environment of Rome (Italy). Prev Vet Med 2006; 77:180-185

32.   Reichler IM. Gonadectomy in Cats and Dogs: A Review of Risks and Benefits. Reprod Domest Anim 2009; 44:29-35

33.   DeTora M, McCarthy RJ. Ovariohysterectomy versus ovariectomy for elective sterilization of female dogs and cats: is removal of the uterus necessary? J Am Vet Med Assoc 2011; 239:1409-1412

34.   Howe LM. Surgical methods of contraception and sterilization. Theriogenology 2006; 66:500-509

35. Williams LS, Levy JK, Robertson SA, Cistola AM, Centonze LA. Use of the anesthetic combination of tiletamine, zolazepam, ketamine, and xylazine for neutering feral cats. J Am Vet Med Assoc 2002; 220:1491-1495

36. Cistola AM, Golder FJ, Centonze LA, McKay LW, Levy JK. Anesthetic and physiologic effects of tiletamine, zolazepam, ketamine, and xylazine combination (TKX) in feral cats undergoing surgical sterilization. J Feline Med Surg 2004; 6:297-303

37. Robertson SA. A review of feral cat control. J Feline Med Surg 2008; 10:366-375

38. Pineda MH, Dooley MP. Surgical and chemical vasectomy in the cat. Am J Vet Res 1984; 45:291-300

39. Fagundes AKF, Oliveira ECS, Tenorio BM, Melo CCS, Nery LTB, Santos FAB, Alves LC, Douglas RH, Silva Jr VA. Injection of a chemical castration agent, zinc gluconate, into the testes of cats results in the impairment of spermatogenesis: A potentially irreversible contraceptive approach for this species? Theriogenology 2014; 81:230-236

40. Oliveira ECS, Fagundes AKF, Melo CCS, Nery LTB, Rêvoredo RG, Andrade TFG, Oliveira-Esquerre K, Kastelic JP, Silva Jr VA. Intratesticular injection of a zinc-based solution for contraception of domestic cats: A randomized clinical trial of efficacy and safety. The Veterinary Journal 2013; 197:307-310

41. Jana K, Samanta PK. Clinical evaluation of non-surgical sterilization of male cats with single intra-testicular injection of calcium chloride. BMC Vet Res 2011; 7:39

42. Plumb DC. Plumb's veterinary drug handbook. Stockholm, Wis.; Ames, Iowa: PharmaVet ; Distributed by Wiley.

43. Burke TJ. Pharmacologic control of estrus in bitch and queen. Vet Clin North Am Small Anim Pract 1982; 12:79-84

44. Peterson ME. Effects of megestrol acetate on glucose tolerance and growth hormone secretion in the cat. Res Vet Sci 1987; 42:354-357

45. Hayden DW, Barnes DM, Johnson KH. Morphologic changes in the mammary gland of megestrol acetate-treated and untreated cats: a retrospective study. Vet Pathol 1989; 26:104-113

46. van Os JL, van Laar PH, Oldenkamp EP, Verschoor JS. Oestrus control and the incidence of mammary nodules in bitches, a clinical study with two progestogens. Vet Q 1981; 3:46-56

47. Evans JM, Sutton DJ. The use of hormones, especially progestagens, to control oestrus in bitches. J Reprod Fertil Suppl 1989; 39:163-173

48. Burke TJ, Reynolds HA, Sokolowski JH. A 280-day tolerance-efficacy study with mibolerone for suppression of estrus in the cat. Am J Vet Res 1977; 38:469-477

49. Gorman SP, Levy JK, Hampton AL, Collante WR, Harris AL, Brown RG. Evaluation of a porcine zona pellucida vaccine for the immunocontraception of domestic kittens (Felis catus). Theriogenology 2002; 58:135-149

50. Levy JK, Mansour M, Crawford PC, Pohajdak B, Brown RG. Survey of zona pellucida antigens for immunocontraception of cats. Theriogenology 2005; 63:1334-1341

51. Eade JA, Roberston ID, James CM. Contraceptive potential of porcine and feline zona pellucida A, B and C subunits in domestic cats. Reproduction 2009; 137:913-922

52. Goericke-Pesch S, Georgiev P, Antonov A, Vodenicharov A, Navarro C, Wehrend A. Reversibility of germinative and endocrine testicular function after long-term contraception with a GnRH-agonist implant in the tom-a follow-up study. Theriogenology 2014; 81:941-946

53. Munson L, Bauman JE, Asa CS, Jochle W, Trigg TE. Efficacy of the GnRH analogue deslorelin for suppression of oestrous cycles in cats. J Reprod Fertil Suppl 2001; 57:269-273

54. Toydemir TS, Kilicarslan MR, Olgac V. Effects of the GnRH analogue deslorelin implants on reproduction in female domestic cats. Theriogenology 2012; 77:662-674

55. Prohaczik A RS, Miller L, Fagerstone K, Driancourt M. Novel non steroidal long term contraceptive approaches for queens. Paper presented at: 6th International Symposium on Canine and Feline Reproduction and 6th Biannual European Veterinary Society for Small Animal Reproduction Congress2008; Vienna, Austria

56. Baker HJ, Griffen B, Smith BF, Braden TD. Immunization of Cats and Dogs with an Anti-GnRH Protein Vaccine with Molecular Adjuvantation. Paper presented at: 2nd International Symposium on Non-Surgical methods for Pet Population Control2004; Breckenridge, CO

57. Robbins SC, Jelinski MD, Stotish RL. Assessment of the immunological and biological efficacy of two different doses of a recombinant GnRH vaccine in domestic male and female cats (Felis catus). J Reprod Immunol 2004; 64:107-119

58.   Wetsel WC, Srinivasan S. Pro-GnRH processing. Progress in Brain Research. Vol Volume 141: Elsevier; 2002:221-241.

59.   Nikolics K, Mason AJ, Szonyi E, Ramachandran J, Seeburg PH. A prolactin-inhibiting factor within the precursor for human gonadotropin-releasing hormone. Nature 1985; 316:511-517

60.   Seeburg PH, Mason AJ, Stewart TA, Nikolics K. The mammalian GnRH gene and its pivotal role in reproduction. Recent Prog Horm Res 1987; 43:69-98

61.   Sealfon SC, Weinstein H, Millar RP. Molecular mechanisms of ligand interaction with the gonadotropin-releasing hormone receptor. Endocr Rev 1997; 18:180-205

62.   Karten MJ, Rivier JE. Gonadotropin-releasing hormone analog design. Structure-function studies toward the development of agonists and antagonists: rationale and perspective. Endocr Rev 1986; 7:44-66

63.   Guarnieri F, Weinstein H. Conformational Memories and the Exploration of Biologically Relevant Peptide Conformations: An Illustration for the Gonadotropin-Releasing Hormone. J Am Chem Soc 1996; 118:5580-5589

64.   Tensen C, Okuzawa K, Blomenrohr M, Rebers F, Leurs R, Bogerd J, Schulz R, Goos H. Distinct efficacies for two endogenous ligands on a single cognate gonadoliberin receptor. Eur J Biochem 1997; 243:134-140

65.   Millar RP, Flanagan CA, Milton RC, King JA. Chimeric analogues of vertebrate gonadotropin-releasing hormones comprising substitutions of the variant amino acids in positions 5, 7, and 8. Characterization of requirements for receptor

binding and gonadotropin release in mammalian and avian pituitary gonadotropes. J Biol Chem 1989; 264:21007-21013

66. Illing N, Troskie BE, Nahorniak CS, Hapgood JP, Peter RE, Millar RP. Two gonadotropin-releasing hormone receptor subtypes with distinct ligand selectivity and differential distribution in brain and pituitary in the goldfish (Carassius auratus). Proc Natl Acad Sci U S A 1999; 96:2526-2531

67. Flanagan CA, Becker, II, Davidson JS, Wakefield IK, Zhou W, Sealfon SC, Millar RP. Glutamate 301 of the mouse gonadotropin-releasing hormone receptor confers specificity for arginine 8 of mammalian gonadotropin-releasing hormone. J Biol Chem 1994; 269:22636-22641

68. Salisbury TB, Binder AK, Nilson JH. Welcoming beta-catenin to the gonadotropin-releasing hormone transcriptional network in gonadotropes. Mol Endocrinol 2008; 22:1295-1303

69. Tsutsumi M, Zhou W, Millar RP, Mellon PL, Roberts JL, Flanagan CA, Dong K, Gillo B, Sealfon SC. Cloning and functional expression of a mouse gonadotropin-releasing hormone receptor. Mol Endocrinol 1992; 6:1163-1169

70. Kakar SS, Musgrove LC, Devor DC, Sellers JC, Neill JD. Cloning, sequencing, and expression of human gonadotropin releasing hormone (GnRH) receptor. Biochem Biophys Res Commun 1992; 189:289-295

71. Chi L, Zhou W, Prikhozhan A, Flanagan C, Davidson JS, Golembo M, Illing N, Millar RP, Sealfon SC. Cloning and characterization of the human GnRH receptor. Mol Cell Endocrinol 1993; 91:R1-6

72. Perrin MH, Bilezikjian LM, Hoeger C, Donaldson CJ, Rivier J, Haas Y, Vale WW. Molecular and functional characterization of GnRH receptors cloned from rat pituitary and a mouse pituitary tumor cell line. Biochem Biophys Res Commun 1993; 191:1139-1144

73. Kaiser UB, Zhao D, Cardona GR, Chin WW. Isolation and characterization of cDNAs encoding the rat pituitary gonadotropin-releasing hormone receptor. Biochem Biophys Res Commun 1992; 189:1645-1652

74. Eidne KA, Sellar RE, Couper G, Anderson L, Taylor PL. Molecular cloning and characterisation of the rat pituitary gonadotropin-releasing hormone (GnRH) receptor. Mol Cell Endocrinol 1992; 90:R5-9

75. Illing N, Jacobs GF, Becker, II, Flanagan CA, Davidson JS, Eales A, Zhou W, Sealfon SC, Millar RP. Comparative sequence analysis and functional characterization of the cloned sheep gonadotropin-releasing hormone receptor reveal differences in primary structure and ligand specificity among mammalian receptors. Biochem Biophys Res Commun 1993; 196:745-751

76. Brooks J, Taylor PL, Saunders PT, Eidne KA, Struthers WJ, McNeilly AS. Cloning and sequencing of the sheep pituitary gonadotropin-releasing hormone receptor and changes in expression of its mRNA during the estrous cycle. Mol Cell Endocrinol 1993; 94:R23-27

77. Weesner GD, Matteri RL. Rapid communication: nucleotide sequence of luteinizing hormone-releasing hormone (LHRH) receptor cDNA in the pig pituitary. J Anim Sci 1994; 72:1911

78. Reinhart J, Mertz LM, Catt KJ. Molecular cloning and expression of cDNA encoding the murine gonadotropin-releasing hormone receptor. J Biol Chem 1992; 267:21281-21284

79. Dohlman HG, Caron MG, Lefkowitz RJ. A family of receptors coupled to guanine nucleotide regulatory proteins. Biochemistry 1987; 26:2657-2664

80. Rispoli LA, Nett TM. Pituitary gonadotropin-releasing hormone (GnRH) receptor: structure, distribution and regulation of expression. Anim Reprod Sci 2005; 88:57-74

81. Keinan D, Hazum E. Mapping of gonadotropin-releasing hormone receptor binding site. Biochemistry 1985; 24:7728-7732

82. Sealfon SC, Millar RP. Functional domains of the gonadotropin-releasing hormone receptor. Cell Mol Neurobiol 1995; 15:25-42

83. Davidson JS, Flanagan CA, Zhou W, Becker, II, Elario R, Emeran W, Sealfon SC, Millar RP. Identification of N-glycosylation sites in the gonadotropin-releasing hormone receptor: role in receptor expression but not ligand binding. Mol Cell Endocrinol 1995; 107:241-245

84. Ji TH, Grossmann M, Ji I. G protein-coupled receptors. I. Diversity of receptor-ligand interactions. J Biol Chem 1998; 273:17299-17302

85. Fromme BJ, Katz AA, Roeske RW, Millar RP, Flanagan CA. Role of aspartate7.32(302) of the human gonadotropin-releasing hormone receptor in stabilizing a high-affinity ligand conformation. Mol Pharmacol 2001; 60:1280-1287

86. Troskie B, Illing N, Rumbak E, Sun YM, Hapgood J, Sealfon S, Conklin D, Millar R. Identification of three putative GnRH receptor subtypes in vertebrates. Gen Comp Endocrinol 1998; 112:296-302

87. Neill JD, Duck LW, Sellers JC, Musgrove LC. A gonadotropin-releasing hormone (GnRH) receptor specific for GnRH II in primates. Biochem Biophys Res Commun 2001; 282:1012-1018

88. Wang L, Bogerd J, Choi HS, Seong JY, Soh JM, Chun SY, Blomenrohr M, Troskie BE, Millar RP, Yu WH, McCann SM, Kwon HB. Three distinct types of GnRH receptor characterized in the bullfrog. Proc Natl Acad Sci U S A 2001; 98:361-366

89. King JA, Millar RP. Evolutionary aspects of gonadotropin-releasing hormone and its receptor. Cell Mol Neurobiol 1995; 15:5-23

90. Benard O, Naor Z, Seger R. Role of dynamin, Src, and Ras in the protein kinase C-mediated activation of ERK by gonadotropin-releasing hormone. J Biol Chem 2001; 276:4554-4563

91. Mulvaney JM, Roberson MS. Divergent signaling pathways requiring discrete calcium signals mediate concurrent activation of two mitogen-activated protein kinases by gonadotropin-releasing hormone. J Biol Chem 2000; 275:14182-14189

92. Morrison DK, Davis RJ. Regulation of MAP kinase signaling modules by scaffold proteins in mammals. Annu Rev Cell Dev Biol 2003; 19:91-118

93. Sim P, Mitchell R, Thorfinn L. Activation of MAP kinase in alpha T3-1 cells by luteinising hormone-releasing hormone. Biochem Soc Trans 1993; 21:357S

94. Roberson MS, Misra-Press A, Laurance ME, Stork PJ, Maurer RA. A role for mitogen-activated protein kinase in mediating activation of the glycoprotein hormone alpha-subunit promoter by gonadotropin-releasing hormone. Mol Cell Biol 1995; 15:3531-3539

95. Mitchell R, Sim PJ, Leslie T, Johnson MS, Thomson FJ. Activation of MAP kinase associated with the priming effect of LHRH. J Endocrinol 1994; 140:R15-18

96. Levi NL, Hanoch T, Benard O, Rozenblat M, Harris D, Reiss N, Naor Z, Seger R. Stimulation of Jun N-terminal kinase (JNK) by gonadotropin-releasing hormone in pituitary alpha T3-1 cell line is mediated by protein kinase C, c-Src, and CDC42. Mol Endocrinol 1998; 12:815-824

97. Kanasaki H, Bedecarrats GY, Kam KY, Xu S, Kaiser UB. Gonadotropin-releasing hormone pulse frequency-dependent activation of extracellular signal-regulated kinase pathways in perifused LbetaT2 cells. Endocrinology 2005; 146:5503-5513

98. Burger LL, Haisenleder DJ, Aylor KW, Marshall JC. Regulation of Lhb and Egr1 gene expression by GNRH pulses in rat pituitaries is both c-Jun N-terminal kinase (JNK)- and extracellular signal-regulated kinase (ERK)-dependent. Biol Reprod 2009; 81:1206-1215

99. Burger LL, Haisenleder DJ, Aylor KW, Marshall JC. Regulation of intracellular signaling cascades by GNRH pulse frequency in the rat pituitary: roles for CaMK II, ERK, and JNK activation. Biol Reprod 2008; 79:947-953

100. Wolfe MW, Call GB. Early growth response protein 1 binds to the luteinizing hormone-beta promoter and mediates gonadotropin-releasing hormone-stimulated gene expression. Mol Endocrinol 1999; 13:752-763

101. Lawson MA, Tsutsumi R, Zhang H, Talukdar I, Butler BK, Santos SJ, Mellon PL, Webster NJ. Pulse sensitivity of the luteinizing hormone beta promoter is determined by a negative feedback loop Involving early growth response-1 and Ngfi-A binding protein 1 and 2. Mol Endocrinol 2007; 21:1175-1191

102. Fortin J, Lamba P, Wang Y, Bernard DJ. Conservation of mechanisms mediating gonadotrophin-releasing hormone 1 stimulation of human luteinizing hormone beta subunit transcription. Mol Hum Reprod 2009; 15:77-87

103. Dobkin-Bekman M, Naidich M, Pawson AJ, Millar RP, Seger R, Naor Z. Activation of mitogen-activated protein kinase (MAPK) by GnRH is cell-context dependent. Mol Cell Endocrinol 2006; 252:184-190

104. Bliss SP, Miller A, Navratil AM, Xie J, McDonough SP, Fisher PJ, Landreth GE, Roberson MS. ERK signaling in the pituitary is required for female but not male fertility. Mol Endocrinol 2009; 23:1092-1101

105. Sundaresan S, Colin IM, Pestell RG, Jameson JL. Stimulation of mitogen-activated protein kinase by gonadotropin-releasing hormone: evidence for the involvement of protein kinase C. Endocrinology 1996; 137:304-311

106. Kolch W, Heidecker G, Kochs G, Hummel R, Vahidi H, Mischak H, Finkenzeller G, Marme D, Rapp UR. Protein kinase C alpha activates RAF-1 by direct phosphorylation. Nature 1993; 364:249-252

107. Duvernay MT, Filipeanu CM, Wu G. The regulatory mechanisms of export trafficking of G protein-coupled receptors. Cell Signal 2005; 17:1457-1465

108. Achour L, Labbe-Jullie C, Scott MG, Marullo S. An escort for GPCRs: implications for regulation of receptor density at the cell surface. Trends Pharmacol Sci 2008; 29:528-535

109. Zhang X, Dong C, Wu QJ, Balch WE, Wu G. Di-acidic motifs in the membrane-distal C termini modulate the transport of angiotensin II receptors from the endoplasmic reticulum to the cell surface. J Biol Chem 2011; 286:20525-20535

110. Dong C, Wu G. Regulation of anterograde transport of alpha2-adrenergic receptors by the N termini at multiple intracellular compartments. J Biol Chem 2006; 281:38543-38554

111. Dong C, Filipeanu CM, Duvernay MT, Wu G. Regulation of G protein-coupled receptor export trafficking. Biochim Biophys Acta 2007; 1768:853-870

112. Peer W. Plasma Membrane Protein Trafficking. In: Murphy AS, Schulz B, Peer W, eds. The Plant Plasma Membrane. Vol 19: Springer Berlin Heidelberg; 2011:31-56.

113. Ellgaard L, Helenius A. Quality control in the endoplasmic reticulum. Nat Rev Mol Cell Biol 2003; 4:181-191

114. Conn PM, Janovick JA. Trafficking and quality control of the gonadotropin releasing hormone receptor in health and disease. Mol Cell Endocrinol 2009; 299:137-145

115. Cooray SN, Chan L, Webb TR, Metherell L, Clark AJ. Accessory proteins are vital for the functional expression of certain G protein-coupled receptors. Mol Cell Endocrinol 2009; 300:17-24

116. Lefkowitz RJ, Pierce KL, Luttrell LM. Dancing with different partners: protein kinase a phosphorylation of seven membrane-spanning receptors regulates their G protein-coupling specificity. Mol Pharmacol 2002; 62:971-974

117. Millar RP, Lu ZL, Pawson AJ, Flanagan CA, Morgan K, Maudsley SR. Gonadotropin-releasing hormone receptors. Endocr Rev 2004; 25:235-275

118. Willars GB, Royall JE, Nahorski SR, El-Gehani F, Everest H, McArdle CA. Rapid down-regulation of the type I inositol 1,4,5-trisphosphate receptor and desensitization of gonadotropin-releasing hormone-mediated Ca2+ responses in alpha T3-1 gonadotropes. J Biol Chem 2001; 276:3123-3129

119. Stojilkovic SS, Catt KJ. Novel aspects of GnRH-induced intracellular signaling and secretion in pituitary gonadotrophs. J Neuroendocrinol 1995; 7:739-757

120. Leanos-Miranda A, Janovick JA, Conn PM. Receptor-misrouting: an unexpectedly prevalent and rescuable etiology in gonadotropin-releasing hormone receptor-mediated hypogonadotropic hypogonadism. J Clin Endocrinol Metab 2002; 87:4825-4828

121. Berger K, Souza H, Brito VN, d'Alva CB, Mendonca BB, Latronico AC. Clinical and hormonal features of selective follicle-stimulating hormone (FSH) deficiency due to FSH beta-subunit gene mutations in both sexes. Fertil Steril 2005; 83:466-470

122. Themmen APN, Huhtaniemi IT. Mutations of gonadotropins and gonadotropin receptors: elucidating the physiology and pathophysiology of pituitary-gonadal function. Endocr Rev 2000; 21:551-583

123. Arnhold IJ, Lofrano-Porto A, Latronico AC. Inactivating mutations of luteinizing hormone beta-subunit or luteinizing hormone receptor cause oligo-amenorrhea and infertility in women. Horm Res 2009; 71:75-82

124. Drake MT, Shenoy SK, Lefkowitz RJ. Trafficking of G protein-coupled receptors. Circ Res 2006; 99:570-582

125. Claing A, Laporte SA, Caron MG, Lefkowitz RJ. Endocytosis of G protein-coupled receptors: roles of G protein-coupled receptor kinases and beta-arrestin proteins. Prog Neurobiol 2002; 66:61-79

126. McArdle CA, Franklin J, Green L, Hislop JN. Signalling, cycling and desensitisation of gonadotrophin-releasing hormone receptors. J Endocrinol 2002; 173:1-11

127. Redding L, Weiner DB. DNA vaccines in veterinary use. Expert review of vaccines 2009; 8:1251-1276

128. Jansen B, Zangemeister-Wittke U. Antisense therapy for cancer--the time of truth. Lancet Oncol 2002; 3:672-683

129. Vugmeyster Y, Harrold J, Xu X. Absorption, distribution, metabolism, and excretion (ADME) studies of biotherapeutics for autoimmune and inflammatory conditions. AAPS J 2012; 14:714-727

130. Leader B, Baca QJ, Golan DE. Protein therapeutics: a summary and pharmacological classification. Nat Rev Drug Discov 2008; 7:21-39

131. Lee SH, Chung BH, Park TG, Nam YS, Mok H. Small-interfering RNA (siRNA)-based functional micro- and nanostructures for efficient and selective gene silencing. Acc Chem Res 2012; 45:1014-1025

132. Antosova Z, Mackova M, Kral V, Macek T. Therapeutic application of peptides and proteins: parenteral forever? Trends Biotechnol 2009; 27:628-635

133. Guo P. The emerging field of RNA nanotechnology. Nat Nanotechnol 2010; 5:833-842

134. Mok H, Park JW, Park TG. Microencapsulation of PEGylated adenovirus within PLGA microspheres for enhanced stability and gene transfection efficiency. Pharm Res 2007; 24:2263-2269

135. Mok H, Park TG. Water-free microencapsulation of proteins within PLGA microparticles by spray drying using PEG-assisted protein solubilization technique in organic solvent. Eur J Pharm Biopharm 2008; 70:137-144

136. Fan NC, Cheng FY, Ho JA, Yeh CS. Photocontrolled targeted drug delivery: photocaged biologically active folic acid as a light-responsive tumor-targeting molecule. Angew Chem Int Ed Engl 2012; 51:8806-8810

137. Li P, Zheng Y, Ran H, Tan J, Lin Y, Zhang Q, Ren J, Wang Z. Ultrasound triggered drug release from 10-hydroxycamptothecin-loaded phospholipid microbubbles for targeted tumor therapy in mice. J Control Release 2012; 162:349-354

138. Kievit FM, Stephen ZR, Veiseh O, Arami H, Wang T, Lai VP, Park JO, Ellenbogen RG, Disis ML, Zhang M. Targeting of primary breast cancers and

metastases in a transgenic mouse model using rationally designed multifunctional SPIONs. ACS Nano 2012; 6:2591-2601

139. Kievit FM, Zhang M. Cancer nanotheranostics: improving imaging and therapy by targeted delivery across biological barriers. Adv Mater 2011; 23:H217-247

140. Kievit FM, Zhang M. Surface engineering of iron oxide nanoparticles for targeted cancer therapy. Acc Chem Res 2011; 44:853-862

141. Rudge S, Peterson C, Vessely C, Koda J, Stevens S, Catterall L. Adsorption and desorption of chemotherapeutic drugs from a magnetically targeted carrier (MTC). J Control Release 2001; 74:335-340

142. Veiseh O, Kievit FM, Ellenbogen RG, Zhang M. Cancer cell invasion: treatment and monitoring opportunities in nanomedicine. Adv Drug Deliv Rev 2011; 63:582-596

143. Fang C, Zhang M. Nanoparticle-based theragnostics: Integrating diagnostic and therapeutic potentials in nanomedicine. J Control Release 2010; 146:2-5

144. Neuberger T, Schöpf B, Hofmann H, Hofmann M, von Rechenberg B. Superparamagnetic nanoparticles for biomedical applications: Possibilities and limitations of a new drug delivery system. J Magn Magn Mater 2005; 293:483-496

145. Buerli T, Pellegrino C, Baer K, Lardi-Studler B, Chudotvorova I, Fritschy JM, Medina I, Fuhrer C. Efficient transfection of DNA or shRNA vectors into neurons using magnetofection. Nat Protoc 2007; 2:3090-3101

146. Park JW, Bae KH, Kim C, Park TG. Clustered magnetite nanocrystals cross-linked with PEI for efficient siRNA delivery. Biomacromolecules 2011; 12:457-465

147. Nakahara T, Yaguchi H, Yoshida M, Miyakoshi J. Effects of exposure of CHO-K1 cells to a 10-T static magnetic field. Radiology 2002; 224:817-822

148. Maeda H, Wu J, Sawa T, Matsumura Y, Hori K. Tumor vascular permeability and the EPR effect in macromolecular therapeutics: a review. J Control Release 2000; 65:271-284

149. Mejias R, Perez-Yague S, Gutierrez L, Cabrera LI, Spada R, Acedo P, Serna CJ, Lazaro FJ, Villanueva A, Morales Mdel P, Barber DF. Dimercaptosuccinic acid-coated magnetite nanoparticles for magnetically guided in vivo delivery of interferon gamma for cancer immunotherapy. Biomaterials 2011; 32:2938-2952

150. Fang C, Bhattarai N, Sun C, Zhang M. Functionalized nanoparticles with long-term stability in biological media. Small 2009; 5:1637-1641

151. Sadhukha T, Wiedmann TS, Panyam J. Inhalable magnetic nanoparticles for targeted hyperthermia in lung cancer therapy. Biomaterials 2013; 34:5163-5171

152. Ruiz-Hernandez E, Baeza A, Vallet-Regi M. Smart drug delivery through DNA/magnetic nanoparticle gates. ACS Nano 2011; 5:1259-1266

153. Sun C, Lee JS, Zhang M. Magnetic nanoparticles in MR imaging and drug delivery. Adv Drug Deliv Rev 2008; 60:1252-1265

154. Larsen EK, Nielsen T, Wittenborn T, Rydtoft LM, Lokanathan AR, Hansen L, Ostergaard L, Kingshott P, Howard KA, Besenbacher F, Nielsen NC, Kjems J. Accumulation of magnetic iron oxide nanoparticles coated with variably sized polyethylene glycol in murine tumors. Nanoscale 2012; 4:2352-2361

155. Chouly C, Pouliquen D, Lucet I, Jeune JJ, Jallet P. Development of superparamagnetic nanoparticles for MRI: effect of particle size, charge and surface nature on biodistribution. J Microencapsul 1996; 13:245-255

156. Mitragotri S, Lahann J. Physical approaches to biomaterial design. Nat Mater 2009; 8:15-23

157. Kohler N, Fryxell GE, Zhang M. A bifunctional poly(ethylene glycol) silane immobilized on metallic oxide-based nanoparticles for conjugation with cell targeting agents. J Am Chem Soc 2004; 126:7206-7211

158. Rebodos RL, Vikesland PJ. Effects of oxidation on the magnetization of nanoparticulate magnetite. Langmuir 2010; 26:16745-16753

159. Lu AH, Salabas EL, Schuth F. Magnetic nanoparticles: synthesis, protection, functionalization, and application. Angew Chem Int Ed Engl 2007; 46:1222-1244

160. Wong RM, Gilbert DA, Liu K, Louie AY. Rapid size-controlled synthesis of dextran-coated, 64Cu-doped iron oxide nanoparticles. ACS Nano 2012; 6:3461-3467

161. Veiseh O, Sun C, Fang C, Bhattarai N, Gunn J, Kievit F, Du K, Pullar B, Lee D, Ellenbogen RG, Olson J, Zhang M. Specific targeting of brain tumors with an optical/magnetic resonance imaging nanoprobe across the blood-brain barrier. Cancer Res 2009; 69:6200-6207

162. Lee JH, Jung MJ, Hwang YH, Lee YJ, Lee S, Lee DY, Shin H. Heparin-coated superparamagnetic iron oxide for in vivo MR imaging of human MSCs. Biomaterials 2012; 33:4861-4871

163. Laurent S, Forge D, Port M, Roch A, Robic C, Vander Elst L, Muller RN. Magnetic iron oxide nanoparticles: synthesis, stabilization, vectorization, physicochemical characterizations, and biological applications. Chem Rev 2008; 108:2064-2110

164. Chastellain M, Petri A, Hofmann H. Particle size investigations of a multistep synthesis of PVA coated superparamagnetic nanoparticles. J Colloid Interface Sci 2004; 278:353-360

165. Reverchon E, Antonacci A. Chitosan Microparticles Production by Supercritical Fluid Processing. Ind Eng Chem Res 2006; 45:5722-5728

166. Zhang Y, Kohler N, Zhang M. Surface modification of superparamagnetic magnetite nanoparticles and their intracellular uptake. Biomaterials 2002; 23:1553-1561

167. Yamazaki M, Ito T. Deformation and instability in membrane structure of phospholipid vesicles caused by osmophobic association: mechanical stress model for the mechanism of poly(ethylene glycol)-induced membrane fusion. Biochemistry 1990; 29:1309-1314

168. McBain SC, Yiu HHP, El Haj A, Dobson J. Polyethyleneimine functionalized iron oxide nanoparticles as agents for DNA delivery and transfection. J Mater Chem 2007; 17:2561-2565

169. Chen XW, Mao QX, Liu JW, Wang JH. Isolation/separation of plasmid DNA using hemoglobin modified magnetic nanocomposites as solid-phase adsorbent. Talanta 2012; 100:107-112

170. Maye MM, Nykypanchuk D, van der Lelie D, Gang O. A simple method for kinetic control of DNA-induced nanoparticle assembly. J Am Chem Soc 2006; 128:14020-14021

171. He X, Huo H, Wang K, Tan W, Gong P, Ge J. Plasmid DNA isolation using amino-silica coated magnetic nanoparticles (ASMNPs). Talanta 2007; 73:764-769

172. Tanaka T, Shibata K, Hosokawa M, Hatakeyama K, Arakaki A, Gomyo H, Mogi T, Taguchi T, Wake H, Tanaami T, Matsunaga T. Characterization of magnetic nanoparticles modified with thiol functionalized PAMAM dendron for DNA recovery. J Colloid Interface Sci 2012; 377:469-475

173. Jiang C, Xu S, Zhang S, Jia L. Chitosan functionalized magnetic particle-assisted detection of genetically modified soybeans based on polymerase chain reaction and capillary electrophoresis. Anal Biochem 2012; 420:20-25

174. Scherer F, Anton M, Schillinger U, Henke J, Bergemann C, Kruger A, Gansbacher B, Plank C. Magnetofection: enhancing and targeting gene delivery by magnetic force in vitro and in vivo. Gene Ther 2002; 9:102-109

175. Veiseh O, Kievit FM, Gunn JW, Ratner BD, Zhang M. A ligand-mediated nanovector for targeted gene delivery and transfection in cancer cells. Biomaterials 2009; 30:649-657

176. Kievit FM, Veiseh O, Bhattarai N, Fang C, Gunn JW, Lee D, Ellenbogen RG, Olson JM, Zhang M. PEI-PEG-Chitosan Copolymer Coated Iron Oxide Nanoparticles for Safe Gene Delivery: synthesis, complexation, and transfection. Adv Funct Mater 2009; 19:2244-2251

177. Wang C, Ding C, Kong M, Dong A, Qian J, Jiang D, Shen Z. Tumor-targeting magnetic lipoplex delivery of short hairpin RNA suppresses IGF-1R overexpression of lung adenocarcinoma A549 cells in vitro and in vivo. Biochem Biophys Res Commun 2011; 410:537-542

178. Dames P, Gleich B, Flemmer A, Hajek K, Seidl N, Wiekhorst F, Eberbeck D, Bittmann I, Bergemann C, Weyh T, Trahms L, Rosenecker J, Rudolph C. Targeted delivery of magnetic aerosol droplets to the lung. Nat Nanotechnol 2007; 2:495-499

179. Risso A, Corrada Y, Barbeito C, Diaz JD, Gobello C. Long-term-release GnRH agonists postpone puberty in domestic cats. Reprod Domest Anim 2012; 47:936-938

180. Miller LA, Gionfriddo JP, Fagerstone KA, Rhyan JC, Killian GJ. The single-shot GnRH immunocontraceptive vaccine (GonaCon) in white-tailed deer: comparison of several GnRH preparations. Am J Reprod Immunol 2008; 60:214-223

181. Levy JK, Miller LA, Cynda Crawford P, Ritchey JW, Ross MK, Fagerstone KA. GnRH immunocontraception of male cats. Theriogenology 2004; 62:1116-1130

182. Levy JK, Friary JA, Miller LA, Tucker SJ, Fagerstone KA. Long-term fertility control in female cats with GonaCon, a GnRH immunocontraceptive. Theriogenology 2011; 76:1517-1525

183. Bliss SP, Navratil AM, Xie J, Roberson MS. GnRH signaling, the gonadotrope and endocrine control of fertility. Front Neuroendocrinol 2010; 31:322-340

184. Naor Z. Signaling by G-protein-coupled receptor (GPCR): studies on the GnRH receptor. Front Neuroendocrinol 2009; 30:10-29

185. Kutzler MA, Weiner DB. DNA vaccines: ready for prime time? Nat Rev Genet 2008; 9:776-788

186. Saxena BB, Clavio A, Singh M, Rathnam P, Bukharovich Y, Reimers T, Jr., Saxena A, Perkins S. Modulation of ovarian function in female dogs immunized with bovine luteinizing hormone receptor. Reprod Domest Anim 2002; 37:9-17

187. Saxena BB, Clavio A, Singh M, Rathnam P, Bukharovich EY, Reimers TJ, Jr., Saxena A, Perkins S. Effect of immunization with bovine luteinizing hormone receptor on ovarian function in cats. Am J Vet Res 2003; 64:292-298

188. Jain CK, Arora S, Khanna A, Gupta M, Wadhwa G, Sharma SK. The ubiquitin-proteasome pathway an emerging anticancer strategy for therapeutics: a patent analysis. Recent Pat Anticancer Drug Discov 2015; 10:201-213

189. Chou B, Hiromatsu K, Okano S, Ishii K, Duan X, Sakai T, Murata S, Tanaka K, Himeno K. Antiangiogenic tumor therapy by DNA vaccine inducing aquaporin-1-specific CTL based on ubiquitin-proteasome system in mice. J Immunol 2012; 189:1618-1626

190. Eslami NS, Shokrgozar MA, Mousavi A, Azadmanesh K, Nomani A, Apostolopoulos V, Day S, Amanzadeh A, Alimohammadian MH. Simultaneous immunisation with a Wilms' tumour 1 epitope and its ubiquitin fusions results in enhanced cell mediated immunity and tumour rejection in C57BL/6 mice. Mol Immunol 2012; 51:325-331

191. Woo SK, Lee JI, Park IK, Yoo YJ, Cho CM, Kang MS, Ha DB, Tanaka K, Chung CH. Multiple ubiquitin C-terminal hydrolases from chick skeletal muscle. J Biol Chem 1995; 270:18766-18773

192. Degorce F, Card A, Soh S, Trinquet E, Knapik GP, Xie B. HTRF: A Technology Tailored for Drug Discovery –A Review of Theoretical Aspects and Recent Applications. Curr Chem Genomics 2009; 3:22-32

193. Naz RK, Gupta SK, Gupta JC, Vyas HK, Talwar AG. Recent advances in contraceptive vaccine development: a mini-review. Hum Reprod 2005; 20:3271-3283

194. Hardy CM, Braid AL. Vaccines for immunological control of fertility in animals. Rev Sci Tech 2007; 26:461-470

195. Cooper DW, Larsen E. Immunocontraception of mammalian wildlife: ecological and immunogenetic issues. Reproduction 2006; 132:821-828

196. Jacob J, Radkevich O, Forni G, Zielinski J, Shim D, Jones RF, Wei WZ. Activity of DNA vaccines encoding self or heterologous Her-2/neu in Her-2 or neu transgenic mice. Cell Immunol 2006; 240:96-106

197. Taylor SC, Posch A. The Design of a Quantitative Western Blot Experiment. BioMed Res Int 2014; 2014:361590

198. Zerani M, Parillo F, Brecchia G, Guelfi G, Dall'Aglio C, Lilli L, Maranesi M, Gobbetti A, Boiti C. Expression of type I GNRH receptor and in vivo and in vitro GNRH-I effects in corpora lutea of pseudopregnant rabbits. J Endocrinol 2010; 207:289-300

199. Wilson AC, Salamat MS, Haasl RJ, Roche KM, Karande A, Meethal SV, Terasawa E, Bowen RL, Atwood CS. Human neurons express type I GnRH receptor and respond to GnRH I by increasing luteinizing hormone expression. J Endocrinol 2006; 191:651-663

200. Santra S, Rao VS, Shanker YG, Rao AJ. Cloning and characterization of bonnet monkey GnRH receptor. Mol Hum Reprod 2000; 6:415-421

201. Albertson AJ, Talbott H, Wang Q, Jensen D, Skinner DC. The gonadotropin-releasing hormone type I receptor is expressed in the mouse cerebellum. Cerebellum 2008; 7:379-384

202. Samoylov AM, Napier ID, Morrison NE, Martin DR, Cox NR, Samoylova TI. Molecular cloning, sequencing, and distribution of feline GnRH receptor (GnRHR) and resequencing of canine GnRHR. Theriogenology 2015; 83:266-275

203. Warne T, Serrano-Vega MJ, Tate CG, Schertler GF. Development and crystallization of a minimal thermostabilised G protein-coupled receptor. Protein Expr Purif 2009; 65:204-213

204. Heydenreich FM, Vuckovic Z, Matkovic M, Veprintsev DB. Stabilization of G protein-coupled receptors by point mutations. Front Pharmacol 2015; 6:82

205. Andréll J, Tate CG. Overexpression of membrane proteins in mammalian cells for structural studies. Mol Membr Biol 2013; 30:52-63

206. Tate CG. Overexpression of mammalian integral membrane proteins for structural studies. FEBS Lett 2001; 504:94-98

207. Hou J, Tyo K, Liu Z, Petranovic D, Nielsen J. Engineering of vesicle trafficking improves heterologous protein secretion in Saccharomyces cerevisiae. Metab Eng 2012; 14:120-127

208. Manoj S, Babiuk LA, van Drunen Littel-van den Hurk S. Approaches to enhance the efficacy of DNA vaccines. Crit Rev Clin Lab Sci 2004; 41:1-39

209. Poizot P, Laruelle S, Grugeon S, Dupont L, Tarascon JM. Nano-sized transition-metal oxides as negative-electrode materials for lithium-ion batteries. Nature 2000; 407:496-499

210. Mahmoudi M, Simchi A, Imani M, Stroeve P, Sohrabi A. Templated growth of superparamagnetic iron oxide nanoparticles by temperature programming in the presence of poly(vinyl alcohol). Thin Solid Films 2010; 518:4281-4289

211. Hans ML, Lowman AM. Biodegradable nanoparticles for drug delivery and targeting. Curr Opin Solid State and Mater Sci 2002; 6:319-327

212. Langer R. Drug delivery and targeting. Nature 1998; 392:5-10

213. Ghendon Y, Markushin S, Krivtsov G, Akopova I. Chitosan as an adjuvant for parenterally administered inactivated influenza vaccines. Arch Virol 2008; 153:831-837

214. Truong-Le VL, Walsh SM, Schweibert E, Mao HQ, Guggino WB, August JT, Leong KW. Gene transfer by DNA-gelatin nanospheres. Arch Biochem Biophys 1999; 361:47-56

215. Pickard MR, Barraud P, Chari DM. The transfection of multipotent neural precursor/stem cell transplant populations with magnetic nanoparticles. Biomaterials 2011; 32:2274-2284

216. Seder RA, Hill AV. Vaccines against intracellular infections requiring cellular immunity. Nature 2000; 406:793-798

217. Leung KC-F, Lee S-F, Wong C-H, Chak C-P, Lai JMY, Zhu X-M, Wang Y-XJ, Sham KWY, Cheng CHK. Nanoparticle–DNA–polymer composites for

hepatocellular carcinoma cell labeling, sensing, and magnetic resonance imaging. Methods 2013; 64:315-321

218. Moraes L, Vasconcelos-dos-Santos A, Santana FC, Godoy MA, Rosado-de-Castro PH, Jasmin, Azevedo-Pereira RL, Cintra WM, Gasparetto EL, Santiago MF, Mendez-Otero R. Neuroprotective effects and magnetic resonance imaging of mesenchymal stem cells labeled with SPION in a rat model of Huntington's disease. Stem Cell Res 2012; 9:143-155

219. Liu CH, Kim YR, Ren JQ, Eichler F, Rosen BR, Liu PK. Imaging Cerebral Gene Transcripts in Live Animals. Journal of Neurosci 2007; 27:713-722

220. Gratton SEA, Ropp PA, Pohlhaus PD, Luft JC, Madden VJ, Napier ME, DeSimone JM. The effect of particle design on cellular internalization pathways. Proc Natl Acad Sci U S A 2008; 105:11613-11618

221. Huang X, Li L, Liu T, Hao N, Liu H, Chen D, Tang F. The Shape Effect of Mesoporous Silica Nanoparticles on Biodistribution, Clearance, and Biocompatibility in Vivo. ACS Nano 2011; 5:5390-5399

222. Zhang L, Dou Y-H, Gu H-C. Sterically induced shape control of magnetite nanoparticles. J Cryst Growth 2006; 296:221-226

223. Gaumet M, Vargas A, Gurny R, Delie F. Nanoparticles for drug delivery: the need for precision in reporting particle size parameters. Eur J Pharm Biopharm 2008; 69:1-9

224. Chouly C, Pouliquen D, Lucet I, Jeune JJ, Jallet P. Development of superparamagnetic nanoparticles for MRI: effect of particle size, charge and surface nature on biodistribution. J Microencapsul 1996; 13:245-255

225. Honary S, Zahir F. Effect of Zeta Potential on the Properties of Nano-Drug Delivery Systems - A Review (Part 2). Trop J Pharm Res 2013; 12:265-273

226. Gupta AK, Naregalkar RR, Vaidya VD, Gupta M. Recent advances on surface engineering of magnetic iron oxide nanoparticles and their biomedical applications. Nanomedicine (Lond) 2007; 2:23-39

227. Dobrovolskaia MA, McNeil SE. Immunological properties of engineered nanomaterials. Nat Nanotechnol 2007; 2:469-478

228. Kim S, Kim JH, Jeon O, Kwon IC, Park K. Engineered polymers for advanced drug delivery. Eur J Pharm Biopharm 2009; 71:420-430

229. Piao Y, Burns A, Kim J, Wiesner U, Hyeon T. Designed Fabrication of Silica-Based Nanostructured Particle Systems for Nanomedicine Applications. Adv Funct Mater 2008; 18:3745-3758

230. Lutz JF, Stiller S, Hoth A, Kaufner L, Pison U, Cartier R. One-pot synthesis of pegylated ultrasmall iron-oxide nanoparticles and their in vivo evaluation as magnetic resonance imaging contrast agents. Biomacromolecules 2006; 7:3132-3138

231. Ding H, Sagar V, Agudelo M, Pilakka-Kanthikeel S, Atluri VS, Raymond A, Samikkannu T, Nair MP. Enhanced blood-brain barrier transmigration using a novel transferrin embedded fluorescent magneto-liposome nanoformulation. Nanotechnology 2014; 25:055101

232. Alexiou C, Jurgons R, Schmid R, Hilpert A, Bergemann C, Parak F, Iro H. In vitro and in vivo investigations of targeted chemotherapy with magnetic nanoparticles. J Magn Magn Mater 2005; 293:389-393

233. Lee JH, Lee HB, Andrade JD. Blood compatibility of polyethylene oxide surfaces. Prog Polym Sci 1995; 20:1043-1079

234. Luo Z, Li P, Deng J, Gao N, Zhang Y, Pan H, Liu L, Wang C, Cai L, Ma Y. Cationic polypeptide micelle-based antigen delivery system: A simple and robust adjuvant to improve vaccine efficacy. J Control Release 2013; 170:259-267

235. Zhuang Y, Ma Y, Wang C, Hai L, Yan C, Zhang Y, Liu F, Cai L. PEGylated cationic liposomes robustly augment vaccine-induced immune responses: Role of lymphatic trafficking and biodistribution. J Control Release 2012; 159:135-142

236. Harris JM, Chess RB. Effect of pegylation on pharmaceuticals. Nat Rev Drug Discov 2003; 2:214-221

237. Fay F, Quinn DJ, Gilmore BF, McCarron PA, Scott CJ. Gene delivery using dimethyldidodecylammonium bromide-coated PLGA nanoparticles. Biomaterials 2010; 31:4214-4222

238. Perez C, Sanchez A, Putnam D, Ting D, Langer R, Alonso MJ. Poly(lactic acid)-poly(ethylene glycol) nanoparticles as new carriers for the delivery of plasmid DNA. J Control Release 2001; 75:211-224

239. Patil YB, Swaminathan SK, Sadhukha T, Ma L, Panyam J. The use of nanoparticle-mediated targeted gene silencing and drug delivery to overcome tumor drug resistance. Biomaterials 2010; 31:358-365

240. Li Z, Yang H, He N, Liang W, Ma C, Shah MA, Tang Y, Li S, Liu H, Jiang H, Guo Y. Solid-phase hybridization efficiency improvement on the magnetic nanoparticle surface by using dextran as molecular arms. J Biomed Nanotechnol 2013; 9:1945-1949

241. Cole AJ, David AE, Wang J, Galban CJ, Hill HL, Yang VC. Polyethylene glycol modified, cross-linked starch-coated iron oxide nanoparticles for enhanced magnetic tumor targeting. Biomaterials 2011; 32:2183-2193

242. Prijic S, Scancar J, Romih R, Cemazar M, Bregar VB, Znidarsic A, Sersa G. Increased cellular uptake of biocompatible superparamagnetic iron oxide nanoparticles into malignant cells by an external magnetic field. J Membr Biol 2010; 236:167-179

243. Alexiou C, Jurgons R, Seliger C, Brunke O, Iro H, Odenbach S. Delivery of superparamagnetic nanoparticles for local chemotherapy after intraarterial infusion and magnetic drug targeting. Anticancer Res 2007; 27:2019-2022

244. Chertok B, David AE, Yang VC. Polyethyleneimine-modified iron oxide nanoparticles for brain tumor drug delivery using magnetic targeting and intra-carotid administration. Biomaterials 2010; 31:6317-6324

245. Chertok B, Moffat BA, David AE, Yu F, Bergemann C, Ross BD, Yang VC. Iron oxide nanoparticles as a drug delivery vehicle for MRI monitored magnetic targeting of brain tumors. Biomaterials 2008; 29:487-496

246. Clogston J, Patri A. Zeta Potential Measurement. In: McNeil SE, ed. Characterization of Nanoparticles Intended for Drug Delivery. Vol 697: Humana Press; 2011:63-70.

247. Vinogradov SV, Bronich TK, Kabanov AV. Nanosized cationic hydrogels for drug delivery: preparation, properties and interactions with cells. Adv Drug Deliv Rev 2002; 54:135-147

248. Rigotti A, Acton SL, Krieger M. The class B scavenger receptors SR-BI and CD36 are receptors for anionic phospholipids. J Biol Chem 1995; 270:16221-16224

249. Pai Kasturi S, Qin H, Thomson KS, El-Bereir S, Cha S-c, Neelapu S, Kwak LW, Roy K. Prophylactic anti-tumor effects in a B cell lymphoma model with DNA vaccines delivered on polyethylenimine (PEI) functionalized PLGA microparticles. J Control Release 2006; 113:261-270

250. Shan Z, Jiang Y, Guo M, Bennett JC, Li X, Tian H, Oakes K, Zhang X, Zhou Y, Huang Q, Chen H. Promoting DNA loading on magnetic nanoparticles using a DNA condensation strategy. Colloids and Surfaces B: Biointerfaces 2015; 125:247-254

251. Grosenbaugh DA, Leard AT, Bergman PJ, Klein MK, Meleo K, Susaneck S, Hess PR, Jankowski MK, Jones PD, Leibman NF, Johnson MH, Kurzman ID, Wolchok JD. Safety and efficacy of a xenogeneic DNA vaccine encoding for human tyrosinase as adjunctive treatment for oral malignant melanoma in dogs following surgical excision of the primary tumor. Am J Vet Res 2011; 72:1631-1638

252. Manthorpe M, Cornefert-Jensen F, Hartikka J, Felgner J, Rundell A, Margalith M, Dwarki V. Gene therapy by intramuscular injection of plasmid DNA: studies on firefly luciferase gene expression in mice. Hum Gene Ther 1993; 4:419-431

253. Levy MY, Barron LG, Meyer KB, Szoka FC, Jr. Characterization of plasmid DNA transfer into mouse skeletal muscle: evaluation of uptake mechanism, expression and secretion of gene products into blood. Gene Ther 1996; 3:201-211

254. Davis HL, Demeneix BA, Quantin B, Coulombe J, Whalen RG. Plasmid DNA is superior to viral vectors for direct gene transfer into adult mouse skeletal muscle. Hum Gene Ther 1993; 4:733-740

255. Mumper R, Ledebur H, Jr., Rolland A, Tomlinson E. Controlled Plasmid Delivery and Gene Expression. In: Lowrie D, Whalen R, eds. DNA Vaccines. Vol 29: Humana Press; 2000:267-286.

256. Pannier AK, Shea LD. Controlled Release Systems for DNA Delivery. Mol Ther 2004; 10:19-26

257. Wahajuddin, Arora S. Superparamagnetic iron oxide nanoparticles: magnetic nanoplatforms as drug carriers. Inter J Nanomedicine 2012; 7:3445-3471

258. Oh N, Park J-H. Endocytosis and exocytosis of nanoparticles in mammalian cells. International Journal of Nanomedicine 2014; 9:51-63

259. Wang S-T, Lin Y, Spicer CD, Stevens MM. Bio-inspired Maillard-Like reactions enable a simple and sensitive assay for colorimetric detection of methylglyoxal. Chem Commun 2015; 51:11026-11029

260. Zakaria HM, Shah A, Konieczny M, Hoffmann JA, Nijdam AJ, Reeves ME. Small molecule- and amino acid-induced aggregation of gold nanoparticles. Langmuir 2013; 29:7661-7673

261. Kim T, Lee K, Gong MS, Joo SW. Control of gold nanoparticle aggregates by manipulation of interparticle interaction. Langmuir 2005; 21:9524-9528

262. Albanese A, Chan WC. Effect of gold nanoparticle aggregation on cell uptake and toxicity. ACS Nano 2011; 5:5478-5489

263. Park HG, Oh JH, Lee JS. Assembly-based titration for the determination of monodisperse plasmonic nanoparticle concentrations using DNA. Anal Chem 2011; 83:4989-4995

264. Zinchenko AA, Sakaue T, Araki S, Yoshikawa K, Baigl D. Single-Chain Compaction of Long Duplex DNA by Cationic Nanoparticles: Modes of Interaction and Comparison with Chromatin. J Phys Chem B 2007; 111:3019-3031

265. Yoshikawa K, Yoshikawa Y, Koyama Y, Kanbe T. Highly Effective Compaction of Long Duplex DNA Induced by Polyethylene Glycol with Pendant Amino Groups. J Am Chem Soc 1997; 119:6473-6477

266. Bloomfield VA. DNA condensation. Curr Opin Struct Biol 1996; 6:334-341

267. Segura T, Volk MJ, Shea LD. Substrate-mediated DNA delivery: role of the cationic polymer structure and extent of modification. J Control Release 2003; 93:69-84

268. Segura T, Shea LD. Surface-Tethered DNA Complexes for Enhanced Gene Delivery. Bioconjug Chem 2002; 13:621-629

269. Quill H, Schwartz RH. Stimulation of normal inducer T cell clones with antigen presented by purified Ia molecules in planar lipid membranes: specific induction of a long-lived state of proliferative nonresponsiveness. J Immunol 1987; 138:3704-3712

270. Mueller DL, Jenkins MK, Schwartz RH. Clonal expansion versus functional clonal inactivation: a costimulatory signalling pathway determines the outcome of T cell antigen receptor occupancy. Annu Rev Immunol 1989; 7:445-480

271. Lamb JR, Skidmore BJ, Green N, Chiller JM, Feldmann M. Induction of tolerance in influenza virus-immune T lymphocyte clones with synthetic peptides of influenza hemagglutinin. J Exp Med 1983; 157:1434-1447

272. Jenkins MK, Schwartz RH. Antigen presentation by chemically modified splenocytes induces antigen-specific T cell unresponsiveness in vitro and in vivo. J Exp Med 1987; 165:302-319

273. Pardoll DM, Beckerleg AM. Exposing the immunology of naked DNA vaccines. Immunity 1995; 3:165-169

274. Hohlfeld R, Engel AG. The immunobiology of muscle. Immunol Today 1994; 15:269-274

275. Austyn JM, Hankins DF, Larsen CP, Morris PJ, Rao AS, Roake JA. Isolation and characterization of dendritic cells from mouse heart and kidney. J Immunol 1994; 152:2401-2410

276. Dubensky TW, Liu MA, Ulmer JB. Delivery systems for gene-based vaccines. Mol Med 2000; 6:723-732

277. Plank C, Zelphati O, Mykhaylyk O. Magnetically enhanced nucleic acid delivery. Ten years of magnetofection-progress and prospects. Adv Drug Deliv Rev 2011; 63:1300-1331

278. Park HY, Noh EH, Chung HM, Kang MJ, Kim EY, Park SP. Efficient generation of virus-free iPS cells using liposomal magnetofection. PLoS One 2012; 7:e45812

279. Ma Y, Zhang Z, Wang X, Xia W, Gu H. Insights into the mechanism of magnetofection using MNPs-PEI/pDNA/free PEI magnetofectins. Int J Pharm 2011; 419:247-254

280. Plank C, Schillinger U, Scherer F, Bergemann C, Remy JS, Krotz F, Anton M, Lausier J, Rosenecker J. The magnetofection method: using magnetic force to enhance gene delivery. Biol Chem 2003; 384:737-747

281. Huth S, Lausier J, Gersting SW, Rudolph C, Plank C, Welsch U, Rosenecker J. Insights into the mechanism of magnetofection using PEI-based magnetofectins for gene transfer. J Gene Med 2004; 6:923-936

282. Berry CC, Wells S, Charles S, Curtis AS. Dextran and albumin derivatised iron oxide nanoparticles: influence on fibroblasts in vitro. Biomaterials 2003; 24:4551-4557

283. Mah C, Fraites TJ, Jr., Zolotukhin I, Song S, Flotte TR, Dobson J, Batich C, Byrne BJ. Improved method of recombinant AAV2 delivery for systemic targeted gene therapy. Mol Ther 2002; 6:106-112

284. Xu ZP, Zeng QH, Lu GQ, Yu AB. Inorganic nanoparticles as carriers for efficient cellular delivery. Chem Eng Sci 2006; 61:1027-1040

285. Prabha S, Zhou WZ, Panyam J, Labhasetwar V. Size-dependency of nanoparticle-mediated gene transfection: studies with fractionated nanoparticles. Int J Pharm 2002; 244:105-115

286. Cui Z, Dierling A, Foldvari M. Non-invasive immunization on the skin using DNA vaccine. Curr Drug Deliv 2006; 3:29-35

287. Nicolas JF, Guy B. Intradermal, epidermal and transcutaneous vaccination: from immunology to clinical practice. Expert Rev Vaccines 2008; 7:1201-1214

288. Lambert PH, Laurent PE. Intradermal vaccine delivery: will new delivery systems transform vaccine administration? Vaccine 2008; 26:3197-3208

289. Glenn GM, Kenney RT. Mass vaccination: solutions in the skin. Curr Top Microbiol Immunol 2006; 304:247-268

290. Gregersen JP. DNA vaccines. Naturwissenschaften 2001; 88:504-513

291. Torres CA, Iwasaki A, Barber BH, Robinson HL. Differential dependence on target site tissue for gene gun and intramuscular DNA immunizations. J Immunol 1997; 158:4529-4532

292. Condon C, Watkins SC, Celluzzi CM, Thompson K, Falo LD, Jr. DNA-based immunization by in vivo transfection of dendritic cells. Nat Med 1996; 2:1122-1128

293. Steele KE, Stabler K, VanderZanden L. Cutaneous DNA vaccination against Ebola virus by particle bombardment: histopathology and alteration of CD3-positive dendritic epidermal cells. Vet Pathol 2001; 38:203-215

294. Barry MA, Johnston SA. Biological features of genetic immunization. Vaccine 1997; 15:788-791

295. Fynan EF, Webster RG, Fuller DH, Haynes JR, Santoro JC, Robinson HL. DNA vaccines: protective immunizations by parenteral, mucosal, and gene-gun inoculations. Proc Natl Acad Sci U S A 1993; 90:11478-11482

296. Tighe H, Corr M, Roman M, Raz E. Gene vaccination: plasmid DNA is more than just a blueprint. Immunol Today 1998; 19:89-97

297. Tanigawa K, Yu H, Sun R, Nickoloff BJ, Chang AE. Gene gun application in the generation of effector T cells for adoptive immunotherapy. Cancer Immunol Immunother 2000; 48:635-643

298. Kent SJ, Zhao A, Best SJ, Chandler JD, Boyle DB, Ramshaw IA. Enhanced T-cell immunogenicity and protective efficacy of a human immunodeficiency virus type 1 vaccine regimen consisting of consecutive priming with DNA and boosting with recombinant fowlpox virus. J Virol 1998; 72:10180-10188

299. Zhang L, Nolan E, Kreitschitz S, Rabussay DP. Enhanced delivery of naked DNA to the skin by non-invasive in vivo electroporation. Biochimica et Biophysica Acta (BBA) - General Subjects 2002; 1572:1-9

300. Liu MA, Ulmer JB. Gene-based vaccines. Mol Ther 2000; 1:497-500

301. Widera G, Austin M, Rabussay D, Goldbeck C, Barnett SW, Chen M, Leung L, Otten GR, Thudium K, Selby MJ, Ulmer JB. Increased DNA vaccine delivery and immunogenicity by electroporation in vivo. J Immunol 2000; 164:4635-4640

302. Rizzuto G, Cappelletti M, Maione D, Savino R, Lazzaro D, Costa P, Mathiesen I, Cortese R, Ciliberto G, Laufer R, La Monica N, Fattori E. Efficient and regulated erythropoietin production by naked DNA injection and muscle electroporation. Proc Natl Acad Sci U S A 1999; 96:6417-6422

303. Drabick JJ, Glasspool-Malone J, King A, Malone RW. Cutaneous transfection and immune responses to intradermal nucleic acid vaccination are significantly enhanced by in vivo electropermeabilization. Mol Ther 2001; 3:249-255

304. Raz E, Carson DA, Parker SE, Parr TB, Abai AM, Aichinger G, Gromkowski SH, Singh M, Lew D, Yankauckas MA, et al. Intradermal gene immunization: the possible role of DNA uptake in the induction of cellular immunity to viruses. Proc Natl Acad Sci U S A 1994; 91:9519-9523

305. Tesoro-Cruz E, Calderon-Rodriguez R, Hernandez-Gonzalez R, Blanco-Favela F, Aguilar-Setien A. Intradermal DNA vaccination in ear pinnae is an efficient route to protect cats against rabies virus. Vet Res 2008; 39:16

306. Lodmell DL, Parnell MJ, Weyhrich JT, Ewalt LC. Canine rabies DNA vaccination: a single-dose intradermal injection into ear pinnae elicits elevated and persistent levels of neutralizing antibody. Vaccine 2003; 21:3998-4002

307. Lodmell DL, Ewalt LC, Parnell MJ, Rupprecht CE, Hanlon CA. One-time intradermal DNA vaccination in ear pinnae one year prior to infection protects dogs against rabies virus. Vaccine 2006; 24:412-416

308. Forg P, von Hoegen P, Dalemans W, Schirrmacher V. Superiority of the ear pinna over muscle tissue as site for DNA vaccination. Gene Ther 1998; 5:789-797

309. Gold JS, Ferrone CR, Guevara-Patino JA, Hawkins WG, Dyall R, Engelhorn ME, Wolchok JD, Lewis JJ, Houghton AN. A single heteroclitic epitope determines cancer immunity after xenogeneic DNA immunization against a tumor differentiation antigen. J Immunol 2003; 170:5188-5194

310. Christadoss P, Poussin M, Deng C. Animal models of myasthenia gravis. Clin Immunol 2000; 94:75-87

311. Zhang M, Obata C, Hisaeda H, Ishii K, Murata S, Chiba T, Tanaka K, Li Y, Furue M, Chou B, Imai T, Duan X, Himeno K. A novel DNA vaccine based on ubiquitin-proteasome pathway targeting 'self'-antigens expressed in melanoma/melanocyte. Gene Ther 2005; 12:1049-1057

312. Mykhaylyk O, Sanchez-Antequera Y, Vlaskou D, Cerda M, Bokharaei M, Hammerschmid E, Anton M, Plank C. Magnetic Nanoparticle and Magnetic Field Assisted siRNA Delivery In Vitro. In: Sioud M, ed. RNA Interference. Vol 1218: Springer New York; 2015:53-106.

313. Prijic S, Prosen L, Cemazar M, Scancar J, Romih R, Lavrencak J, Bregar VB, Coer A, Krzan M, Znidarsic A, Sersa G. Surface modified magnetic nanoparticles for immuno-gene therapy of murine mammary adenocarcinoma. Biomaterials 2012; 33:4379-4391

314. Kubo T, Sugita T, Shimose S, Nitta Y, Ikuta Y, Murakami T. Targeted delivery of anticancer drugs with intravenously administered magnetic liposomes in osteosarcoma-bearing hamsters. Int J Oncol 2000; 17:309-315

315. Porgador A, Irvine KR, Iwasaki A, Barber BH, Restifo NP, Germain RN. Predominant role for directly transfected dendritic cells in antigen presentation to CD8+ T cells after gene gun immunization. J Exp Med 1998; 188:1075-1082

316. Sbai H, Schneider J, Hill AV, Whalen RG. Role of transfection in the priming of cytotoxic T-cells by DNA-mediated immunization. Vaccine 2002; 20:3137-3147

317. Toki S, Omary RA, Wilson K, Gore JC, Peebles RS, Pham W. A comprehensive analysis of transfection-assisted delivery of iron oxide nanoparticles to dendritic cells. Nanomedicine : nanotechnology, biology, and medicine 2013; 9:1235-1244

318. Yoshida M, Babensee JE. Molecular aspects of microparticle phagocytosis by dendritic cells. J Biomater Sci Polym Ed 2006; 17:893-907

319. Babensee JE. Interaction of dendritic cells with biomaterials. Semin Immunol 2008; 20:101-108

320. Yoshida M, Babensee JE. Poly(lactic-co-glycolic acid) enhances maturation of human monocyte-derived dendritic cells. J Biomed Mater Res A 2004; 71A:45-54

321. Peachman KK, Rao M, Alving CR. Immunization with DNA through the skin. Methods 2003; 31:232-242

322. Donnelly JJ, Wahren B, Liu MA. DNA vaccines: progress and challenges. J Immunol 2005; 175:633-639

323. Akbari O, Panjwani N, Garcia S, Tascon R, Lowrie D, Stockinger B. DNA vaccination: transfection and activation of dendritic cells as key events for immunity. J Exp Med 1999; 189:169-178